THESIS ON NATURAL AND EXACT SCIENCES B189

Internal Geochemical Stratification of Bentonites (Altered Volcanic Ash Beds) and its Interpretation

SVEN SIIR

TUT PRESS

TALLINN UNIVERSITY OF TECHNOLOGY
Institute of Geology

This dissertation was accepted for the defence of the degree of Doctor of Philosophy in Earth Sciences on June 10, 2015.

Supervisor: Dr. Tarmo Kiipli, Institute of Geology at Tallinn University of Technology

Co-supervisor: Prof. Alvar Soesoo, Institute of Geology at Tallinn University of Technology

Opponents: Associate Prof. Sigitas Radzevičius, Vilnius University

Dr. Sten Suuroja, Head of Department, Geological Survey of Estonia

Defence of the thesis: August 10, 2015 at Tallinn University of Technology, Ehitajate tee 5, Tallinn, 19086, Estonia

Declaration: *Hereby I declare that this doctoral thesis, my original investigation and achievement, submitted for the doctoral degree at Tallinn University of Technology has not been submitted for doctoral or equivalent academic degree elsewhere.*

Sven Siir

ISSN 1406-4723
ISBN 978-9949-23-819-4 (publication)
ISBN 978-9949-23-820-0 (PDF)

LOODUS- JA TÄPPISTEADUSED B189

Bentoniitide (muutunud vulkaanituhkade) geokeemiline sisestratifikatsioon ja selle interpretatsioon

SVEN SIIR

TTÜ KIRJASTUS

CONTENTS

INTRODUCTION 7
1. GEOLOGICAL BACKGROUND AND MATERIALS 9
2. METHODS 12
3. RESULTS 14
3.1 X-ray diffractometry (XRD) 14
3.2 Phenocrysts 16
3.3 Sedigraf 17
3.4 X-ray fluorescence (XRF) 17
4. DISCUSSION 21
4.1 Comparison of bentonites with clay from carbonate rocks 21
4.2 Diagenetic alteration 21
4.3 Multiple versus single eruption hypothesis for source of material forming bentonite 24
4.4 Role of mixing of material during transport and emplacement 25
4.5 Environmental effects of the ash falls and interaction of ash-water-sediment system 25
4.6 Discrimination of bentonites from different eruptions 27
5. CONCLUSIONS 28
ACKNOWLEDGEMENTS 29
REFERENCES 30
ABSTRACT 39
KOKKUVÕTE 40
ELULOOKIRJELDUS 42
CURRICULUM VITAE 43
PUBLICATIONS 45

LIST OF ORIGINAL PUBLICATIONS

The thesis is based on the following papers, in the text referred to in Roman numerals as listed below.

I – Dahlquist, P.; Calner, M.; Kallaste, T.; Kiipli, T.; **Siir, S**. 2012. Geochemical variations within the mid-Silurian Grötlingbo Bentonite (Gotland, Sweden)—discriminating between magmatic composition, ash transport fractionation and diagenetic effects. *GFF*, **134**, 273-282.

II – Kiipli, E.; Kiipli, T.; Kallaste, T.; **Siir, S**. 2012. Al_2O_3/TiO_2 ratio of the clay fraction of Late Ordovician–Silurian carbonate rocks as an indicator of paleoclimate of the Fennoscandian Shield. Elsevier. *Palaeogeography, Palaeoclimatology, Palaeoecology*, **365/366**, 312-320.

III – Kiipli, T.; Kallaste, T.; Nielsen, A.; Schovsbo, N.; **Siir, S**. 2014. Geochemical discrimination of the Upper Ordovician Kinnekulle Bentonite in the Billegrav-2 drill core section, Bornholm, Denmark. *Estonian Journal of Earth Sciences*, **63**, 264–270.

IV – **Siir, S**., Kallaste, T., Kiipli, T. & Hints, R. 2015. Internal stratification of two thick Ordovician bentonites of Estonia: deciphering primary magmatic, sedimentary, environmental and diagenetic signatures. *Estonian Journal of Earth Sciences*, **64**, 2, 140-158.

The co-authorship of the papers reflects that they were part of collaborative research projects. For Paper IV, the author was responsible for sample collection, analysis, data interpretation and writing of the paper; for papers I and II, the author participated in sample preparation, analysis and interpretation, and for Paper III, the author participated in sample collection, preparation, interpretation and manuscript preparation.

INTRODUCTION

In the sense of geological time, volcanic ash fallout is an „instantaneous“ event and can be used for precise regional correlation of sedimentary sections (Hageman and Sjelnaes 1955; Kolata and Frost 1987; Huff and Kolata 1989; Bergström et al. 1998; Emerson et al. 2004; Kiipli et al. 2006, 2008b, 2010b, 2010c, 2011, 2012a, 2012b, 2014a; Inanli et al. 2009; Ray 2007; Ray et al. 2011, 2013; Batchelor 2014b; Sell et al. 2015). The idea of using volcanic ash beds for correlations in stratigraphy was first proposed by Thorarinsson (1944). Over the succeeding decades, tephrochronology has intensively grown, forming an important branch of Quaternary science today (Wastegård and Davies 2009; Austin et al. 2014). Researchers studying volcanic ash beds (bentonites) for correlation in hundreds of millions of years old rocks, are faced with complicated challenges, since volcanic ash has considerably altered over time, appearing mostly as clay bands of various composition today. The composition of authigenic clay has lost most of its original signatures and, therefore, bulk composition cannot be used for identification of particular eruption layers. In the last decades of the 20th century (Potts 2003), developments in laboratory analytical techniques offered new possibilities for solving identification problems of altered volcanic ash. Today, micro-analytical techniques allow to study compositions of well-preserved micro-phenocrysts—apatite, biotite, sanidine and zircon (Batchelor and Clarkson 1993; Batchelor 2014a, 2009; Sell and Samson 2011; Kallaste and Kiipli 2006; Bauert et al. 2014). From the bulk composition of bentonites, only a restricted list of immobile elements can be used for constructing correlations (Zielinski 1985).

Altered volcanic ash interbeds (bentonites) also carry information, which helps reconstruct tectonomagmatic environments in volcanic source areas (Huff et al. 1993, 2000, 2014; Batchelor and Evans 2000; Batchelor 2009; Hetherington et al. 2011, Kiipli et al. 2014b) and diagenetic environments of sedimentary rocks (Altaner et al. 1984; Kepežinskas 1994; Hints et al. 2006, 2008; Somelar et al. 2010; Williams et al. 2013), as well as determine the direction to the volcanic source (Huff et al. 1992; Bergström et al. 1995; Torsvik and Rehnstöm 2003; Kiipli et al. 2013). Isotopic datings of well-preserved phenocrysts in bentonites are used for refining the geological time scale (Bergström et al. 2008; Huff 2008; Cramer et al. 2012, 2015; Sell et al. 2013; Svensen et al. 2015).

In the Baltoscandian Region, Bergström et al. (1995) applied trace element geochemistry in combination with palaeontological data and thickness of the beds for correlation and named the thickest Ordovician bed the “Kinnekulle”

K-bentonite, which was studied more closely in papers III and IV. BII, Sinsen and Grötlingbo bentonites (Paper I and IV) are 30–90 cm thick bentonite layers, which allow to trace internal geochemical stratification and to compare bentonitic clay bands with terrigenous clays (Paper II). While in recent sediments, volcanic glass composition has been used for identification of particular eruption layers (Sarna-Wojcicki et al. 1987; Turney et al. 2008), in Palaeozoic rocks, all glass has been altered and only small ratios of immobile elements and well-preserved phenocryst crystals can be used for geological correlations. Since Al, Th, Nb, Zr, Cr and Ti are generally considered immobile during the conversion of volcanic ash into bentonitic clay (Winchester and Floyd 1977; Kiipli et al. 2008c, 2008d, 2013), ratios of these elements can be used for interpretation of source magma composition. This concept was challenged by the present study (Paper IV), where highly or slightly mobile elements Si, K, Mg, Rb, Ga and Y were used for tracing compositional changes that had occurred during the conversion of volcanic ash into bentonitic clay. Besides element mobility in diagenetic processes, change of source magma composition during long-lasting volcanic eruptions and fractionation of ash components in air transport and re-deposition in sedimentary basins can also influence the final bentonite composition. In addition, accumulation of volcanic ash from several eruptions into a single bentonite bed has been proposed to be a cause of compositional variability (Bergström et al. 1997). In bentonites, the result of all these processes occurs as internal compositional stratification, which complicates the identification and correlation of layers.

The main aim of the present PhD study was deciphering the causes of within-bed natural variability. Since, during the formation of the bentonite, geochemical processes occur inside the ash layer as well as between volcanic ash and the surrounding environment, the current study focused on describing the changes that took place during the diagenesis. Understanding these processes will form a solid foundation for further studies in the field of volcanic stratigraphy.

1. GEOLOGICAL BACKGROUND AND MATERIALS

Ordovician and Silurian sedimentary rocks are exposed in North and Central Estonia and on the Baltic Sea islands belonging to Estonia, Sweden and Denmark (Paper III). In Scandinavia, Palaeozoic rocks can be found in several isolated areas, which have escaped post-Palaeozoic erosion. Ordovician and Silurian in subsurface extend in all the East Baltic countries and northern Poland and Belarus; they have also been established by drilling and seismic studies under the central and southern Baltic Sea. These rocks have deposited in stable platform (Baltica palaeocontinent) conditions and are represented by limestones and dolomites in shallow-shelf palaeo-environments and by shales and marlstones in deep-shelf settings (Raukas & Teedumäe 1997). In the Late Ordovician Sandbian time, the small continent of Avalonia approached Baltica (Cocks and Fortey 2009; Waldron et al. 2014) and brought an active volcanic zone close enough to supply Ordovician sediments on the Baltic Basin with volcanic ashes. In the Billegrav-2 core from Bornholm (Denmark), bentonites from 40 separate volcanic eruptions have been recognized in total (Paper III). Later, in the Ordovician Katian and the Silurian, Baltica and Avalonia approached Laurentia (today`s North America) and the convergence of these continents resulted in intensive volcanism, which, once again, sent volcanic ash from a large number of eruptions to the sediments in the Baltic Basin (Fig. 1). Bentonites from altogether 150 volcanic eruptions have been established in the East Baltic Silurian (Kiipli et al. 2013).

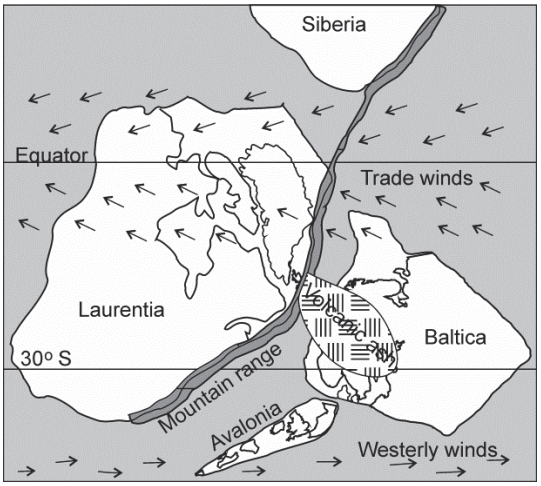

Fig. 1. Palaeogeography of the Late Ordovician (Katian) time. Modified from Huff et al. (2014). Volcanic ash cloud according to Kiipli et al. (2015).

Thick bentonite beds and host rocks were sampled from four drill cores located in Estonia, Sweden and Denmark (Fig. 2):

1. The Grötlingbo Bentonite (Paper I) was sampled from the Hunninge-1 core (Gotland, Sweden) and includes the topmost Slite Marl through the Fröjel, Halla and basal Klinteberg formations, Upper-Homerian (Calner et al. 2006). The Grötlingbo Bentonite was divided into eight samples, spaced by 5 cm and weighing 15–20 g each. Two additional samples were taken as reference at 0.1 and 0.5 m below and above the bentonite, respectively. The underlying and overlying rocks are micritic limestones with sparse coated grains (Fig. 2).
2. The study material for Paper IV was collected from the Kuressaare (K-3) drill core, Saaremaa Island (Estonia), where the Kinnekulle Bentonite marking the boundary of the Haljala and Keila stages is 40 cm thick and BII in the middle of the Pirgu Stage is 30 cm thick. Host rocks of the Kinnekulle Bentonite are limestones and of the BII Bentonite argillaceous marlstones. Based on the facies framework of the Baltic Palaeobasin, the Ordovician sedimentary section of the Kuressaare (K-3) drill core belongs to the transition zone between proximal shallow and deeper shelf-sea areas (Põlma, 1967). During sampling, both bentonites were divided into eight equal parts, BII samples being 3.75 cm and Kinnekulle samples 5 cm thick. The amount of study material was about 15–20 g per sample. Host rock samples were taken for comparison at 5 cm and 30 cm below, 5 cm and 15 cm above the Kinnekulle Bentonite, and 3 cm, 10 cm and 20 cm below and above the BII Bentonite layer.
3. For Paper III, 76 geochemical samples from the c. 12 m thick Sandbian part of the Billegrav-2 drill core (Bornholm, Denmark) were collected (Schovsbo et al. 2011). The Sandbian strata lie unconformably on the thin Komstad Limestone (basal Dapingian) and are, in turn, overlain by grey and black shales of the Katian Age; these strata are assigned to the Dicellograptus Shale. A conspicuous feature of the Sandbian Section is that c. 50% of the section is formed by volcanogenic sediment altered into clay, i.e. bentonite. The other half of the section is formed by grey, often silicified shale. In addition, the bentonites contain much chert. The section includes two thick (80 and 90 cm) bentonite layers and thick intervals, where bentonite material predominates, separated only by thin terrigenous mudstone interbeds. The aim of the Paper III was to demonstrate the possibilities and problems of geochemical identification of individual volcanic eruption layers and to identify the Kinnekulle Bentonite in the Billegrav-2 drill core section on Bornholm.

4. The majority of samples in Paper II were taken from the Laeva-13 drill core. The samples cover the upper part of the Middle–Ordovician (from the Volkhov Stage) to Silurian (Juuru Stage). The samples from host rocks were used for comparison with bentonites.

   Figs. 2 and 3 show the lithology, stratigraphy and location of samples.

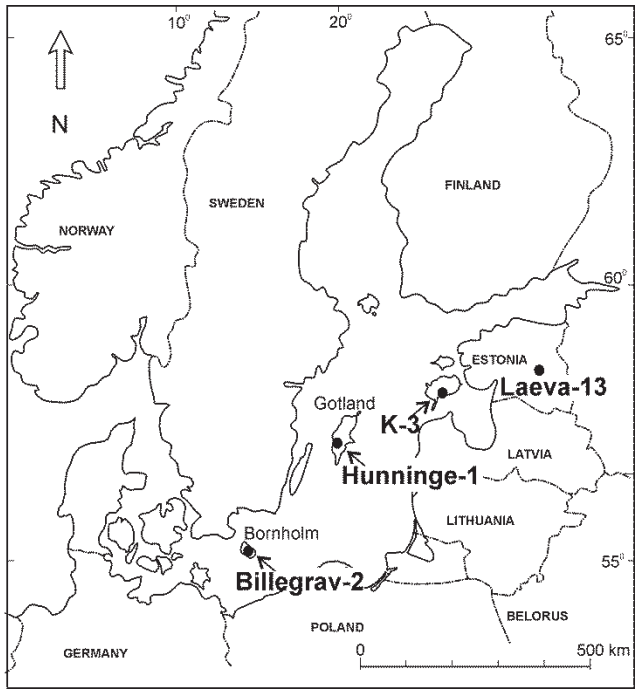

Fig. 2. Location of the studied drill core sections.

2. METHODS

Major chemical components and trace elements were determined by the XRF method using a Bruker S4 Pioneer spectrometer. The X-ray tube with Rh-anode and the maximum working power of 3 kW was used. Eight grams of fine powder (grains not larger than 50 μm) of samples was mixed with eight drops of 5% Mowiol solution in distilled water, and pressed. The pellets were dried for 2 hours at 105° C. The samples were then measured and preliminary results calculated by using the manufacturer`s standard methods MultiRes and GeoQuant. More than ten international and in-house reference materials were used to refine the analytical results.

Grain material for x-ray diffractometry (XRD) and microanalyses (EDXRF) was separated, using the following procedure: about two grams of bentonite samples were dispersed ultrasonically during two minutes in 50 ml of 0.1% Na-pyrophosphate solution. The remaining Na-pyrophosphate suspension was slowly poured away. The pouring process was done carefully so as not to lose the separated grains. The procedure was repeated. Next, 25ml of 1:4 HCl solution was added to the separated grain material for dissolving carbonate minerals, and the matter was treated with ultrasound until the acid solution became warm and started to evaporate slightly; the process took about 3 minutes. According to our experience, this procedure extracts most grains larger than 0.04 mm from the bentonite sample.

XRD measurements of bulk sample and grain fraction were performed on a D-8 Advance instrument from Bruker AXS, using Fe-filtered Co radiation. TOPAS and EVA software and Microsoft Excel were used to analyse the measured diffraction patterns. As an exception, XRD measurements for Paper I were performed by HZG-4 diffractometer (Freiberger Präzisionmechanik, 1985).

Microanalyses of grains were done using an energy-dispersive X-ray instrument, connected to scanning electron microscope, under low vacuum (30 Pa) conditions. The electron beam was generated at 20 kV and 650 pA. The basaltic glass BBM-1G, distributed by the International Association of Geoanalysts, was measured together with the studied grains and used as a reference. On the basis of these measurements, Al, Si and Fe concentrations were corrected linearly by a few percent of the concentration. According to repetitive measurements by BBM-1G, the precision of measurements was better than 0.4%.

Grain size analyses were made by the laser scattering particle size distribution analyser LA-950V2 of Horiba Ltd (Japan).

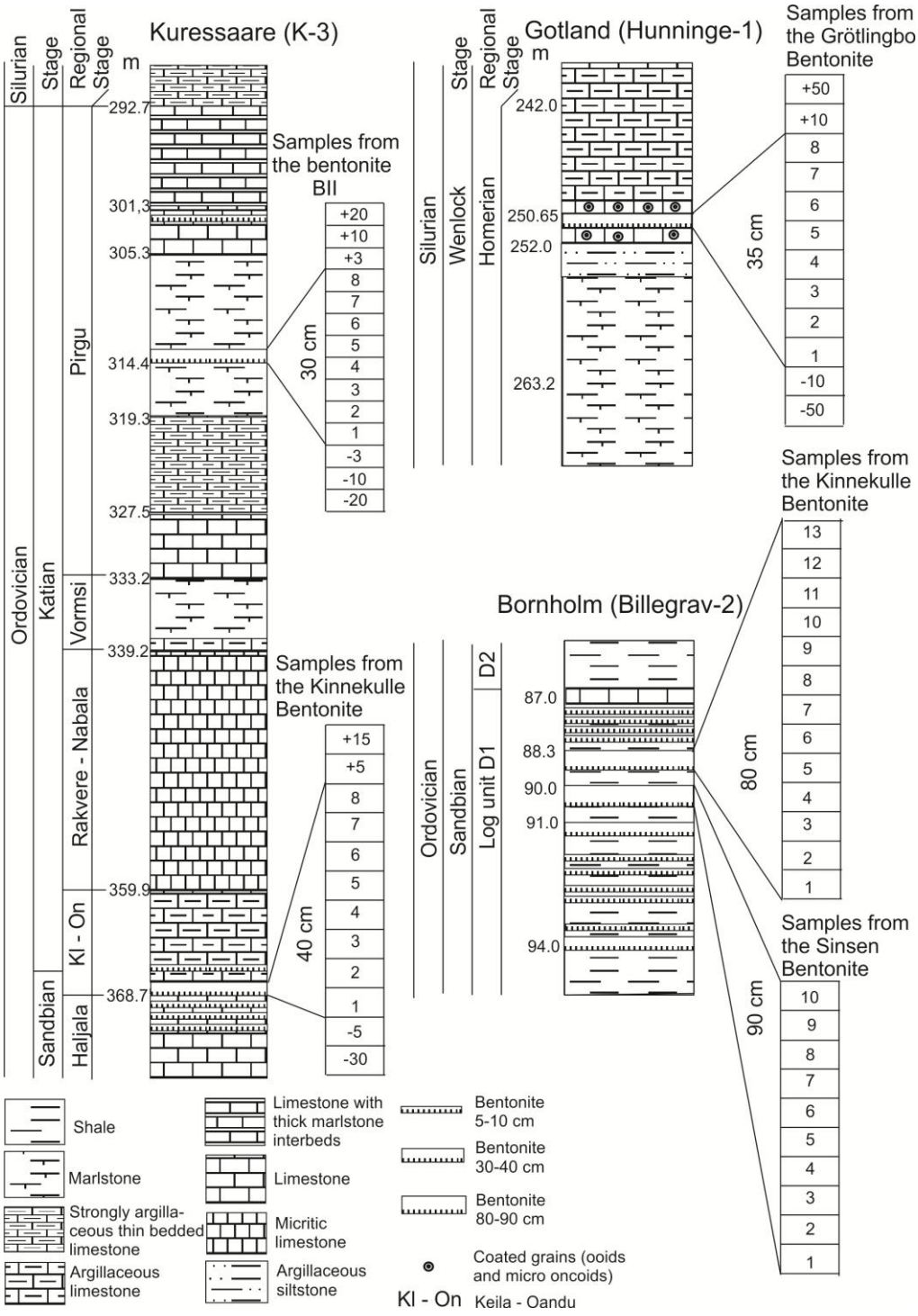

Fig. 3. Stratigraphic position of the studied bentonites.

3. RESULTS

3.1 X-ray diffractometry (XRD)

Among the Grötlingbo Bentonite samples, a broad reflection at 11.2–11.5Å indicated illite–smectite as the main mineral component in all the samples (Fig.4).

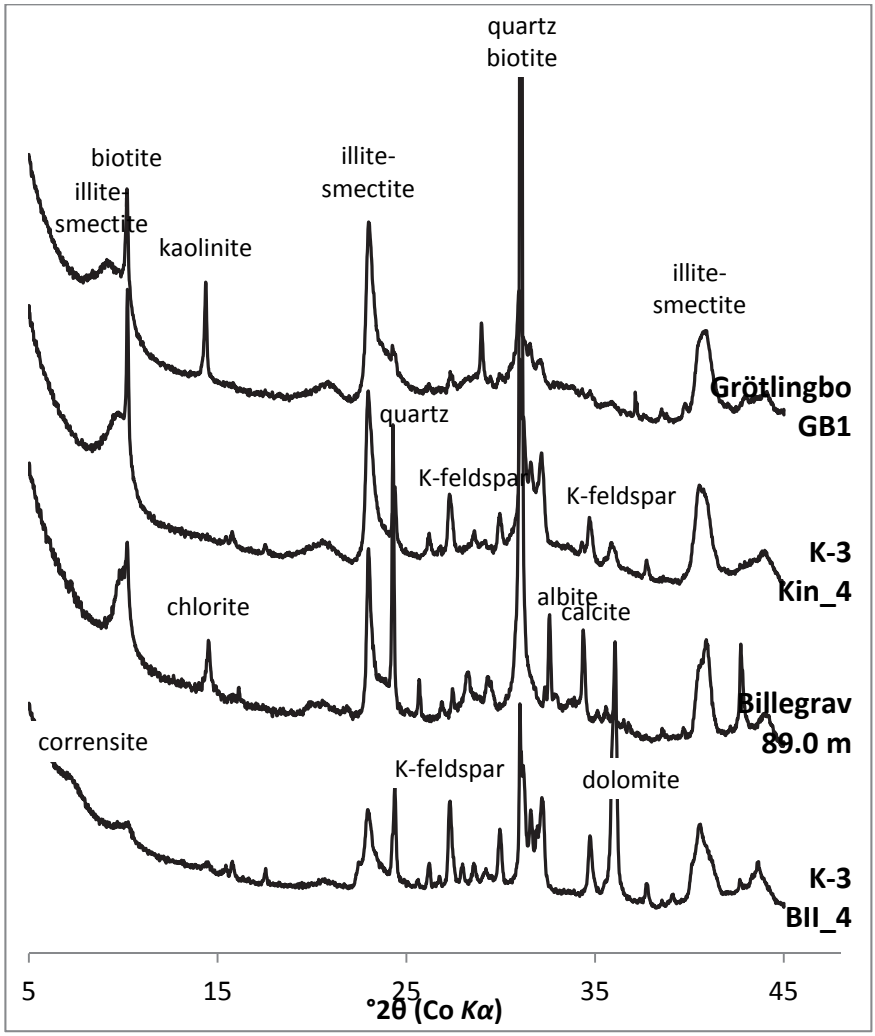

Fig. 4. XRD patterns of the original/untreated samples from the Grötlingbo, Kinnekulle-K3, Kinnekulle-Blg2 and BII bentonites. The BII Bentonite revealed stronger reflections of corrensite and dolomite; the Kinnekulle Bentonite in the middle samples—biotite, quartz and calcite; the Grötlingbo Bentonite—quartz, biotite, kaolinite and much less intensive dolomite.

Kaolinite and biotite reflections were the strongest in the lowermost sample (GB1) and decreased upwards. Samples GB3–GB6, in the middle of the bentonite bed, were characterised by weak kaolinite and biotite reflections. Biotite was almost absent in the two uppermost samples (GB7 and GB8), but the kaolinite reappeared in the uppermost sample (GB8). Starting from sample GB4, a small portion of quartz appeared, increasing upwards. From sample GB5 upwards, minor portions of dolomite were detected. The uppermost sample (GB8) contained some calcite.

Three out of four host rock samples of the Grötlingbo Bentonite revealed calcite and quartz reflections with much less intensive dolomite. Only at the depth of 250 cm below, at the base of the bentonite, dolomite reflection was almost as strong as that of calcite, suggesting the presence of a significant portion of the mineral.

Main minerals detected throughout the Pirgu (BII) Bentonite layer were illite-smectite, chlorite-smectite and K-feldspar, plus quartz and dolomite (Fig.4). From those minerals, chlorite-smectite (corrensite) is only known from bentonites of the Pirgu Stage in Estonia (Hints et al. 2006, Kiipli et al. 2015). Lower samples of the BII Bentonite with their minor amounts of calcite and pyrite were mineralogically quite similar to sample 1. Starting from sample 3, small portions of quartz and dolomite appeared, and the amount of these phases consistently increased towards the upper boundary of the bentonite layer. In the upper part of the bentonite (samples 7 and 8), traces of calcite were observed again. The content of illitic layers in the illite-smectite of bentonites of the Pirgu Stage in the East Baltic has been previously reported to vary between 71 and 74% (Hints et al. 2006).
Lower host rock of the BII Bentonite was mostly composed of calcite and dolomite, with smaller amounts of quartz, illite, K-feldspar, chlorite and traces of pyrite. The host rock just above the bentonite was composed mainly of calcite, but there were also traces of K-feldspar, quartz and dolomite. Ten centimetres above the bentonite, the dolomitization and quartz component increased; however, this sample was still highly calcitic. The trend continued up to 20 cm above the bentonite layer, whereafter the rock composition gradually became similar to the rock below the bentonite. In the transition zone, similarly to bentonites, the clay fraction of the host rocks of the Pirgu Stage also contained abundant chlorite-smectite (Paper II).

The mineral composition of the Kinnekulle Bentonite has been previously studied in the Pääsküla exposure, northern Estonia (Hints et al. 1997), where mineral assemblage of the bentonite was reported to be composed of

potassium feldspar and illite-smectite. The same minerals in the Kinnekulle Bentonite occur over the entire northern and central region of Estonia (Kiipli et al. 2007) and the content of illitic layers in illite-smectite in the East Baltic area varies between 71 and 87%.
In the Kinnekulle Bentonite from the K-3 drill core, illite-smectite occurs as the predominant mineral phase with its highest concentrations in the middle of the bentonite layer. K-feldspar content is lower than in North-Estonian settings, but similarly to those sections, the content reaches its maximum at the upper and lower boundaries of the layer (samples 1, 2 and 8).

Bentonites in the Billegrav-2 section were predominantly formed of highly illitic illite-smectite with broad XRD reflection at 10.4 Å. Differently from the East Baltic and Gotland, bentonites contained chlorite and albite as important minor minerals. Frequently, the abundant finely disperged authigenic quartz formed a significant portion of bentonites and host rock. Bentonites and host rocks in the Billegrav-2 contained plenty of thin Mn-rich calcite veins, indicated by the shift in the 104 calcite XRD reflection.

3.2 Phenocrysts

Among the studied 113 grains of magmatic phenocrysts in the Grötlingbo Bentonite, 42% were biotites and 42% kaolinised feldspars. Minor phenocrysts were quartz (5%), Ti-oxides (4%), zircon (4%) and apatite (3%). Biotite in the Grötlingbo Bentonite was rich in Mg. The Kinnekulle Bentonite contained iron-rich biotites. In BII, biotite was absent. In the Grötlingbo Bentonite, biotite was kaolinised, especially in lower and upper samples. Content of biotite in both the Grötlingbo and Kinnekulle bentonites decreased upwards, but its composition was stable throughout the section. In bentonites from the Billegrav-2 section, biotites were strongly chloritized, as evidenced by the expansion of biotite flakes observed under the microscope and the chlorite peak on bulk XRD patterns.
According to XRD analysis, K-Na-Ca sanidine composition was constant throughout bentonite sections, averaging at 25.2±0.6 mol% of $(Na,Ca)AlSi_3O_8$ in the Kinnekulle Bentonite, 43.8±0.4 mol% in the BII bed and 18 mol% in the Grötlingbo Bentonite. As previous studies in our laboratory have shown, sanidine phenocrysts are absent in bentonites from Bornholm exposures (Toivo Kallaste, personal communication), which is why they were not studied in the Billegrav-2 section.

3.3 Sedigraph

Grain size of bentonite was analysed in Paper I and silicate matter of carbonate rocks in Paper II. Both results showed a bimodal distribution of grain size (Fig. 5). Most frequent clay particles in bentonites were 0.12 µm and in carbonate clays 0.28 µm in diameter. Smaller-frequency peaks in bentonites also occurred at 0.28 µm. Silty material in bentonites had predominantly smaller grain size than in carbonate rocks with peaks at 3.9 and 5.5 µm, correspondingly. In contrast, concentration of larger grains of over 30 µm was higher in bentonite. In the Grötlingbo Bentonite, the grain size in samples GB1 to GB5 decreased upwards. The content of grains larger than 40 µm decreased upwards throughout the bentonite layer. In carbonate rocks of the Laeva Section, silicate material was formed mostly of clay and silt, only in Oandu, Pirgu and Porkuni stages some sandy material occurred. The concentration of clay particles in the silicate material of carbonate rocks varied between 22 and 77 % (Fig. 5).

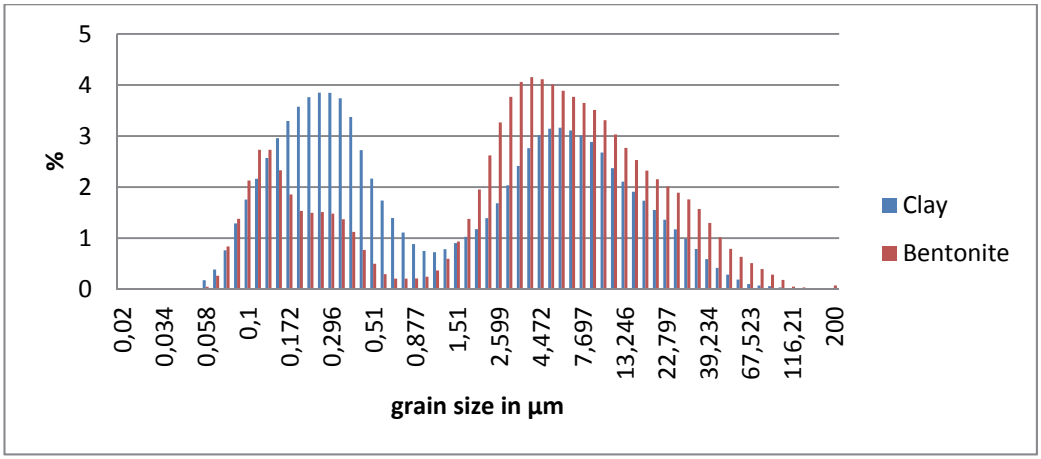

Fig. 5. Comparison of average grain size in bentonites and silicate part of carbonate rocks.

3.4 X-ray fluorescence (XRF)

In Fig. 6, bentonite compositions were compared with compositions of clay from carbonate rocks. Ti- and Al-graphs showed a clear discrepancy between clay and bentonite samples. Titanium content in bentonite samples never exceeded 0.6%, but in clay samples its concentration began at 0.6% and increased, giving a positive correlation with Al. Besides titanium, the most effective elements in discriminating bentonites from host rocks were Fe, Cr,

Ni, Cu and V. The amounts of the elements in bentonites were significantly lower than in the silicate part of the host rock. Titanium as an immobile element should have remained constant throughout the bentonite layer. In reality, its concentration increased in the upper part of the Kinnekulle-K3 Bentonite, which could be explained by a calcareous terrigenous admixture. Because of the process, CaO and Cr values also grew (Paper IV). The elements indicated a terrigenous admixture in bentonites. In the Grötlingbo Bentonite and BII bentonites, a rise in the concentration of the elements was observed (Fig. 7). The admixture of calcareous terrigenous material in the BII Bentonite started already in the middle of the bentonite layer, together with a noticeable rise in titanium content. The bottommost samples of the Grötlingbo Bentonite had 1.5–2 times less titanium than the rest, and the chromium content was the lowest in the first three samples, which implies that the lowermost part of the bentonite in its composition was the closest to that of the inital magma. The Kinnekulle Bentonite revealed homogenous concentration of the elements; terrigenous admixture could be noticed only in the uppermost sample. For discrimination of particular bentonite layers, immobile elements Zr, Nb, Th and Ti are useful. The BII Bentonite was remarkably different from others because of its high content of MgO (between 9 and 13%), in the Kinnekulle and Grötlingbo bentonites, MgO ranges only between 4–5%.

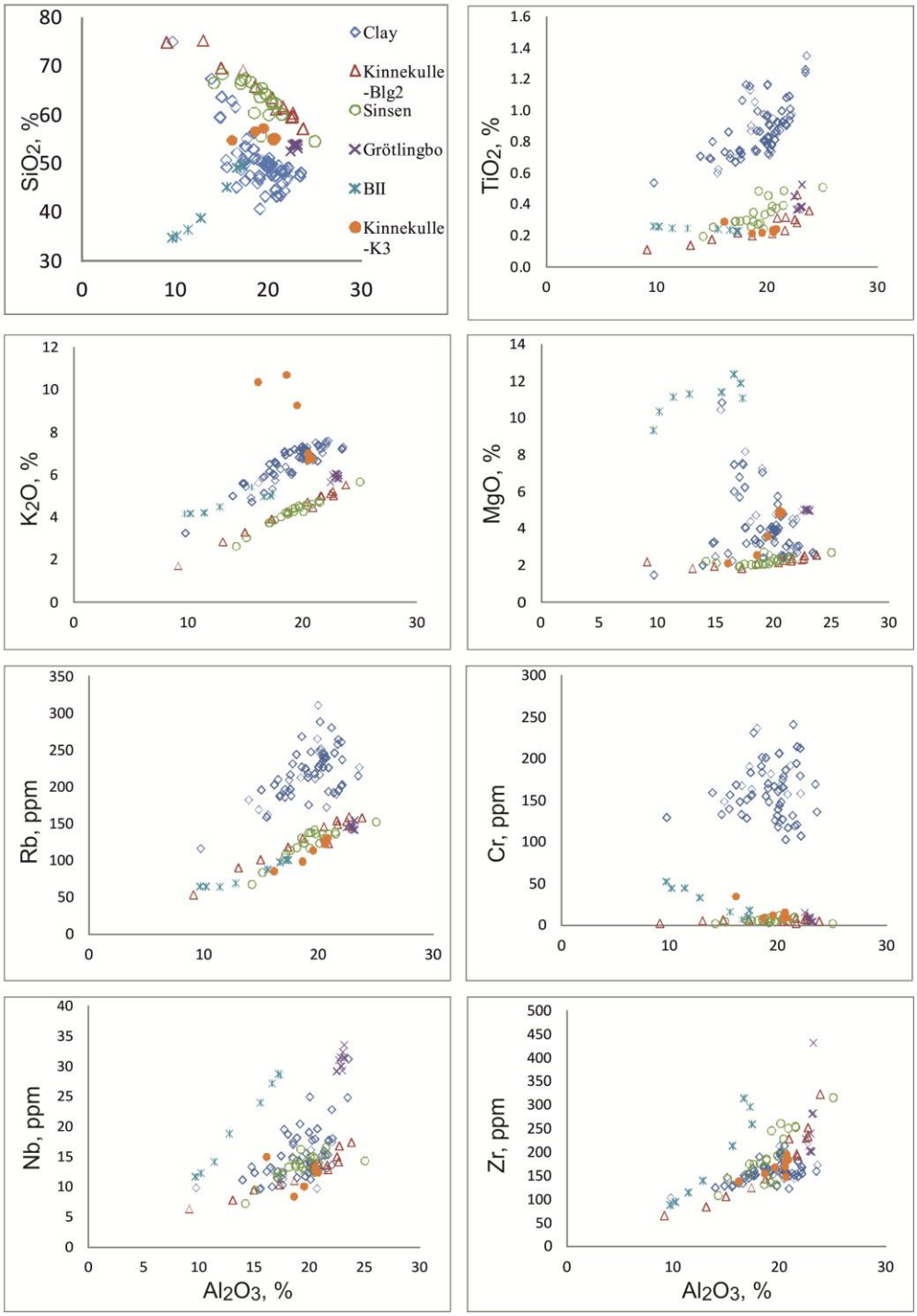

Fig. 6. Comparison of element concentrations in bentonites and in clays of carbonate rocks. X-axis represents Al_2O_3 content in all graphs.

Element concentrations throughout the thick bentonite layers varied significantly (Fig. 7). For example, the content of the most important major component, SiO_2, varied from 35% in the upper part of the BII Bentonite to more than 70% in the upper part of the Kinnekulle Bentonite. The amounts of other major and trace elements differed as well (see Discussion).

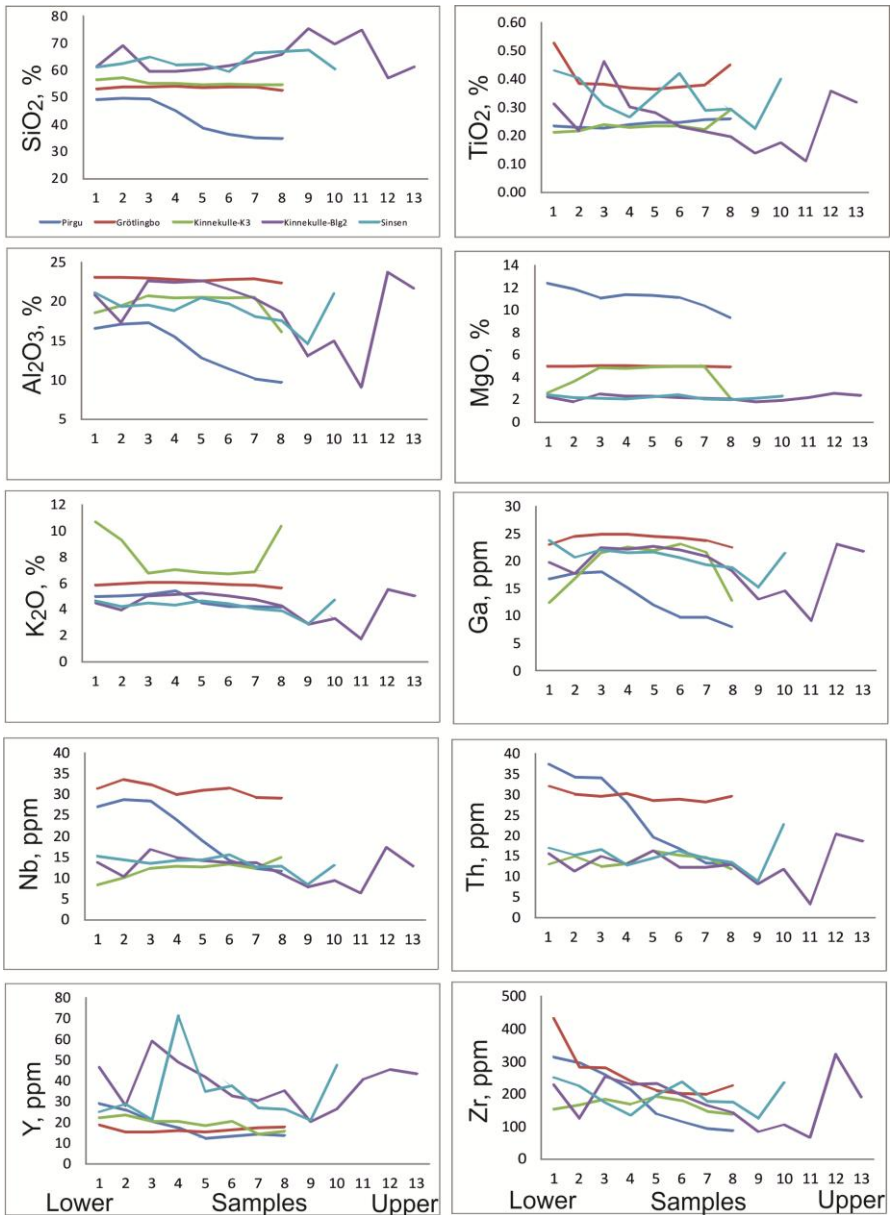

Fig. 7. Geochemical profiles through thick bentonite layers. X-axis represents samples in bentonite beds (No 1 designates the bottommost sample).

4. DISCUSSION

4.1 Comparison of bentonites and clays from carbonate rock sections

Depending on diagenetic conditions, major components—SiO_2, K_2O and MgO—can discriminate bentonite from clay in a particular case, but not in general (Fig. 6). The same is true for immobile trace elements Nb and Zr. The most universal discriminators are usually Cr and TiO_2, due to the evolved nature of most source magmas of bentonites that determine the predominating low concentrations of these elements. In contrast, terrigenous clays are generated from the average material of all rocks in the weathering areas, characterized by remarkably higher content of Cr and TiO_2. Rb concentrations also help discriminate bentonites from clays quite well, but the reason for it is less clear. All bentonites show a good correlation in Rb and Al_2O_3 contents, while clays show the highest Rb and Al_2O_3 concentrations. In general, Rb concentrations are relatively high in evolved magmatic rocks and lower in the average rock material (Turekian and Wedepohl 1961). This, however, is in contradiction with our observations. Evidently, Rb concentrations are not determined by the source material, but by the environmental conditions of clay formation and diagenesis.

Hydrodynamics, which has removed the finest matter from terrigenous clay materials to more distal areas, is lacking in bentonites and could have caused the relative abundance of extremely fine-grained clay material in bentonites. Comparable shift in size of fine silt in the clastic material could have been caused by similar reasons and account for the presence of authigenic silicate component in bentonites. Frequent occurrence of fine sand-size material in bentonites is caused by the pyroclastic component. Clay in terrigenous material is composed of illite and minor chlorite (Paper II), rarely of corrensite. In silt fractions, quartz, muscovite, orthoclase, microcline and albite predominate (Kiipli et al. 2008a). The mineralogical nature of different grain fractions in bentonites needs to be investigated further.

4.2 Diagenetic alteration

While in evolved source magmas SiO_2 contents are high (e.g., between 60 and 80%), in bentonites the concentrations are typically significantly lower (e.g., between 40 and 60%), indicating dissolution and removal of silica during transformation of volcanic ash into authigenic minerals. For the Kinnekulle Bentonite, the source magma composition has been determined from glass inclusions in quartz phenocrysts (Huff et al. 1996). These analyses showed

approximately 78% of SiO_2 and 13% of Al_2O_3. In K-3, SiO_2 contents are much lower—around 55%. Accumulation of authigenic chert below (less frequently above) thick ash beds (Grim and Güven 1978) could indicate export of SiO_2 from the ash beds. In our case, unusually high SiO_2 contents reaching 80% (Fig. 7) in the silicate part of the host rock, below the Kinnekulle Bentonite, most likely point to silica leaching from the bentonite (Paper IV). The absence of elevated SiO_2 contents above the BII Bentonite suggests that either (1) early release of silica was mostly completed before the deposition of layers above, or (2) the system was opened enough to support effective migration of dissolved silica. In accordance with this discussion, thick Kinnekulle and Sinsen bentonites in the Billegrav-2 core have significantly elevated contents of SiO_2. Thick volcanic ash deposits clearly retarded the removal of silica, which was accumulated as authigenic chert in bentonites and host sediments.

Among other major components, Na_2O, so common in source magmas, has almost completely been dissolved and removed; only small amounts of it have preserved within sanidine phenocrysts in all bentonites.
The rest of the less soluble residual material has been altered into clay minerals and authigenic potassium feldspar. During authigenic mineral formation, the ash could also have assimilated some elements from the surrounding environment, whereas the set of assimilated elements could be different, depending on the environment. Most remarkable is the incorporation of Mg during the alteration process of primary ash of the BII Bentonite. Mg is low in the evolved source magmas (for example, 0.07% in source magma of the Kinnekulle ash, Huff et al. 1996), i.e., the observed 11–12% of MgO in the BII Bentonite and 5% in the Kinnekulle Bentonite should be predominantly of authigenic origin. Hints et al. (2006) explained the formation of high-Mg chlorite-smectite-rich bentonites under the influence of saline evaporitic waters from sabkhas of the Pirgu Age. Although hypersaline sediments of the Pirgu Age are unknown in Estonia, sedimentary diagenetic dolomites occur in directly younger Hirnantian sediments. So it is possible that the initially lagoonal environments existed also at the Pirgu Age and the primary sediments have been eroded later. Outflow of lagoonal waters along the sea-bottom to the open sea of the transition zone can explain the partial dolomitization of host rocks of the Pirgu Age and account for the occurrence of chlorite-smectite in host rocks (Paper II). Fortey and Cocks (2005), who showed, based on the movement of tropical fauna to lower latitudes, a global warming in Katian, support higher temperature at the Pirgu time, possibly favouring development of evaporitic settings. In contrast, limestones around the Kinnekulle Bentonite are believed to have deposited in cold water conditions, since at the time the Baltica plate was located in intermediate

latitudes of the southern hemisphere (Torsvik & Rehnström 2003). Deposited under normal marine conditions, the ash of Kinnekulle Bentonite was mostly converted to illite-smectite during alteration, the illitization process has likely been controlled by external K-flux (Somelar et al. 2010).

Similarly to illite-smectite, the formation of authigenic K-feldspar in bentonites needs an external source of K. High potassium contents reaching 10% at the margins of the Kinnekulle Bentonite could not have been supplied by volcanic ash, whose initial K_2O content was only 4% (Huff et al. 1996). In other sections, K_2O contents can exceed 15% (Kiipli et al. 2007). A number of hypotheses have been put forward to explain the formation of K-feldspar and the incorporation of additional potassium into bentonites. Kiipli et al. (2007) proposed that high pH in shallow-sea environments enables incorporation of cations from seawater, favouring the formation of feldspars instead of clay minerals. Hints et al. (2008b) suggested that authigenic feldspar in Estonian bentonites might be product of recrystallization of early diagenetic metastable zeolites, formed due to interaction of ash and the juxtaposed highly alkaline calcareous muds. Somelar et al. (2010) concluded that regional saline fluids flowing into sedimentary rocks significantly after the deposition time caused a significant influx of potassium controlling illitization of smectite in the Early Silurian bentonites.

However, late diagenetic formation of K-feldspar (or its precursor phase) in bentonites is somewhat problematic, since in the studied sections, bentonites of different composition alternate closely. For example, in the Kuressaare drill core, bentonite at 368.7 m is composed of illite-smectite with K-feldspar addition at its margins, at 314.4 m—chlorite-smectite with illite-smectite (present study), at 215.7 m—7 cm of pure K-feldspar, at 214 m to 158 m—16 thin bentonite layers consisting of illite-smectite, including a K-feldspar layer at 184.8 m (Kallaste et al. 2006, Kiipli et al. 2006). At Põõsaspea exposure (North-West Estonia), in the upper part of the Kinnekulle Bentonite, Hints et al. (2008a) found a layer of sedimentary breccia, where angular grains consist of pure K-feldspar while the fine-grained mass of breccia contains terrigenous clay and carbonates. This lithology indicates that the hardened layer in the upper part of the bentonite had already formed before a storm event brecciated it, strongly supporting the early start of recrystallization of primary ash.

Considering Al_2O_3 (13% in source magma and 20% in bentonite) immobile during the conversion of volcanic ash into clay and feldspar, it is evident that, compared with source magma, concentrations of immobile elements in the Kinnekulle Bentonite have increased by factor of 1.5. According to our previous analyses on the East Baltic materials, Ti, Zr, Th and Nb have been considered immobile (Kiipli et al. 2008d, 2013). The present data from the BII Bentonite, where maximum Nb content directly below the bentonite exceeds significantly the common values in silicate parts of the host rock, indicate

small-scale mobility of this element during the conversion of volcanic ash (Paper IV). Although small-scale mobility to the distance of a few centimetres does not exclude the use of Nb in source magma interpretation, researchers should still be wary when using this element in particular cases. In the samples of the Kinnekulle Bentonite, for example, the ratio of Nb/Y, commonly used for discriminating magma series (Winchester & Floyd 1977) was found to vary from 0.4 to 0.9. This considerable variation depends largely on the irregular distribution of Y, the content of which in beds was likely controlled by combined factors, such as input of pyroclastic apatite and leaching of the element near the upper contact of the ash bed.

4.3 Multiple- versus single-eruption hypothesis for determining the source of bentonite-forming material

To explain the origin of some of the major Early Palaeozoic bentonites, the multiple-eruption hypothesis has been put forward (Huff et al. 2010). Nevertheless, in all the studied bentonites, the composition of primary magmatic phenocrysts was found to be stable in their vertical sections, as evidenced by the high-precision XRD data on volcanic sanidine. Furthermore, good correspondence between XRD and EDXRF data exists in sanidine's compositional data. Also Mg/(Mg+Fe) atom ratio in biotite in the Kinnekulle Bentonite was found to be stable. The observed stability of composition of primary phenocrysts proves that most likely, the original magmatic material for all the studied bentonites originates from a single source.

On the other hand, notable grain size difference of pyroclastic minerals was documented across the section of the Kinnekulle Bentonite. As a rule, larger grain material from volcanic ash clouds falls first and, consequently, the lower part of the bentonite should contain larger grains than the upper part. However, while grain size in the Grötlingbo and BII bentonites perfectly follows this rule, in the Kinnekulle Bentonite, the maximum primary grain size was found only in the second and third sample from below. This could be indicative of a relatively long duration of the Kinnekulle eruption. Deposition of larger grains in the middle of the eruption could be caused by a temporary rise in the power of the eruption, or by a change in the wind direction. The BII Bentonite, whose pyroclastic grain distribution shows no obvious signatures of primary volcanogenic or air-transport-induced heterogeneity, probably originated from the eruption of a shorter duration. The recorded immobile trace element distribution patterns in the studied sections do not contradict the concept of bentonites originating from a single eruption. However, variations in the content of some minor elements (e.g., Zr, Rb, P_2O_5) in the Kinnekulle

bed could reflect notable variations in the input of pyroclastic minerals during sedimentation.

4.4 Role of mixing of material during transport and emplacement

In the Grötlingbo and Pirgu (BII) bentonites, Zr content is the highest in samples from lower layers, decreasing upwards. The trend cannot be explained by redeposition; it rather points to the fractionation of the material during air-transport. It is likely that phenocrysts (e.g., zircon) that are heavier and larger than vitric particles deposited faster and accumulated in the lower part of the ash bed. In case of the Kinnekulle and Sinsen bentonites, the heterogeneity of the primary ash layer is signalled by somewhat irregular distribution of Zr across the section, with its highest concentrations in the middle of the section.
Ash deposition in shallow-water marine settings could have been accompanied by considerable redeposition and mixing of primary ash with regular marine sediments. In the Kinnekulle Bentonite, terrigenous and calcareous admixture is noticeable only in the uppermost sample, as evidenced by the slightly elevated values of CaO and Cr.
In case of the BII Bentonite, however, the data suggest that the upper part of the bentonite layer was likely mixed with marine calcareous mud and terrigenous material. Based on the absence of carbonate material and low contents of Ti, Cr and V, the lower 3–4 samples represent pure bentonite. Beginning with sample 4, the admixture of terrigenous and carbonate sedimentary material increases upwards, as can be seen from the growing contents of dolomite in bulk samples (Fig.4) and rise in Ti, Cr and V concentrations. Thus, geochemical trends indicate that the full section of the primary ash layer of the BII Bentonite was formed in combination of two physical processes: (1) direct fall-out of the ash from the atmosphere; (2) reworking and re-deposition of the ash during transport from shallow to deeper marine environments.
Similarly to the BII Bentonite, the upper part of the Grötlingbo Bentonite is also redeposited and contains much terrigenous and carbonate material. Heavy zircon crystals accumulated in the lower part of the Grötlingbo Bentonite, expressing higher Zr concentrations (Fig. 7).

4.5 Environmental effects of ashfalls and interaction of the ash–water–sediment system

Some previous works have reported a remarkable decrease in diversity of marine life after the deposition of the thick Kinnekulle Bentonite (Hints et al.

2003, Vincent et al. 2012), and interpreted those variations as consequences of environmental perturbations caused by volcanic eruptions. The geochemical signatures recorded in bentonites and their host rocks during the current study demonstrate that both large ashfalls, but more notably that of the Kinnekulle ashfall, triggered environmental changes in marine settings where they deposited. The direct effect of the ashfall can be read from the peaks of sulphur below and above the Kinnekulle Bentonite. Sulphur fixation in sediments occurs when decay of organic material proceeds in an anoxic environment via microbial sulphate reduction. In the lower contact of primary ash layer, life forms on the sea-bottom likely died after being abruptly buried under the ash layer, which initially could have been as much as a metre thick, thus promoting development of anoxia below beds. Additionally, water-soluble ash leachates could have provided an extra source of sulphate for sulphate reduction near the freshly deposited ash layer. It is also possible that ashfall was accompanied by toxification of the water column, which, in turn, caused mass mortality. Dead organic matter, due to its better flotation properties, could have deposited to the seafloor slower than volcanic dust. Consequently, it could have accumulated in the upper layers of the ash bed, thus explaining sulphur accumulation in the upper layer of the bentonite. Alternatively, ashfall could have triggered the increase of primary production through fertilizing the water column with essential macro- and micronutrients (e.g., Duggen et al. 2010). The resultant rise in the flux of organic matter to the shallow sea-bottom could have promoted quick consumption of free oxygen and sulphate reduction.

The absence of sulphur peaks at the margins of the BII Bentonite could have been caused by shorter duration of the eruption and a smaller amount of ash reaching the sedimentation area. Violet patches in the host rock are also indicative of an environment with better oxygenated sediments and probably with lower bioproductivity during the deposition of the BII. Lower sulphur values in the bentonite of the Pirgu Stage could also reflect suppressed microbial sulphate reduction in a marine environment of increased salinity.

An outstanding feature in case of both studied bentonites in the Kuressaare Section is finding P and Ca peaks in the host rock directly above the bentonite. This effect is greater above the thicker Kinnekulle Bentonite and less significant above the thinner BII bentonite. Note that in the Kinnekulle bed, just below the Ca- and P-rich host rock, the previously discussed sulphur peak occurs as well. The increased productivity after the ashfall, bottom oxygen deficit, enhanced sulphate reduction and increased alkalinity near the sediment–water interface could possibly all have favoured the precipitation of calcium carbonate from the dissolved Ca-hydrocarbonate. The enrichment of P, which is the fundamental limiting nutrient for marine life (Filippelli 2002, Kiipli et al. 2010a), is more controversial. Phosphorus is mostly remineralized

as organic matter breaks down and is deposited on to the sea-bottom, and most of it will be externally recycled in shallow marine environments. Studies of modern volcanic ashes indicate that some ashfalls might provide a considerable extra source of phosphorus for marine environments through rapid release of the element from the ash (Jones and Gislason, 2008). The recorded P_2O_5 values in the Kinnekulle and BII bentonites are rather low; however, it does not exclude the possibility that some of the phosphorus was released during the very early stages of ash transformation. Enrichment of P above the studied bentonites could have been induced either (1) by release of P during anoxic breakdown of organic matter under the increased flux of organic matter to the sea-bottom, or (2) by possible desorption of phosphorous species or leaching of phosphorus from ash particles, and fixation thereafter in the alkaline mud above the ash beds.

4.6 Discrimination of bentonites from different eruptions

Immobile and low-mobility elements, for example Al, Ti, Ga, Nb, Th, Y and Zr can be used for discriminating bentonites. X–Y graphs (Fig. 6 and 8) conclude that, in composition, the Kinnekulle and Sinsen bentonites are very similar. In all likelihood, the source of both eruptions was the same volcano. As the two bentonites are separated from one another by 20 cm of host rock, the aforementioned eruptions definitely occurred some time apart. Due to the various diagenetic changes (removal of SiO_2, Na_2O and incorporation of MgO and K_2O), the best way to use immobile elements for identification of bentonites is to apply ratios of immobile elements (Kiipli et al. 2013, Paper III). Therefore, I used immobile element/Al_2O_3 ratios to discriminate different eruptions (Fig.8).

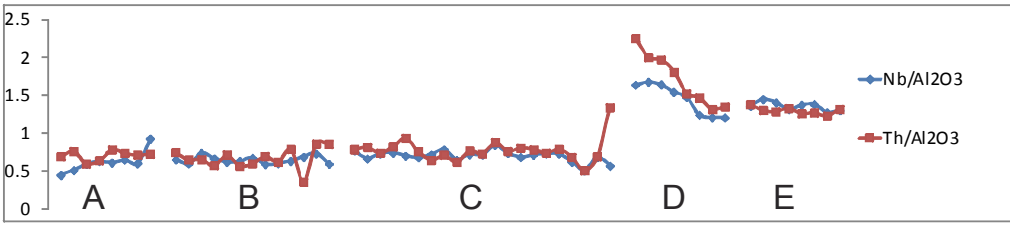

Fig. 8. Nb and Th ratios to Al_2O_3 discriminate different eruptions. A – Kinnekulle K-3, B – Kinnekulle Bgl-2, C – Sinsen, D – BII, E - Grötlingbo

Nb and Th ratios to Al_2O_3 show that the Kinnekulles and Sinsen bentonites clearly differ from the BII and Grötlingbo bentonites. The number of bentonites of the Ordovician Grefsen Series clearly differs from that of other Ordovician bentonites by their high Zr contents (Batchelor 2014a, Paper III).

Since bentonites from repetitive eruptions from the same volcanic source exhibit quite similar compositions, in addition to ratios of immobile elements, other methods such as analyses of well-preserved phenocrysts must be applied, in order to obtain reliable results.

5. CONCLUSIONS

1. Most likely, all the studied thick bentonites formed from a single volcanic eruption, as the stability of composition of phenocrysts through the entire section of the bentonite confirms. Sanidine phenocryst compositions that have been used in many previous studies for proving the correlations of volcanic ash beds, remain stable throughout the vertical section and are therefore a good discrimination criterion. Phenocrysts from the redeposited parts of bentonites can also be used for correlation. With the advanced XRD technologies, sanidine composition can be analysed quite precisely (±0.5 mol%). In the Grimstrop Bentonite (Paper III), the interval between 87.25 and 87.82 m in the Billegrav-2 core thin shale interbeds indicate that this thick bentonite formed from several volcanic eruptions.
2. The Kinnekulle Bentonite, one of the major volcanic ash beds of the Phanerozoic, has formed from an eruption of a longer duration, whose maximum extent reached as far as the East Baltic area. The pyroclastic mineral grain-size distribution and immobile trace element composition point to the layered and heterogeneous nature of the primary ash bed.
3. The Grötlingbo and BII bentonites formed from a less voluminous eruption of a shorter duration and their full thickness was accumulated from redeposition of the volcanic material in shallow-sea areas.
4. For a reliable trace-element-based correlation of thick bentonites, it is useful to conduct a bulk chemical composition study on a number of samples covering the whole section. Lower layers of the bentonites originating from direct ashfalls are of correlative value. However, the mobility of trace elements should be checked in advance.

5. The Kinnekulle, and to a lesser extent, the BII ashfall had notable effect on the chemistry of the juxtaposed marine sediments. Peak concentrations of calcium and phosphorus directly above both bentonites and the increased sulphur content near bentonite contacts prove that the ash fall triggered significant fluctuations in biotic and geochemical cycles in shallow marine settings.
6. The best geochemical discriminators of bentonites from terrigenous clays are TiO_2 and Cr.

ACKNOWLEDGEMENTS

I am very grateful to my supervisors, Dr. Tarmo Kiipli and Prof. Alvar Soesoo, and to my colleague, Dr. Toivo Kallaste, for their support and advice throughout the master's and doctoral studies. I would also like to thank my co-authors Enli Kiipli, Rutt Hints, Peter Dahlqvist, Mikael Calner, Arne T. Nielsen and Niels H. Schovsbo.
European Social Fund's Doctoral Studies and International Programme DoRa supported this research along with the Estonian Ministry of Education and Research with its target research project No. SF0140016s09.

REFERENCES

Altaner, S.P., Hower, J., Whitney, G., Aronson, J.L. 1984. Model for K-bentonite formation: Evidence from zoned K-bentonites in the disturbed belt, Montana. Geology **12**, 412–415.

Austin, W.E.N., Abbott, P.M., Davies, S., Pearce, N.J.G., Wastegard, S. 2014. Marine tephrochronology: an introduction to tracing time in the ocean. In: Austin, W.E.N., Abbott, P.M., Davies, S., Pearce, N.J.G., Wastegard, S. (eds) Marine Tephrochronology, *Geological Society Special Publication* **398**, 1–5.

Batchelor, R.A. 2009. Geochemical "Golden Spike" for Lower Palaeozoic metabentonites. *Earth and Environmental Science Transactions of the Royal Society of Edinburgh* **99**, 177–187.

Batchelor, R.A. 2014a. Geochemistry of Upper Ordovician metabentonites and their cognate apatite microphenocrysts from Norway and Sweden. *GFF* **136**, 387–397.

Batchelor, R.A. 2014b. Metabentonites from the Sandbian Stage (Upper Ordovician) in Scotland - a geochemical comparison with their equivalents in Baltoscandia. *Scottish Journal of Geology* **50**, 159–163.

Batchelor, R.A., Clarkson, E.N.K. 1993. Geochemistry of a Silurian metabentonite and associated apatite from the North Esk Inlier, Pentland Hills. *Scottish Journal of Geology* **29**, 123–130.

Batchelor, R.A., Evans, J. 2000. Use of strontium isotope ratios and rare earth elements in apatite microphenocrysts for characterization and correlation of Silurian metabentonites: a Scandinavian case study. *Norsk Geologisk Tidsskrift* **80**, 3–8.

Bauert, H., Isozaki, Y., Holmer, L.E., Aoki, K., Sakata, S., Hirata, T. 2014: New U–Pb zircon ages of the Sandbian (Upper Ordovician) "Big K-bentonite" in Baltoscandia (Estonia and Sweden) by LA-ICPMS. *GFF* **136**, 30–33.

Bergström, S.M., Huff, W.D., Kolata, D.R. 1998. The lower Silurian Osmundsberg K-bentonite. Part I: Stratigraphic position, distribution, and palaeogeographic significance. *Geological Magazine* **135**, 1–13.

Bergström, S.M., Huff, W.D., Kolata, D.R., Bauert, H. 1995. Nomenclature, stratigraphy, chemical fingerprinting, and areal distribution of some Middle Ordovician K-bentonites in Baltoscandia. *Geologiska Föreningens i Stockholm Förhandlingar (GFF)* **117**, 1–13.

Bergström, S.M., Huff, W.D., Kolata, D.R., Yost, D.A., Hart, C. 1997. A unique Middle Ordovician K-bentonite bed succession at Röstånga, S. Sweden. *GFF* **119**, 231–244.

Bergström, S.M., Toprak, F.Ö., Huff, W.D., Mundil, R. 2008. Implications of a new, biostratigraphically well-controlled, radio-isotopic age for the lower Telychian Stage of the Llandovery Series (Lower Silurian, Sweden). *Episodes* **31**, 309–314.

Calner, M., Kozłowska, A., Masiak, M., Schmitz, B. 2006. A shoreline to deep basin correlation chart for the middle Silurian coupled extinction-stable isotopic event. *GFF* **128**, 79–84.

Cocks, L.R.M., Fortey, R.A. 2009. Avalonia: a long-lived terrane in the Lower Palaeozoic? In: Bassett, M.G. (ed) Early Palaeozoic Peri-Gondwana Terranes: New Insights From Tectonics And Biogeography, *Geological Society Special Publication* **325**, 141–155.

Cramer, B.D., Condon, D.J., Söderlund, U. Marshall, C., Worton, G.J., Thomas, A.T., Calner, M., Ray, D.C., Perrier, V., Boomer, I., Patchett, P.J., Jeppsson, L. 2012. U-Pb (zircon) age constraints on the timing and duration of Wenlock (Silurian) paleocommunity collapse and recovery during the "Big Crisis". Geological Society of America Bulletin **124**, 1841–1857.

Cramer, B.D., Schmitz, M.D., Huff, W.D., Bergström, S.M. 2015. High-precision U–Pb zircon age constraints on the duration of rapid biogeochemical events during the Ludlow epoch (Silurian period). *Journal of the Geological Society* **172**, 157–160.

Duggen, S., Olgun, N., Croot, P., Hoffmann, L., Dietze, H., Delmelle, P., Teschner, C. 2010. The role of airborne volcanic ash for the surface ocean biogeochemical iron-cycle. *Biogeosciences* 7, 827–844.

Emerson, N.R., Simo, J.A., Byers, C.W., Fournelle, J. 2004. Correlation of (Ordovician, Mohawkian) K-bentonites in the upper Mississippi valley using apatite chemistry: implications for stratigraphic interpretation of the mixed

carbonate-siliciclastic Decorah Formation. *Palaeogeography, Palaeoclimatology, Palaeoecology* **210**, 215–233.

Filippelli, G.M. 2002. The global phosphorus cycle. In: Kohn, M., Rakovan, J., Hughes, J. (eds) Phosphates: Geochemical, Geobiological, and Materials Importance. *Mineralogy & Geochemistry* **48**, pp 391–425.

Fortey, R. A., Cocks, L. R. M. 2005. Late Ordovician global warming—The Boda event. *Geology* **33,** 405–408.

Grim, R.E. & Güven, N. 1978. Bentonites, Geology, Mineralogy, Properties and Uses. *Developments in Sedimentology* **24**, pp 256.

Hagemann, F., Spjeldnaes, N. 1955. The Middle Ordovician of the Oslo Region, Norway. 6. Notes on bentonites (K-bentonites) from the Oslo-Asker region. *Norsk Geologisk Tidsskrift* **35**, 29–52.

Hetherington, C.J., Nakrem, H.A., Potel, S. 2011. Note on the composition and mineralogy of upper Silurian bentonites from the Ringerike District: implications for local and regional stratigraphic correlation and sedimentation. *Norwegian Journal of Geology* **91**, 181–192.

Hints, L., Männik, P., Hints, O., Hints, R. 2008a. Discovery of the Ordovician Kinnekulle K-bentonite at Põõsaspea cliff, NW Estonia. *Estonian Journal of Earth Sciences* **57**, 192–196.

Hints, O., Kallaste, T., Kiipli, T. 1997. Mineralogy and micropalaeontology of the Kinnekulle altered volcanic ash bed (Ordovician) at Pääsküla, North Estonia. *Proceedings of the Estonian Academy of Sciences Geology* **46**, 107–118.

Hints, O., Hints, L., Meidla, T., Sohar, K. 2003. Biotic effects of the Ordovician Kinnekulle ash-fall recorded in northern Estonia. *Bulletin of the Geological Society of Denmark* **50**, 115–123.

Hints, R., Kirsimäe, K., Somelar, P., Kallaste, T., Kiipli, T. 2006. Chloritization of Late Ordovician K-bentonites from the northern Baltic Palaeobasin – influence from source material or diagenetic environment? *Sedimentary Geology* **191**, 55–66.

Hints, R., Kirsimäe, K., Somelar, P., Kallaste, T., Kiipli, T. 2008b. Multiphase Silurian bentonites in the Baltic Palaeobasin. *Sedimentary Geology* **209**, 69–79.

Huff, W.D. 2008. Ordovician K-bentonites: Issues in interpreting and correlating ancient tephras. *Quaternary International* **178**, 276–287.

Huff, W.D., Bergström, S.M., Kolata, D.R. 1992. Gigantic Ordovician ash fall in North America and Europe: Biological, tectonomagmatic and event stratigraphic significance. *Geology* **20**, 875–878.

Huff, W.D., Bergström, S.M., Kolata, D.R. 2000. Silurian K-bentonites of the Dnestr Basin, Podolia, Ukraine. *Journal of the Geological Society* **157**, 493–504.

Huff, W.D., Bergström, S.M., Kolata, D.R. 2010. Ordovician explosive volcanism. In: Finney, S.C., Berry, W.B.N. (eds). The Ordovician Earth System. *The Geological Society of America Special Paper* **466***,* 13–28.

Huff, W.D., Dronov, A.V., Sell, B., Kanygin A.V., Gonta, T.V. 2014. Traces of explosive volcanic eruptions in the Upper Ordovician of the Siberian Platform. *Estonian Journal of Earth Sciences* **63**, 244–250.

Huff, W.D., Kolata, D.R. 1989. Correlation of K-bentonite beds by chemical fingerprinting using multivariate statistics. In: Cross, T. A. (ed) Quantitative dynamic stratigraphy, Prentice Hall, pp 567–577.

Huff, W.D., Kolata, D.R., Bergström, S.M., Zhang, Y.S. 1996. Large-magnitude Middle Ordovician volcanic ash falls in North America and Europe: dimensions, emplacement and post emplacement characteristics. *Journal of Volcanology and Geothermal Research* **73**, 285–301.

Huff, W.D., Merriman, R.J., Morgan, D.J., Roberts, B. 1993. Distribution and tectonic setting of Ordovician K-bentonites in the United Kingdom. *Geological Magazine* **130**, 93–100.

Inanli, F.Ö., Huff, W.D., Bergström, S.M. 2009. The Lower Silurian (Llandovery) Osmundsberg K-bentonite in Baltoscandia and the British Isles: Chemical fingerprinting and regional correlation. *GFF* **131**, 269–279.

Jones, M.T., Gislason, S.R. 2008. Rapid releases of metal salts and nutrients following the deposition of volcanic ash into aqueous environments. *Geochimica Cosmochimica Acta* **72**, 3661–3680.

Kepežinskas, K., Laškovas, J., Šimkevičius, P., 1994. The Ordovician metabentonites of the Baltic region as a reflection of volcanic activity in the Iapetus paleo-ocean–Tornquist Sea. Geologija **16**, 34–42.

Kallaste, T., Kiipli, T. 2006. New correlations of Telychian (Silurian) bentonites in Estonia. *Proceedings of the Estonian Academy of Sciences, Geology* **55**, 241–251.

Kiipli, E., Kallaste, T. Kiipli, T. 2008a. Hydrodynamic control of sedimentation in the Ordovician (Arenig-Caradoc) Baltic Basin. *Lethaia* **41**, 127–137.

Kiipli, E., Kiipli, T., Kallaste, T. 2006. Identification of the O-bentonite in the deep shelf sections with implication on stratigraphy and lithofacies, East Baltic Silurian. *GFF* **128**, 255–260.

Kiipli, E., Kiipli, T., Kallaste, T., Ainsaar, L. 2010a. Distribution of phosphorus in the Middle and Upper Ordovician Baltoscandian carbonate palaeobasin. *Estonian Journal of Earth Sciences* **59**, 247–255.

Kiipli, T., Dahlquist, P., Kallaste, T., Kiipli, E., Nõlvak, J. 2015. Upper Katian (Ordovician) bentonites in the East Baltic, Scandinavia and Scotland: geochemical correlation and volcanic source interpretation. *Geological Magazine*, dx.doi.org/10.1017/S001675681400051X.

Kiipli, T., Einasto, R., Kallaste, T., Nestor, V., Perens, H., Siir, S. 2011. Geochemistry and correlation of volcanic ash beds from the Rootsiküla Stage (Wenlock-Ludlow) in the eastern Baltic. *Estonian Journal of Earth Sciences* **60**, 207–219.

Kiipli, T., Jeppsson, L., Kallaste, T., Söderlund, U. 2008b. Correlation of Silurian bentonites from Gotland and the East Baltic using sanidine phenocryst composition, and biostratigraphical consequences. *Journal of the Geological Society* **165**, 211–220.

Kiipli, T., Kallaste, T. 2006. Wenlock and uppermost Llandovery bentonites as stratigraphic markers in Estonia. Latvia and Sweden. *GFF* **128**, 139–146.

Kiipli, T., Kallaste, T., Nestor, V. 2010b. Composition and correlation of volcanic ash beds of Silurian age from the eastern Baltic. *Geological Magazine* **147**, 895–909.

Kiipli, T., Kallaste, T., Nestor, V. 2012a. Correlation of upper Llandovery – lower Wenlock bentonites in the När (Gotland, Sweden) and Ventspils D3 (Latvia) drill cores: role of volcanic ash clouds and shelf sea currents in determining bentonite areal distribution. *Estonian Journal of Earth Sciences* **61**, 295–306.

Kiipli, T., Kallaste, T., Kiipli, E., Radzevicius, S. 2013. Correlation of Silurian bentonites based on the immobile elements in the East Baltic and Scandinavia. *GFF* **135**, 152–161.

Kiipli, T., Kallaste, T., Nestor, V., Loydell, D.K. 2010c. Integrated Telychian (Silurian) K-bentonite chemostratigraphy and biostratigraphy in Estonia and Latvia. *Lethaia* **43**, 32–44.

Kiipli, T., Kiipli, E., Kallaste, T., Hints, R., Somelar, P. & Kirsimäe, K. 2007. Altered volcanic ash as an indicator of marine environment, reflecting pH and sedimentation rate – example from the Ordovician Kinnekulle bed of Baltoscandia. *Clays and Clay Minerals* **55**, 177–188.

Kiipli, T., Orlova, K., Kiipli, E., Kallaste, T. 2008c. Use of immobile trace elements for the correlation of Telychian bentonites on Saaremaa Island, Estonia, and mapping of volcanic ash clouds. *Estonian Journal of Earth Sciences* **57**, 39–52.

Kiipli, T., Radzevičius, S., Kallaste, T. 2014a. Silurian bentonites in Lithuania: correlations based on sanidine phenocryst composition and graptolite biozonation - interpretation of volcanic source regions. *Estonian Journal of Earth Sciences* **63**, 18–29.

Kiipli, T., Radzevicius, S., Kallaste, T., Kiipli, E., Siir, S., Soesoo, A., Voolma, M. 2012b. The Geniai Tuff in the southern East Baltic area – a new correlation tool near the Aeronian/Telychian stage boundary, Llandovery, Silurian. *Bulletin of Geosciences* **87**, 695–704.

Kiipli, T., Soesoo, A., Kallaste, T. 2014b. Geochemical evolution of Caledonian volcanism recorded in the sedimentary rocks of the eastern Baltic region. In: Corfu, F., Gasser, D. & Chew, D.M. (eds) New Perspectives on the

Caledonides of Scandinavia and Related Areas, *Geological Society of London Special Publications* **390**, 177–192.

Kiipli, T., Soesoo, A., Kallaste, T., Kiipli, E. 2008d. Geochemistry of Telychian (Silurian) K-bentonites in Estonia and Latvia. *Journal of Volcanology and Geothermal Research* **171**, 45 - 58.

Kolata, D.R., Frost, J.K. 1987. Chemical correlation of K-bentonite beds in the Middle Ordovician Decorah Subgroup, upper Mississippi Valley. *Geology* **15**, 208–211.

Potts, P.J. 2003. Handbook of Rock Analysis. Viridian Publishing, Woking, Surrey UK, 622 pp.

Põlma, L. 1967. On the transitional area between the northern and axial lithofacies zones of the East Baltic Ordovician. *Proceedings of the Estonian Academy of Sciences - Chemistry Geology,* **16**, 272–275 (in Russian).

Raukas, A., Teedumäe, A. 1997. Geology and mineral resources of Estonia. *Estonian Academy Publishers*, Tallinn, 436 pp.

Ray, D.C. 2007. The correlation of Lower Wenlock Series (Silurian) bentonites from the Lower Hill Farm and Eastnor Park boreholes, Midland Platform, England. *Proceedings of the Geologists Association* **118**, 175–185.

Ray, D.C., Collings, A.V.J., Worton, G.J., Jones, G. 2011. Upper Wenlock bentonites from Wren's Nest Hill, Dudley; comparisons with prominent bentonites along Wenlock Edge, Shropshire, England. *Geological Magazine* **148**, 670–681.

Ray, D.C., Richards, T.D. Brett, C.E., Morton, A., Brown, A.M. 2013. Late Wenlock sequence and bentonite stratigraphy in the Malvern, Suckley and Abberley Hills, England. *Palaeogeography, Palaeoclimatology, Palaeoecology* **389**, 115–127.

Sarna-Wojcicki, A.M., Morrison, S.D., Meyer, C.E., Hillhouse, J.W. 1987. Correlation of upper Cenozoic tephra layers between sediments of te western United States and eastern Pacific Ocean and comparison with biostratigraphic and magnetostratigraphic age data. *Geological Society of America Bulletin* **98**, 207–223.

Sell, B., Ainsaar, L., Leslie, S. 2013. Precise timing of the Late Ordovician (Sandbian) super-eruptions and associated environmental, biological, and climatological events. *Journal of the Geological Society* **170**, 711–714.

Sell, B.K., Samson, S.D., Mitchell, Ch.E., McLaughlin, P.I., Koenig, A.E., Leslie, S.A. 2015. Stratigraphic correlations using trace elements in apatite from Late Ordovician (Sandbian-Katian) K-bentonites of eastern North America. *Bulletin of the Geological Society of America*, doi: 10.1130/B31194.1

Sell, B.K., Samson, S.D. 2011. A tephrochronologic method based on apatite trace-element chemistry. *Quaternary Research* **76**, 157–166.

Schovsbo, N.H., Nielsen, A.T., Klitten, K., Mathiesen, A., Rasmussen, P. 2011. Shale gas investigations in Denmark: Lower Palaeozoic shales on Bornholm. *Geological Survey of Denmark and Greenland Bulletin* **23**, 9–14.

Somelar, P., Kirsimäe, K., Hints, R., Kirs, J. 2010. Illitization of Early Paleozoic K-Bentonites in the Baltic Basin: decoupling of burial- and fluid-driven processes. *Clays and Clay Minerals* **58**, 388–398.

Svensen, H.H., Hammer, Ø, Corfu, F. 2015. Astronomically forced cyclicity in the Upper Ordovician and U–Pb ages of interlayered tephra, Oslo Region, Norway. *Palaeogeography, Palaeoclimatology, Palaeoecology* **418**, 150–159.

Thorarinsson, S. 1944. Tefrokronologiska studier på Island: Þjórsárdalur och dess förödelse. Thesis (doctoral). Stockholms Högskola. 217 pp.

Torsvik, T.H., Rehnström, E.F. 2003. The Tornquist Sea and Baltic Avalonia docking. *Tectonophysics* **362**, 67–82.

Turekian, K.K., Wedepohl, K.H., 1961. Distribution of the elements in some major units of the Earth`s crust. *Geological Society of America Bulletin*, **72**, 175–191.

Turney, C.S.M., Blockley, S.P.E., Lowe, J.J., Wulf, S., Nick P. Branch, N.P., Mastrolorenzo, G., Swindle, G., Nathan, R., Pollard, A.M. 2008. Geochemical characterization of Quaternary tephras from the Campanian Province, Italy. *Quaternary International* **178**, 288–305.

Vincent, P., Meidla, T., Tinn, O. 2012. Biotic response to explosive volcanism: Ostracod recovery after Ordovician ash-falls. *Palaeogeography, Palaeoclimatology, Palaeoecology* **365,** 166–183.

Waldron, J.V.F., Schofield, D.I., Murphy, J.B., Thomas, C.W. 2014. How was the Iapetus Ocean infected with subduction? *Geology* **42**, 1095–1098

Wastegård, S., Davies, S.M. 2009. An overview of distal tephrochronology in northern Europe during the last 1000 years. Journal of Quaternary Science, special issue: Climates of the Past: Evidence from Natural and Documentary Archives 24, 500–512.

Winchester, J.A., Floyd, P.A. 1977. Geochemical discrimination of different magma series and their differentiation products using immobile elements. *Chemical Geology* **20***,* 325–343.

Williams, L.B., Srodon, J., Huff, W.D., Clauder, N., Hervig, R.L. 2013. Light element distributions (N, B, Li) in Baltic Basin bentonites record organic sources. *Geochimica et Cosmochimica Acta* **120**, 582–599.

Zielinski, R.A. 1985. Element mobility during alteration of silicic ash to kaolinite – a study of tonstein. *Sedimentology* **32**, 567–579.

ABSTRACT

Volcanic ash beds altered into bentonites form perfect marker horizons for correlation of sedimentary sections, enable interpretation of tectonomagmatic environments in volcanic source areas and help construct a geological time-scale using radiometric dating of well-preserved minerals. For a reliable interpretation, we need to know the within-bed compositional variability to compare it with between-bed variations. The aim of the study was to describe and interpret from the analysed data the geochemical and mineralogical heterogeneity of bentonite beds. To achieve these goals, a number of samples were collected, with the aim of obtaining detailed distribution patterns of elements in the vertical sections of bentonites, and compositional variations of the thick bentonite beds under study. The acquired data were compared with compositions of host rocks and clay fractions of terrigenous material (see Paper II). The thesis concentrated on studying five thick (30 to 90 cm) bentonites, four from the Upper-Ordovician — two Kinnekulle Bentonites, the Sinsen Bentonite and the Pirgu (BII) Bentonite—, and one from Silurian Wenlock: the Grötlingbo Bentonite.

Compositional changes throughout the thick bentonites were studied, using XRF, XRD and SEM analysing techniques, which enabled to detect main chemical components, trace elements, mineral composition, amount and composition of biotite and sanidine micro-phenocrysts. Signs of ash-transport fractionation, redeposition of volcanic ash, also the differentiation from the terrigenous clay and diagenetic redistribution of the volcanic? material were described and interpreted.

The stability of sanidine and biotite phenocryst compositions throughout the vertical sections of bentonites indicates that all bentonites originated from a single eruption. The observed stable composition of pyroclastic sanidine in the vertical section of bentonites confirms the reliability of sanidine-based “fingerprinting” of the altered volcanic ash beds. Trace element distribution in bentonites and in host rocks indicates that Zr, Ga, Nb, Ti and Th were immobile during volcanic ash alteration and carry information from primary ash composition. Immobile trace elements, especially Zr, indicate fractionation of material during air-transport. Some redistribution of Nb and Ti, as well as Y, occurred near the contacts of bentonites with the host rock. Mobile elements (Mg, K, Si) indicate significant redistribution of materials during diagenesis. Considerable geochemical variations, including high sulphur content, near the upper and lower contacts of the Kinnekulle Bentonite, as well as elevated calcium and phosphorus concentrations in host rocks of both bentonites, suggest that the studied large ash-falls caused notable perturbations in shallow marine and early post-sedimentary environment.

KOKKUVÕTE

Bentoniit, peamiselt savimineraalidest koosnev pehme ja poorne kivim, on tekkinud vulkaanidest pärineva püroklastilise materjali ümberkristalliseerumisel. Bentoniidiks muutunud vulkaanilise tuha vahekihid settekivimites pakuvad võimalust geoloogiliste läbilõigete väga täpseks korrelatsiooniks, aga samuti lähtevulkaanide geotektoonilise keskkonna ja magmatüübi väljaselgitamiseks. Bentoniite moodustavaid mineraale saab radioaktiivsete isotoopide abil dateerida ja rakendada geoloogilise ajaskaala ülesehitamiseks ning täpsustamiseks. Peamiseks probleemiks nende ülesannete lahendamisel on kihtidesisese ja kihtidevahelise koostiselise variatsiooni eristamine.

Käesoleva doktoritöö sisuks oli paksude (30 kuni 90 cm) bentoniidikihtide sisemise geokeemilise variatsiooni uurimine ja interpreteerimine. Uurimuses kasutati Ülem-Ordoviitsiumist pärit Kinnekulle, Sinseni ja Pirgu (BII) bentoniite ning Silurist (Wenlock) Grötlingbo bentoniiti. Töö esmane eesmärk oli välja selgitada, millised keemilised tunnused iseloomustavad algset purskematerjali, millised kujunevad tuha fraktsioneerumisel õhutranspordi ja veekeskkonnas ümbersetitamise käigus ja millised kujunevad sette sees keemiliste elementide liikumise tagajärjel. Teine eesmärk oli saadud andmestiku alusel interpreteerida bentoniitide lähtematerjali päritolu, kuhjumist ja bentoniidi teket ning eristumist terrigeensetest savidest. Selle eesmärgi saavutamiseks uuriti detailsete prooviseeriate abil paksude bentoniitide kihisisese koostise varieeruvust ja võrreldi saviga ümbriskivimist. Selleks, et saavutada parimat võimalikku detailsust bentoniidikihtide kirjeldamisel, jaotati uuritav bentoniidiläbilõige mitmeks osaks ning analüüsiti iga osa eraldi, kirjeldades sealjuures kihisiseseid füüsikalisi ja keemilisi muutusi. Bentoniidikihtide tuvastamiseks ja interpreteerimiseks kasutati XRF, XRD ja SEM analüüsimeetodeid, mille alusel määrati uuritavates kihtides keemiliste põhikomponentide ja mikroelementide sisaldust, mineraalset koostist, biotiidi hulka ja koostist ning sanidiini koostist.

Välimeetoditega on bentoniitse ja terrigeense savi eristamine tihti küsitav, aga laboratoorse XRF analüüsi andmed pakuvad täiendavaid võimalusi. Kõige paremini saab savisid eristada Cr ja Ti abil, sest nende sisaldused bentoniidis on tunduvalt madalamad kui terrigeensetes savides. XRD analüüsi andmetel koosnevad bentoniidid valdavalt illiit-smektiidist, kloriit-smektiidist, K-päevakivist ja kaoliniidist. Terrigeensetes savides on aga põhikomponendid illiit, kvarts ja K-päevakivi. Püroklastilise materjali diageneesil bentoniidiks toimub mobiilsete elementide sisse- (Mg, K) või väljakanne (Si ja Na), mis annab võimaluse iseloomustada keskkonda ja settetingimusi, kuid ei kirjelda tuhakihi algset koostist. Väheliikuvate (Ga, Y) ja immobiilsete (Th, Ti, Al, Zr) elementide ning fenokristallide (sanidiin, biotiit, apatiit, tsirkoon) alusel on võimalik tuvastada ja korreleerida erinevaid kihte. Immobiilsete elementide

alusel saab järeldada, et tihti on toimunud märgatav vulkaanituha komponentide fraktsioneerumine õhutranspordi ja merebasseinis ümbersettimise käigus. Fenokristallide koostise stabiilsus uuritud kihtide vertikaalläbilõikes kinnitab, et kõik uuritud paksud bentoniidid on pärit ühest vulkaanipurskest, mitte pole tekkinud mitme erineva purskematerjali kuhjumisel.

Uuritud bentoniidikihtide paksuse ja võimalike lähtevulkaanide suure kauguse alusel võib järeldada, et tegemist on olnud väga võimsate pursetega, mis katsid tuhaga laialdasi alasid. Võimsad vulkaanipursked mõjutavad elukeskkonda nii otseselt, mattes enda alla suuri alasid, kui ka kaudselt, põhjustades temperatuuri langust. Kinnekulle ja Grötlingbo bentoniidialuse kõrvalkivimi väävli kõrgenenud kontsentratsioon näitab (artikkel IV), et orgaaniline materjal on kõdunenud hapnikuvaeses keskkonnas. Väävlisisalduse tõusu on märgata Grötlingbo ja Kinnekulle bentoniidi nii alumises kui ka ülemises kihis, kuna surnud elustiku põhjasadenemine on toimunud aeglasemalt kui tuhakihi sadenemine. Väävlisisalduse kasvu on vähem märgata BII bentoniidis, millest võib järeldada, et tuha mõju eluskeskkonnale oli tunduvalt väiksem. Vulkaanituha mõju keskkonnale näitavad ka fosfori ja kaltsiumi suuremad sisaldused kivimis vahetult Kinnekulle Bentoniidi kohal.

ELULOOKIRJELDUS

Isikuandmed

Ees- ja perekonnanimi: Sven Siir
Sünniaeg ja -koht: 09.12.1984 Eestis
Kodakondsus: Eesti
E-posti aadress: sven.siir@ttu.ee

Hariduskäik

Islandi Vulkanoloogia Instituut, Tefrokronoloogia suvekool (2012).
Tallinna Tehnikaülikool, doktorantuur (2010-2014), Maa-teadused.
Tallinna Tehnikaülikool, magistriõpe (2008-2010), Maa-teadused, kraad kaitstud 2010 teemal: "Vulkaaniliste kihtide korrelatsioon nelja Saaremaa puuraugu põhjal".
Tartu Ülikool, bakalaureuse õpe (2005-2008), keskkonnatehnoloogia, kraad kaitstud 2008.

Keelteoskus

Eesti keel	emakeel
Inglise keel	kesktase

Teenistuskäik

Alates 2015 Semetron AS – radioloogia-meditsiinitehnika insener
Alates 2008-2014 TTÜ Geoloogia Instituut – insener

Ekspeditsioonid

Taani Geoloogiateenistus Kopenhaagen, Billegrav-2 puursüdamiku uurimine ja geokeemiliste proovide võtmine (2013)
Eesti Geoloogiakeskus, Keila, Kuressaare K-3 puursüdamiku uurimine ja geokeemiliste proovide võtmine (2011)
Professor Kristel Sundbladi geoloogiline ekspeditsioon Soomes (2010)

Teadustegevus

Teadustegevuse valdkonnaks on geokeemia ja XRF meetod geokeemias.

CURRICULUM VITAE

Personal data

Name: Sven Siir
Date and place of birth: 12.09.1984, Estonia
E-mail address: sven.siir@ttu.ee

Education

University of Island, Summer School on Tephra Studies (2012)
Tallinn University of Technology, doctorate (2010-...), Earth Sciences
Tallinn University of Technology, master (2008-2010) Earth Sciences
University of Tartu, bachelor`s degree (2005-2008) Environmental Technology

Language competence

Estonian	native language
English	average

Professional employment

Since 2015 Semetron AS – medical equipment (radiology) engineer
Since 2008 till 2014 Institute of Geology at TUT – engineer

Expeditions

Geological survey of Estonia, Keila. Kuressaare K-3 drill core studying and samples collecting (2013).
Geological survey of Denmark, Copenhagen. Billegrav-2 drill core studying and samples collecting (2011).
Geological fieldtrip in Finland by Prof. Krister Sundblad (2010).

Research activity

Main scientific interest: geochemistry and XRF method in geochemistry.

PUBLICATIONS

I – Dahlquist, P.; Calner, M.; Kallaste, T.; Kiipli, T.; **Siir, S**. 2012. Geochemical variations within the mid-Silurian Grötlingbo Bentonite (Gotland, Sweden)—discriminating between magmatic composition, ash transport fractionation and diagenetic effects. *GFF*, **134**, 273-282.

GFF volume 134 (2012), pp. 273–282.
A Scandinavian Journal of Earth Sciences

Article

Geochemical variations within the mid-Silurian Grötlingbo Bentonite (Gotland, Sweden): discriminating between magmatic composition, ash transport fractionation and diagenetic effects

PETER DAHLQVIST[1], MIKAEL CALNER[2], TOIVO KALLASTE[3], TARMO KIIPLI[3] and SVEN SIIR[3]

Dahlqvist, P., Calner, M., Kallaste, T., Kiipli, T. & Siir, S., 2012: Geochemical variations within the mid-Silurian Grötlingbo Bentonite (Gotland, Sweden): discriminating between magmatic composition, ash transport fractionation and diagenetic effects. *GFF*, Vol. 134 (Pt. 1, December), pp. 273–282. © Geologiska Föreningen. doi: 10.1080/11035897.2012.759147.

Abstract: This paper reports on the geochemistry of the mid-Silurian Grötlingbo Bentonite, a ca. 0.1–0.4-m-thick and regionally important bentonite bed in Sweden and the East Baltic area. A series of eight samples, spaced by 5 cm, were taken from the Hunninge-1 drillcore in Gotland, Sweden, and were analysed in order to establish the vertical element composition and variation in the bentonite. The results show that the Götlingbo Bentonite originates from one source magma and from one single eruption. The lowermost 0.1–0.15 m of the bentonite (compacted) was deposited from air-transport fall-out, whereas the upper portions have been reworked in a shallow-marine environment and re-deposited. Vertical differences in Ti and Zr within the Grötlingbo Bentonite mean that regional correlation of the bed may need several samples at each locality to be reliable.

Keywords: Sweden; Grötlingbo Bentonite; Gotland; Silurian.

[1]*Geological Survey of Sweden, Kiliansgatan 10, SE-223 50 Lund, Sweden; peter.dahlqvist@sgu.se*
[2]*Department of Geology, Lund University, Sölvegatan 12, SE-223 62 Lund, Sweden*
[3]*Institute of Geology, Tallinn University of Technology, Ehitajate 5, 19086 Tallinn, Estonia*
Manuscript received 19 October 2012. Revised manuscript accepted 10 December 2012.

Introduction

Volcanic ash beds in sedimentary successions have frequently been used for precise regional correlation of sedimentary sections (Bergström et al. 1995; Kiipli & Kallaste 2006; Kiipli et al. 2008a, 2010a, 2010b; Ray et al. 2011; Cramer et al. 2012) and for reconstruction of the tectonomagmatic environments in volcanic source areas (Batchelor 2009; Hetherington et al. 2011). Various methods for such fingerprinting exist, and the composition of magmatic phenocrysts apatite (Batchelor et al. 1995; Ray 2007; Sell & Samson 2011), biotite (Batchelor 2003) and sanidine (Kiipli & Kallaste 2002) and trace element characteristics (Batchelor & Jeppson 1999; Batchelor & Evans 2000; Huff et al. 2000; Inanli et al. 2009; Kiipli et al. 2008b) have all been used for characterisation and interpretation of ash beds. The vertical chemical and mineralogical composition of individual ash beds is not homogeneous, but varies due to the successive change in magma composition during long-lasting eruptions and due to physical fractionation of ash in air transport and during settling in water basins (Fisher & Schmincke 1984). Various diagenetic processes further change the ash after deposition (Kiipli et al. 2007; Hints et al. 2008). Being aware of the relative scale and importance of these variations and understanding their reasons is an ultimate prerequisite for a successful analysis of chemical and mineralogical signatures and, in the end, for a reliable correlation of individual ash beds.

The aim of this paper was to describe the internal stratigraphy and evaluate vertical compositional variations in the mid-Silurian (Late Wenlock) Grötlingbo Bentonite, one of the thickest bentonites in the Silurian of the Baltic basin (Jeppsson & Calner 2003; Calner et al. 2006; Kiipli et al. 2008c, 2011; Cramer et al. 2012).

Geological background and stratigraphy

The Grötlingbo Bentonite has been documented in several drillcores and outcrops in the Baltic region (Fig. 1; Calner et al. 2006; Kiipli et al. 2008c, 2011). The wide geographical extent makes this conspicuous bentonite an excellent marker bed for correlation between shallow and deep water sections in the basin (Calner et al. 2006; Kiipli et al. 2008c). Based on a sample from the locality Hörsne 3 in eastern Gotland, the Grötlingbo Bentonite has recently been dated by means of high-precision isotope dilution U–Pb (zircon) dating to a weighted mean $^{206}Pb/^{238}U$ age of 428.47 ± 0.72 Ma (Cramer et al. 2012). According to Kiipli et al. (2008c, 2011), the ash derived from a source volcano with a rhyolitic composition, probably located to the west–northwest of the Baltic basin, within the Laurentia–Baltica collisional zone.

For this study, we have sampled the Hunninge-1 core from the Klintehamn area in western Gotland (Fig. 1). Here, the base of the Grötlingbo Bentonite is situated 0.76 m above the

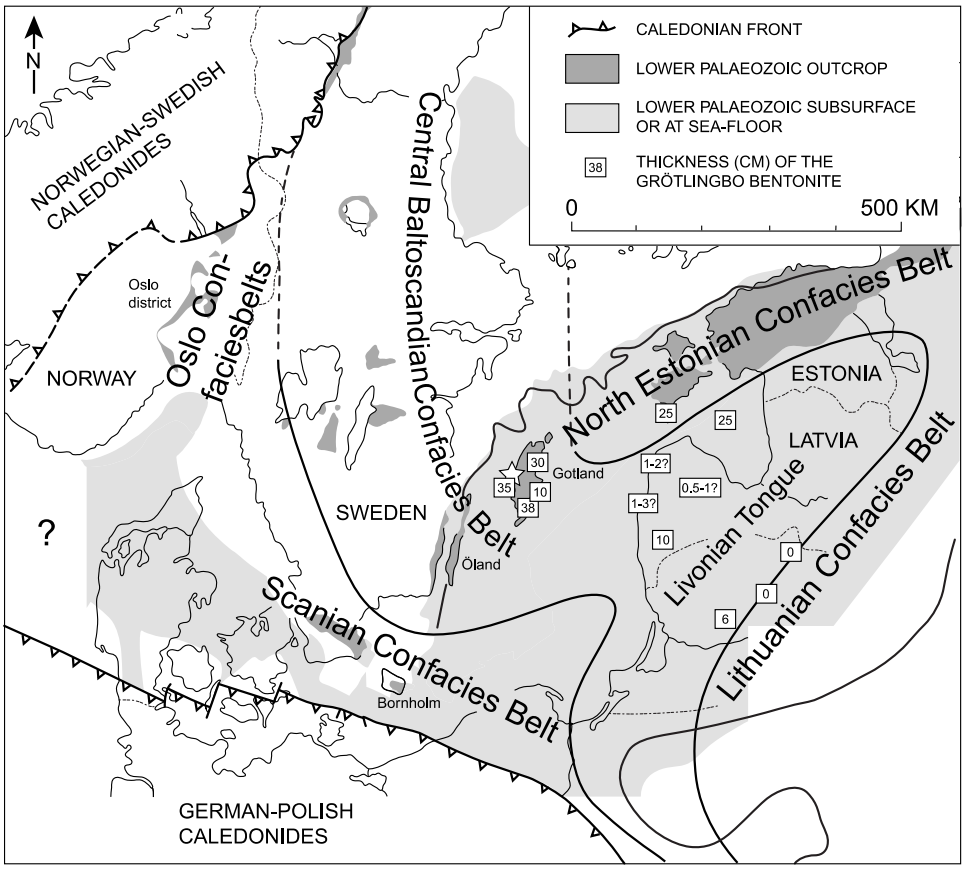

Fig. 1. Map of Scandinavia and the East Baltic region showing the location of the Hunninge-1 drillcore in western Gotland (star) and locations where the Grötlingbo Bentonite has been identified (white boxes with thickness in centimetres). Note the near restriction of the bentonite to the Livonian Tongue and the Central Baltoscandian Confacies Belt. Modified from Kiipli et al. (2008c).

unconformable top of the Slite Group, in the Bara Oolite Member of the Halla Formation (Calner et al. 2006, chart 1). In this area, the Bara Oolite Member is less than a metre thick and constitutes an argillaceous, slightly silty and fine-grained limestone, at some levels with fairly abundant micro-oncoids. The mid-Silurian stratigraphic interval in Gotland is particularly well investigated because of a global turnover in marine biotas – the Mulde Event – and an associated, global positive excursion in $\delta^{13}C$ (Calner et al. 2006, 2012; Calner 2008). For stratigraphical context of the Grötlingbo Bentonite in Gotland and its relationship with sequence stratigraphy, extinctions of the Mulde Event and the mid-Silurian global carbon isotope anomaly, see Calner & Jeppsson (2003) and Calner et al. (2006, chart 1). The geochemistry of bentonites and their associated apatite phenocrysts from the adjacent Slite and Mulde formations has been described by Batchelor & Jeppson (1999). A summary of Wenlock bentonites on the Baltic craton, including a discussion on the distribution and correlation of the Grötlingbo Bentonite, was made by Kiipli et al. (2008c).

Materials and methods

Material was sampled from the Hunninge-1 core (N: 6364427 O: 1647619), drilled in June 2004 in the Hunninge quarry northeast of Klintehamn in western Gotland (Figs. 1 and 2; Calner et al. 2006). The core, which is stored at the Department of Geology, Lund University, is 45 m long in total, has a diameter of 39 mm and includes the topmost Slite Marl through the Fröjel, Halla and basal Klinteberg formations. Eight samples, spaced by 5 cm and each with a weight between 15 and 20 g, were taken through the ~35-cm-thick bentonite (Fig. 3). Two additional samples were taken as reference at 0.1 and 0.5 m below and above the bentonite, respectively. The underlying and overlying rocks are micritic limestones with sparse coated grains.

Major and trace elements were determined using a S4 instrument produced by Bruker AXS (Germany), on pressed powder pellets. Measurements and initial calibrations were made using producers software MultiRes and GeoQuant. With both programs, samples were measured twice, e.g. four measurements were made for each sample. Initial results were

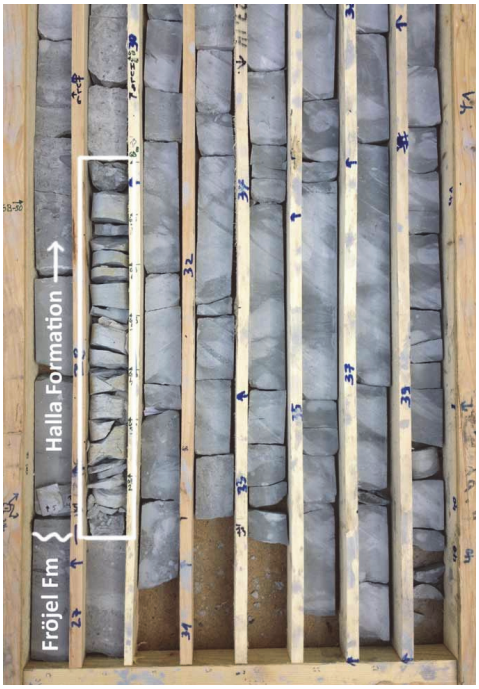

Fig. 2. Portion of the Hunninge-1 core showing the 37 cm thick Grötlingbo Bentonite (within the white box) in the basal part of the Halla Formation. The undulating white line shows the unconformable boundary between the Fröjel (Slite Group) and Halla formations.

corrected using linear coefficients and constants calculated from measurements of ca. 20 international (Govindaraju 1995) and Estonian (Kiipli et al. 2000) reference materials of claystones and acidic to intermediate magmatic rocks. The average result of the four measurements is reported in Table 1.

X-ray diffractometry (XRD) of the bulk samples on a HZG-4 instrument was applied for identification of major minerals.

For grain size analyses, 2.0–3.5 g of each bentonite sample was suspended ultrasonically in a 0.1% tetrasodium pyrophosphate solution in deionised water. After 2–3 s, the suspension was poured into a plastic bottle. This operation was repeated twice. According to our experience, this procedure extracts most of the grains larger than 0.04 mm from the bentonite sample. After drying, the grain material was divided by a 0.1 mm sieve into two parts and the fractions with particles smaller and larger than 0.1 mm, respectively, were weighed. The results are given in weight % of the initial sample.

When suspended in water, the material (mostly with a grain size smaller than 0.04 mm) was analysed with respect to grain size by the laser scattering particle size distribution analyser LA-950V2 of HORIBA Ltd (Japan). Instrument measurements based on the Mie scattering theory and results are given in volume %.

The grain fraction from the bentonite samples was studied by means of an energy-dispersive X-ray microanalyser, connected to a scanning electron microscope, at low vacuum (30 Pa) conditions. The electron beam was generated by 20 kV and 650 pA. The composition of 146 grains from the Grötlingbo Bentonite was analysed. The basaltic glass BBM-1G, distributed by the International Association of Geoanalysts, was measured together with the studied grains and used as a reference. On the basis of these measurements, Al, Si and Fe concentrations were corrected by a few per cent. According to repetitive measurements of BBM-1G, the precision of measurements was better than ± 0.4%.

Results

X-ray diffractometry

Three out of four host rock samples revealed calcite and quartz reflections with much less intensive dolomite. Only at the depth of −50 cm below, the base of the bentonite dolomite reflection is almost as strong as calcite, suggesting the presence of a significant portion of that mineral.

Among the bentonite samples, a broad reflection at 11.2–11.5 Å indicates illite–smectite as the main mineral component in all samples (Fig. 4). Kaolinite and biotite reflections are strongest in the lowermost sample (GB1) and decrease upwards. The third to sixth samples (GB3–GB6), in the middle of the bentonite bed, are characterised by weak kaolinite and biotite reflections. Biotite is almost absent in the two uppermost samples (GB7 and GB8), but kaolinite appears again in the uppermost sample (GB8). Starting from the fourth sample (GB4), a small portion of quartz is present and increases upwards. From the fifth sample (GB5), minor portions of dolomite are detected. The uppermost sample (GB8) contains some calcite.

X-ray fluorescence

SiO_2 concentrations in the silicate part of the host limestone are at the level of ca. 70% (Fig. 3), suggesting a substantial portion of sandy or silty material. A low content of clay minerals in the silicate portion of the host limestones is indicated by relatively low contents of Al_2O_3, K_2O and Rb. This composition is in accordance with the global sea level lowstand at that time (Calner et al. 2006; Johnson 2006; Kiipli et al. 2010c). Several elements in the bentonite, e.g. Fe_2O_3, Cr, Ni, Cu and V, occur in significantly lower concentrations than in the silicate portion of the host rock. These elements can be used as indicators of the terrigenous admixture in the bentonite.

Concentration trends within the bentonite can be grouped into four types (Fig. 5):

1. The concentrations of the following components increase upwards through the bentonite: LOI, CaO, Na_2O, Cr and Ni. If the information from the XRD analysis is also considered, that quartz and dolomite occur in the upper part of bentonite, we can assign these trends to the relative increase of terrigenous admixture upwards in the bentonite bed.
2. Decreasing trends of concentrations in the lower part of the bentonite: P_2O_5, Cl, Zr, Zn and Rb. These trends are related to the upward decreasing contents of phenocrysts: P_2O_5 and Cl with apatite, Zr with zircon and Rb and Zn with biotite.
3. Elements with higher concentrations in the lowermost and uppermost parts of the bentonite, respectively: Y, TiO_2, V, Fe_2O_3, S, As and Pb. The terrigenous component in the upper part and high content of phenocrysts in the lower part cause the rise of TiO_2, V, Y and Fe_2O_3 concentrations in both ends of the bentonite. For S, As, Pb (not shown in Fig. 5) and

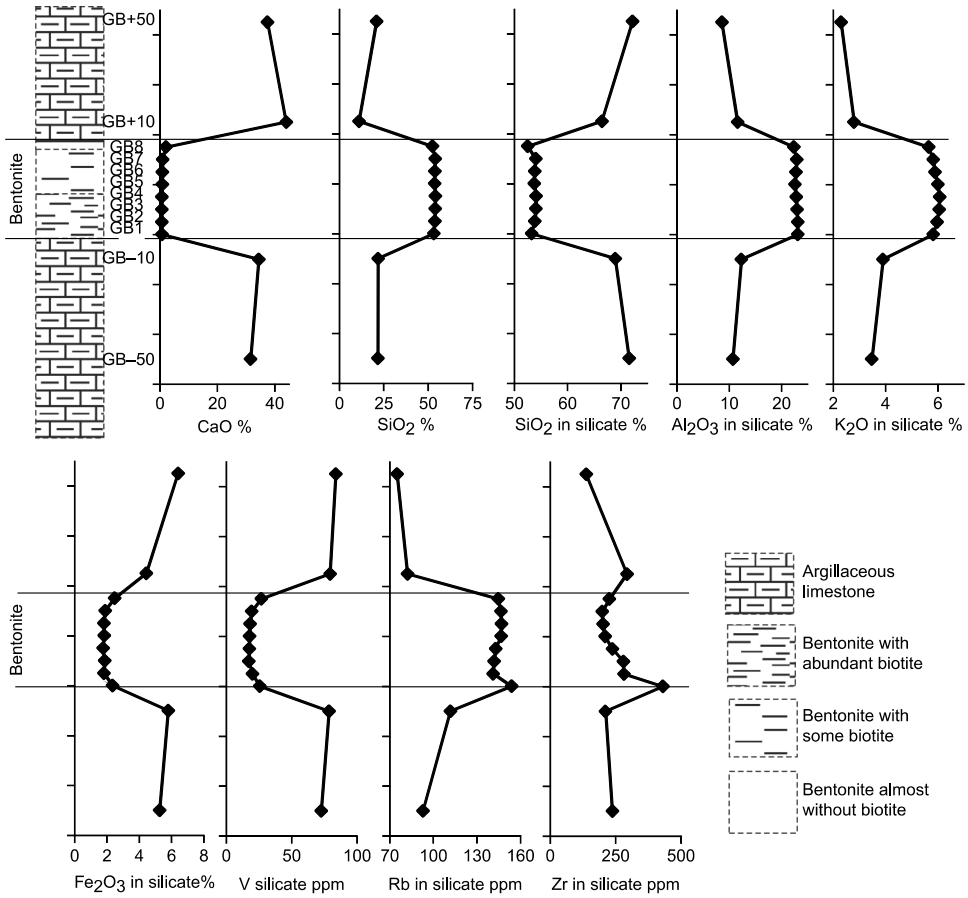

Fig. 3. Distribution of CaO and SiO_2 in Grötlingbo Bentonite and in host rock. Elements in silicate (SiO_2, Al_2O_3, K_2O, Fe_2O_3, V, Rb and Zr) are calculated for host rock as follows: concentration in a silicate portion of host rock = coefficient × measured concentration. Coefficient = 100/(100 – LOI – CaO – MgO).

Fe_2O_3, the occurrence of pyrite in the lowermost and uppermost parts of the bentonite may play some role.

4. Elements having higher concentrations in the middle part of the bentonite: SiO_2, K_2O, MgO, Ga and Sr. These trends represent diagenetic effects transforming the volcanic ash to clay, resulting in more kaolinite near the contacts of the bentonite. Surprisingly, even Ga, commonly considered as an immobile element (Winchester & Floyd 1977), follows this trend.

Grain size

The grain size measurements on clay material suspended in water (mostly <0.04 mm) show a bimodal distribution within all samples, especially when calculated as a mean for all the samples within the Grötlingbo bentonite (Fig. 6). The overall grain size decreases upwards from sample GB1 to GB5 and then increases, which may be due to the above discussed decrease in phenocryst content and the upward increase in terrigenous admixture. Maximal grain sizes are ~ 200 μm (0.2 mm) in these analyses.

Measurements of the fraction of extracted grains (>0.04 mm) show an upward decrease of total amount of grains >0.04 mm and coarse grains >0.1 mm (Fig. 7). This overall upward decrease is due to a decrease in phenocrysts.

If combining the weighted % for grains >0.04 mm and calculated volume % of the clay (mostly <0.04 mm), the pattern of an upward decrease in medium grain size is even stronger (see Figs. 6 and 7).

Phenocrysts

One hundred and thirteen grains, of the total 146 measured, could be classified as fragments of magmatic phenocrysts. The reminder were illite–smectite, pyrite and in the uppermost sample calcite. Biotite (42%) and kaolinitised feldspars (42%) dominate among phenocryst material (Fig. 7). Minor

Table 1. X-ray fluorescence results.

Sample	GB-50	GB-10	GB1	GB2	GB3	GB4	GB5	GB6	GB7	GB8	GB + 10	GB + 50
cm (to bottom)	−50	−10	0	5	10	15	20	25	30	35	45	85
LOI 920° (%)	32.55	31.15	6.94	7.07	6.93	7.16	6.95	7.06	7.24	7.79	37.92	31.94
SiO_2 (%)	21.7	21.9	53.3	53.9	54.1	54.1	53.8	53.9	54.1	52.6	11.1	21.0
TiO_2 (%)	0.160	0.195	0.527	0.385	0.384	0.369	0.366	0.372	0.380	0.450	0.084	0.116
Al_2O_3 (%)	3.3	3.9	23.1	23.1	23.0	22.8	22.6	22.8	22.9	22.4	1.9	2.5
MnO (%)	0.121	0.066	0.021	0.013	0.013	0.009	0.011	0.011	0.012	0.018	0.051	0.063
MgO (%)	5.47	2.59	4.96	4.99	5.06	5.03	5.02	5.01	4.99	4.90	1.28	1.40
CaO (%)	31.61	34.47	0.76	0.67	0.65	0.69	0.86	0.84	0.96	2.16	44.06	37.53
Na_2O (%)	0.21	0.16	0.20	0.19	0.19	0.20	0.21	0.20	0.21	0.22	0.07	0.10
K_2O (%)	1.06	1.24	5.83	5.98	6.05	6.07	6.01	5.90	5.83	5.65	0.47	0.67
Fe_2O_3 (%)	1.60	1.85	2.37	1.83	1.87	1.78	1.84	1.83	1.91	2.49	0.75	1.87
P_2O_5 (%)	0.110	0.046	0.109	0.078	0.080	0.079	0.073	0.072	0.071	0.072	0.052	0.066
Cl (%)	0.043	0.033	0.024	0.020	0.018	0.017	0.016	0.016	0.016	0.017	0.032	0.032
S (%)	0.207	0.357	0.141	0.069	0.064	0.104	0.099	0.120	0.145	0.272	0.092	0.589
F (%)	0.04	0.07	0.57	0.59	0.57	0.61	0.60	0.61	0.60	0.52	0.06	0.03
As (ppm)	3.2	5.5	2.6	0.3	0.7	0.7	1.2	1.9	1.2	4.3	1.1	9.4
Ba (ppm)	88	83	217	146	139	124	125	121	124	155	23	40
Ce (ppm)	<50	<50	<50	<50	<50	<50	<50	<50	<50	<50	<50	<50
Co (ppm)	<5	<5	<5	<5	<5	<5	<5	<5	<5	<5	<5	<5
Cr (ppm)	15.9	23.8	4.3	5.0	3.6	7.0	8.3	9.4	9.5	15.3	11.4	14.1
Cu (ppm)	4.9	7.6	4.9	2.0	2.3	3.1	3.4	4.5	4.6	7.0	3.4	6.9
Ga (ppm)	4.7	7.3	23.0	24.6	24.9	24.9	24.5	24.3	23.8	22.4	4.7	5.0
La (ppm)	<30	<30	<30	<30	<30	<30	<30	<30	<30	<30	<30	<30
Mo (ppm)	<5	<5	<5	<5	<5	<5	<5	<5	<5	<5	<5	<5
Nb (ppm)	3.9	4.8	31.4	33.5	32.3	30.0	31.0	31.5	29.3	29.2	2.5	3.1
Ni (ppm)	8.5	11.4	5.8	4.0	2.8	5.0	4.9	4.7	6.3	8.8	4.6	11.3
Pb (ppm)	8.3	21.1	6.5	1.4	1.3	5.1	3.9	6.1	7.1	15.0	1.6	27.6
Rb (ppm)	28	36	154	141	142	143	147	147	147	145	14	22
Sr (ppm)	353	294	209	221	220	226	232	232	227	201	664	361
Th (ppm)	<5	<5	32.0	30.1	29.6	30.4	28.5	29.0	28.2	29.6	<5	<5
U (ppm)	<5	<5	6.2	10.3	9.5	11.1	10.1	9.5	9.1	7.2	<5	<5
V (ppm)	22.1	25.0	25.8	20.3	17.4	17.8	17.9	18.4	19.6	27.1	13.3	24.4
Y (ppm)	12.9	17.1	18.7	15.4	15.5	16.2	15.2	16.4	17.5	17.8	16.3	20.5
Zn (ppm)	17.1	15.8	37.9	15.7	17.3	14.9	15.1	16.1	18.0	24.9	6.4	62.2
Zr (ppm)	72	67	432	283	281	239	211	203	200	227	49	40

Note: Numbers are the average of four results for each sample.

phenocrysts are quartz (5%), Ti-oxides (4%), zircon (4%) and apatite (3%).

Biotite is Mg-rich (Table 2). In the lower (GB1) and upper samples (GB8), the biotite is strongly kaolinitised and kaolinite lenses occur between unaltered biotite layers. In samples GB2 and GB7, kaolinisation of biotite is weaker; and in samples GB4 and GB6, from the middle part of the bentonite, biotite is well preserved without signs of kaolinitisation. In order to exclude

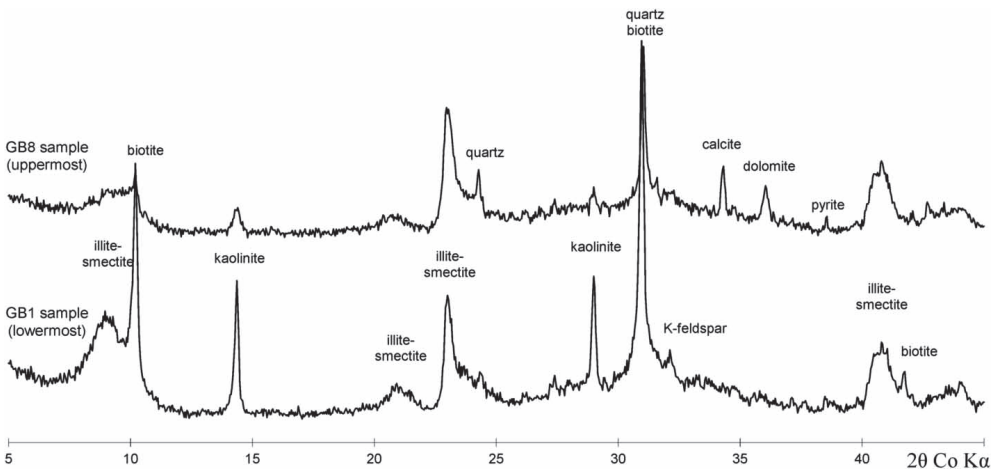

Fig. 4. XRD patterns of original/untreated samples from the Grötlingbo Bentonite. Lower sample reveals stronger reflections of kaolinite and biotite; in the upper sample quartz, dolomite and calcite reflections, indicating redeposition of the volcanic ash material appear.

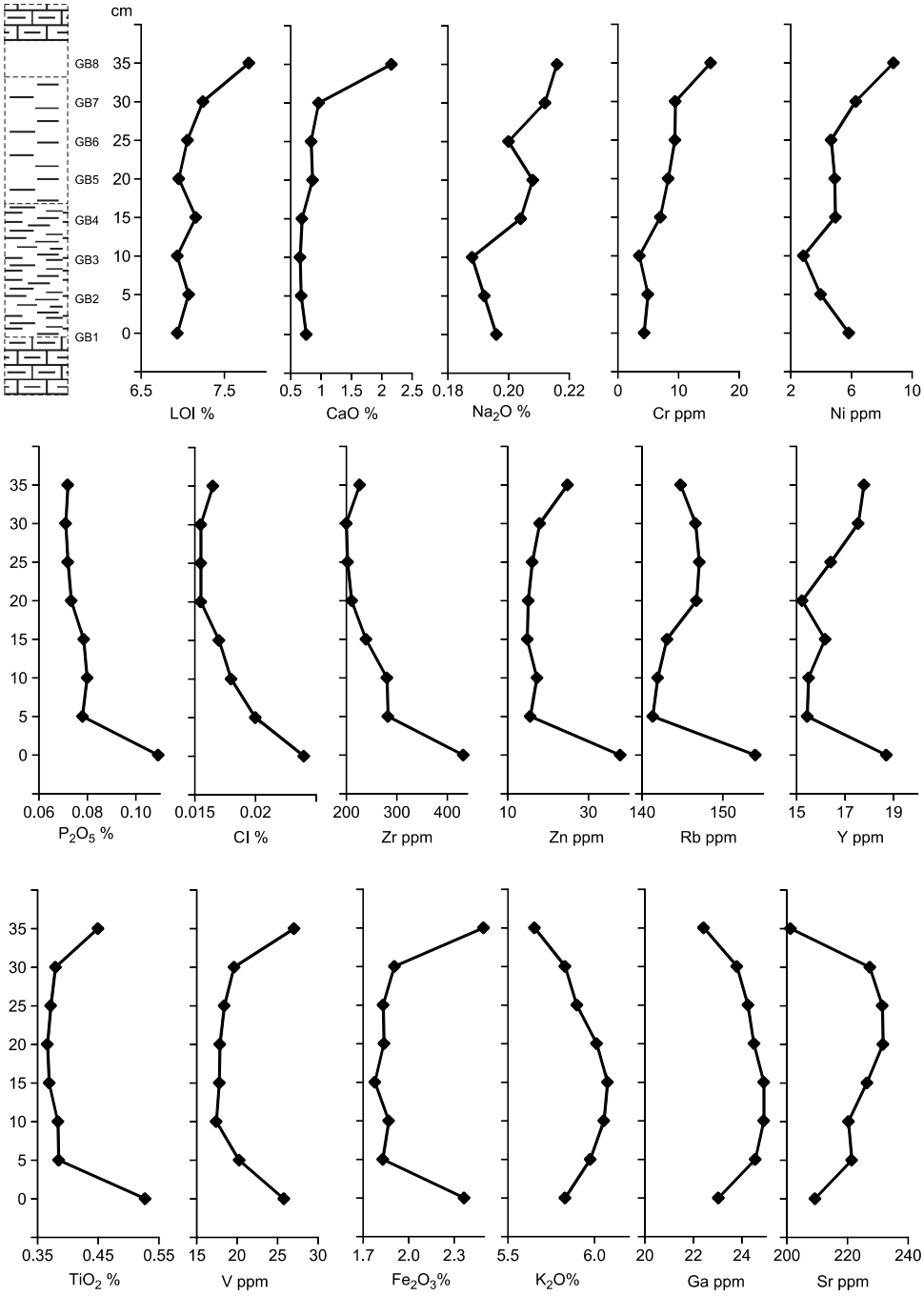

Fig. 5. Distribution of key elements within the Grötlingbo Bentonite.

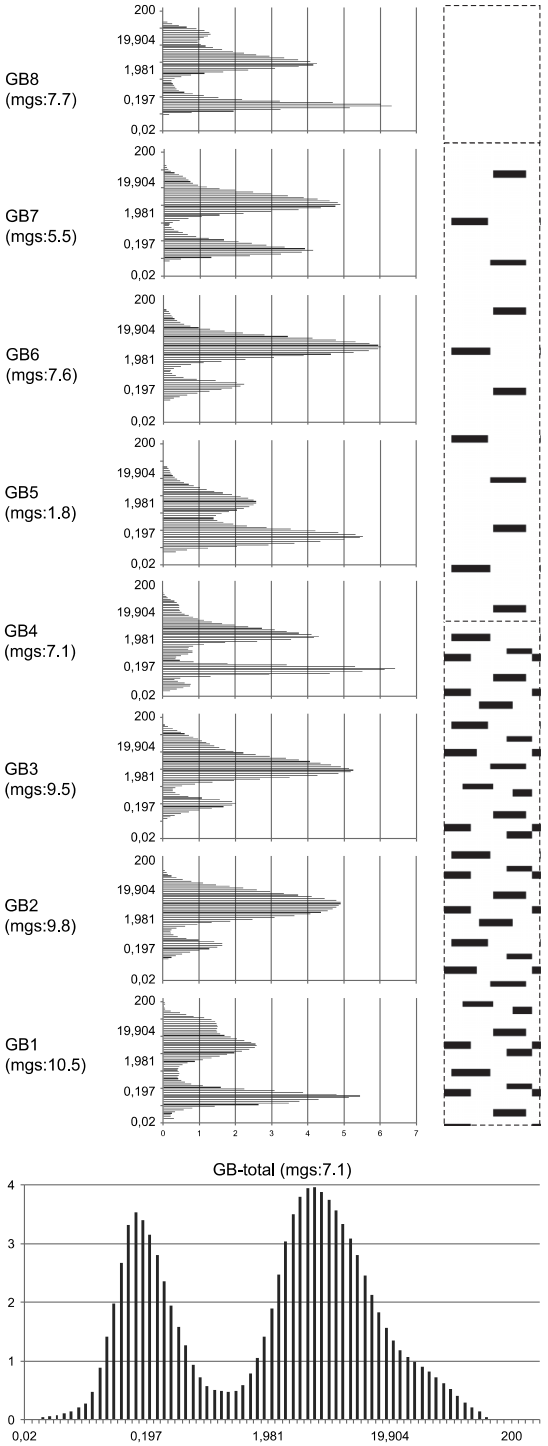

Fig. 6. Grain size distribution for each of the samples within the Grötlingbo Bentonite and the total (below) for all samples. *y*-Axis in % and *x*-axis in μm. mgs, mean grain size in μm. Note that a portion of grains being >0.04 mm is included here, not having been removed during separation.

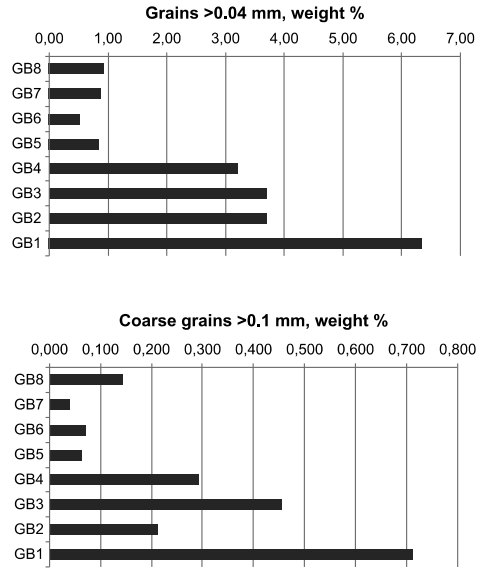

Fig. 7. Grain size distribution for grains >0.04 mm (above) and coarse grains (>0.1 mm, below) for each of the samples within the Grötlingbo Bentonite.

the altered biotites in the calculation of the average composition of biotite (Table 2), only results with $K_2O > 8\%$ and $S < 0.5\%$ are used. In samples GB6 and GB7, biotite dominates and kaolinitised feldspars are less frequent. Despite the significant compositional variation of biotites, largely exceeding measuring uncertainty (see standard deviations in Table 2), there are no differences or trends in biotite composition between samples.

Feldspars are mostly close to the pure end-member K-feldspars indicating authigenic origin (Table 2); only two grains contained significant portions of $NaAlSi_3O_8$ (12–16 mol%) and $CaAl_2Si_2O_8$ (3–5 mol%) components typical of the magmatic feldspars. K-feldspars were associated with kaolinite in the same grains. Often the interior of the grain is kaolinite, surrounded by a thin coating of unaltered K-feldspar (Fig. 8). But the opposite, i.e. K-feldspar in the centre of the grain and kaolinite lenses at the grain margins, is also common. Kaolinitised feldspars are most abundant in samples GB1, GB4 and GB8.

Discussion

The identical composition of biotite in all samples indicates that source magma composition did not change during the time of the volcanic eruption and confirms that the Grötlingbo Bentonite originates from one single eruption. Accordingly, all observed

Table 2. Composition of grains in Grötlingbo Bentonite.

	Biotite		K-feldspar		K–Na-feldspar		Kaolinite	
	Average	SD	Average	SD	Average	SD	Average	SD
Number	45		7		2		36	
Weight %								
Na_2O	0.56	0.12	0.11	0.05	1.40	0.14	0.14	0.10
MgO	12.75	0.91	0.23	0.12	0.22	0.05	0.43	0.18
Al_2O_3	15.52	0.74	19.06	0.62	17.80	0.05	42.87	0.84
SiO_2	39.48	0.88	62.37	0.72	62.42	1.01	53.10	0.57
P_2O_5	0.05	0.14	0.11	0.21	0.48	0.15	0.13	0.20
K_2O	8.72	0.39	14.40	0.73	12.85	0.50	0.75	0.27
CaO	0.17	0.09	0.19	0.13	0.67	0.17	0.22	0.17
TiO_2	4.48	0.27	0.13	0.02	0.28	0.04	0.16	0.14
FeO	17.72	1.43	0.61	0.08	0.77	0.20	0.80	0.32
Index in chemical formula								
Na	0.09	0.02	0.01	0.01	0.14	0.02		
K	0.91	0.02	0.98	0.01	0.83	0.01		
Mg	1.53	0.10						
Fe	1.19	0.09	0.02	0.00	0.03	0.01		
Ti	0.27	0.01	0.00	0.00	0.01	0.00		
Ca	0.01	0.01	0.01	0.01	0.04	0.01		
Al	1.26	0.03	1.05	0.03	0.99	0.01	1.95	0.02
Si	2.73	0.03	2.92	0.03	2.96	0.02	2.05	0.02

Notes: Indexes are calculated according to the following idealised chemical formulas: biotite, $(K,Na)_1(Mg,Fe,Ti,Ca)_3(Al,Si)_4O_{10}(OH,F)_2$; feldspars, $(K,Na,Ca)_1(Al,Si,Ti,Fe)_4O_8$; kaolinite, $Al_2Si_2O_5(OH)_4$.

compositional variations of the bulk bentonite belong to the physical fractionation during air transport, re-deposition of the ash and subsequent diagenetic effects.

Geochemical trends indicate that the full section of the Grötlingbo Bentonite formed under a combination of two physical processes:

1. Direct fall-out of the ash from the atmosphere. The lower 10–15 cm (compacted) has accumulated in that way.
2. Reworking and re-deposition of the ash from shallow-marine environments and land. The upper 20–25 cm has been reworked in a marine environment by wave activity and/or currents and also river influx cannot be excluded.

Diagenetic effects can be different in different environments. For example, in the Middle Ordovician Kinnekulle K-bentonite in North Estonia (Kiipli et al. 2007), a significant portion of potassium was imported from the surrounding environment, forming authigenic potassium feldspar layers in the upper and lower parts of the bentonite. In our case, Mg has probably been imported from the marine environment into forming illite–smectite as Mg is commonly relatively low in rhyolitic source magmas. In accordance with the high Zr/Ti ratio, a rhyolitic source magma was proposed for the Grötlingbo Bentonite by Kiipli et al. (2011), whereas the Zr/TiO_2–Nb/Y plot of Winchester & Floyd (1977) suggests a trachyandesitic composition. Contemporaneous bentonites from the Slite Group and the distal portions of the Halla Formation (Mulde Brick-clay Member; cf. Batchelor & Jeppsson 1999) indicate dacitic affinities. The export of silica and other elements and compaction of the initial ash layer significantly decrease the thickness of the bentonite. For example, 50% of the initial SiO_2 can be lost during ash alteration (Huff et al. 1996; Kiipli et al.

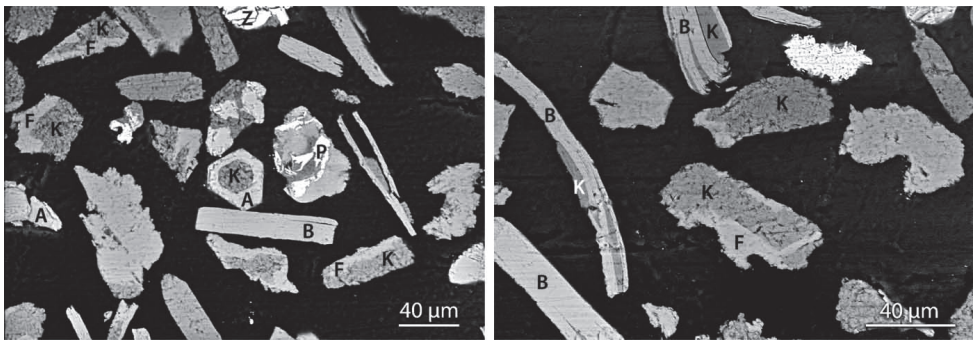

Fig. 8. Pyroclastic grains from the lower part (GB1) of the Grötlingbo Bentonite. B, biotite; K, kaolinite; A, apatite; Z, zircon; P, pyrite; F, potassium feldspar. In the right photograph, the rhombic shape of the kaolinised part of the middle feldspar indicates a rhombic shape of the primary plagioclase phenocryst. Authigenic potassium feldspar forms coatings on primary plagioclase phenocrysts. Less stable plagioclase was later replaced by kaolinite, but more stable K-feldspar coatings are preserved. Biotite flakes are also partly kaolinitised.

2006). Kaolinisation has also decreased the content of several elements near the contacts of the bentonite (see above).

The association of kaolinite and K-feldspar in grains and partial kaolinisation of biotite indicate a series of diagenetic changes of the original ash. A possible alteration scenario of the ash could be as follows:

1. Devitrification of glass particles and the formation of illite–smectite.
2. Growth of the authigenic K-feldspar coatings on the plagioclase grains.
3. Kaolinisation of the plagioclase and biotite.

The initial presence of plagioclase grains among pyroclastic material can be supposed from the fact that kaolinite has mostly replaced materials being more sensitive to alteration than K-feldspar and biotite, but more resistant compared with volcanic glass. Plagioclase is a common phenocryst in unaltered volcanic rocks, but is rarely found in bentonites. K-feldspar and K–Na sanidine are common in kaolinite-rich bentonites (e.g. Kiipli et al. 2010a), which indicates that these minerals are stable during kaolinite formation processes.

All of the above discussed also influence concentrations of the mobile and immobile elements. For regional or intercontinental correlation of bentonites, mostly immobile elements Al, Ti, Zr, Nb and Th are useful (Kiipli et al. 2008b). Within the Grötlingbo Bentonite, the concentration of Zr in the lower part is twice higher than in the rest of the bentonite. TiO_2 is 1.5 times higher in the lower part than in the middle part of the bentonite. Al, Nb and Th show less variation. Therefore, 1.5–2 times differences in Ti and Zr do not exclude correlation between two localities. For a reliable correlation, analysis of the composition in several samples through the full section of the bentonite is recommended. Alternatively, the lowermost 10 cm is most likely to reflect the original ash composition free from re-working.

Conclusions

Geochemical analysis of the mid-Silurian Grötlingbo Bentonite has shown that

1. The identical composition of biotite within the bentonite indicates that source magma composition did not change and confirms that the Grötlingbo Bentonite originates from one single eruption.
2. The compositional variations within the bentonite are most likely due to the physical fractionation during air transport, reworking and re-deposition of parts of the ash and subsequent diagenetic effects.
3. Vertical differences in Ti and Zr within the Grötlingbo Bentonite mean that regional correlation of the bed may need several samples at each locality to be reliable.

Acknowledgements. – This study is a contribution to IGCP591, Estonian Science Foundation project no 8963 and the Estonian Ministry of the Education and Science target financing project SF0140016s09. We also acknowledge the two anonymous reviewers for their comments that improved this paper.

References

Batchelor, R.A., 2003: Geochemistry of biotite in metabentonites as an age discriminant, indicator of regional magma sources and potential correlating tool. *Mineralogical Magazine 67*, 807–817.

Batchelor, R.A., 2009: (2008): Geochemical "Golden Spike" for Lower Palaeozoic metabentonites. *Earth and Environmental Science Transactions of the Royal Society of Edinburgh 99*, 177–187.

Batchelor, R.A., Weir, J.A. & Spjeldnæs, N., 1995: Geochemistry of Telychian metabentonites from Vik, Ringerike District, Oslo region. *Norsk Geologisk Tidsskrift 75*, 219–228.

Batchelor, R.A. & Evans, J., 2000: Use of Strontium isotope ratios and rare earth elements in apatite phenocrysts for characterisation and correlation of Silurian metabentonites: a Scandinavian case study. *Norsk Geologisk Tidsskrift 80*, 3–8.

Batchelor, R.A. & Jeppsson, L., 1999: Wenlock bentonites from Gotland, Sweden: geochemistry, sources and potential as chemostratigraphic markers. *Geological Magazine 136*, 661–669.

Bergström, S.M., Huff, W.D., Kolata, D.R. & Bauert, H., 1995: Nomenclature, stratigraphy, chemical fingerprinting, and areal distribution of some Middle Ordovician K-bentonites in Baltoscandia. *Geologiska Föreningens i Stockholm Förhandlingar (GFF) 117*, 1–13.

Calner, M., 2008: Silurian global events – at the tipping point of climate change. *In* Ashraf M.T. Elewa (ed.): *Mass extinctions*, 21–58. Springer-Verlag, Berlin and Heidelberg.

Calner, M. & Jeppsson, L., 2003: Carbonate platform evolution and conodont stratigraphy during the middle Silurian Mulde Event, Gotland, Sweden. *Geological Magazine 140*, 173–203.

Calner, M., Kozłowska, A., Masiak, M. & Schmitz, B., 2006: A shoreline to deep basin correlation chart for the middle Silurian coupled extinction-stable isotopic event. *GFF 128*, 79–84.

Calner, M., Lehnert, O. & Jeppsson, L., 2012: New chemostratigraphic data through the Mulde Event interval (Silurian, Wenlock), Gotland, Sweden. *GFF 134*, 65–67.

Cramer, B.D., Condon, D.J., Söderlund, U., Marshall, C., Worton, G.J., Thomas, A.T., Calner, M., Ray, D.C., Perrier, V., Boomer, I., Patchett, P.J. & Jeppsson, L., 2012: U–Pb (zircon) age constraints on the timing and duration of Wenlock (Silurian) paleocommunity collapse and recovery during the 'Big Crisis'. *Bulletin of the Geological Society of America 124*, 1841–1857.

Fisher, R.V. & Schmincke, H.U., 1984: *Pyroclastic rocks*, 472 pp. Springer-Verlag, Berlin, Heidelberg, New York, Tokyo.

Govindaraju, K., 1995: 1995 working values with confidence limits for twenty six CRPG, ANRT and IWG-GIT geostandards. *Geostandards Newsletter 19* (*Special Issue*), 1–32.

Hetherington, C.J., Nakrem, H.A. & Potel, S., 2011: Note on the composition and mineralogy of upper Silurian bentonites from the Ringerike District: implications for local and regional stratigraphic correlation and sedimentation. *Norwegian Journal of Geology 91*, 181–192.

Hints, R., Kirsimäe, K., Somelar, P., Kallaste, T. & Kiipli, T., 2008: Multiphase Silurian bentonites in the Baltic Palaeobasin. *Sedimentary Geology 209*, 69–79.

Huff, W.D., Bergström, S.M. & Kolata, D.R., 2000: Silurian K-bentonites of the Dnestr Basin, Podolia, Ukraine. *Journal of the Geological Society of London 157*, 493–504.

Huff, W.D., Kolata, D.R. & Bergström, S.M., 1996: Large-magnitude Middle Ordovician volcanic ash falls in North America and Europe: dimensions, emplacement and post-emplacement characteristics. *Journal of Volcanology and Geothermal Research 73*, 285–301.

Inanli, F.Ö., Huff, W.D. & Bergström, S.M., 2009: The Lower Silurian (Llandovery) Osmundsberg K-bentonite in Baltoscandia and the British Isles: chemical fingerprinting and regional correlation. *GFF 131*, 269–279.

Jeppsson, L. & Calner, M., 2003: The Silurian Mulde Event and a scenario for secundo-secundo events. *Transactions of the Royal Society of Edinburgh: Earth Sciences 93*, 135–154.

Johnson, M.E., 2006: Relationship of Silurian sea-level fluctuations to oceanic episodes and events. *GFF 128*, 115–121.

Kiipli, T., Batchelor, R.A., Bernal, J.P., Cowing, C., Hagel-Brunnstrom, M., Ingham, M.N., Johnson, D., Kivisilla, J., Knaack, C., Kump, P., Lozano, R., Michiels, D., Orlova, K., Pirrus, E., Rousseau, R.M., Ruzicka, J., Sandstrom, H. & Willis, J.P., 2000: Seven sedimentary rock reference samples from Estonia. *Oil Shale 17*, 215–223.

Kiipli, T., Einasto, R., Kallaste, T., Nestor, V., Perens, H. & Siir, S., 2011: Geochemistry and correlation of volcanic ash beds from the Rootsiküla Stage (Wenlock-Ludlow) in the eastern Baltic. *Estonian Journal of Earth Sciences 60*, 207–219.

Kiipli, T., Jeppsson, L., Kallaste, T. & Söderlund, U., 2008a: Correlation of Silurian bentonites from Gotland and the East Baltic using sanidine phenocryst composition, and biostratigraphical consequences. *Journal of the Geological Society 165*, 211–220.

Kiipli, T. & Kallaste, T., 2002: Correlation of Telychian sections from shallow to deep sea facies in Estonia and Latvia based on the sanidine composition of bentonites. *Proceedings of the Estonian Academy of Sciences, Geology 51*, 143–156.

Kiipli, T. & Kallaste, T., 2006: Wenlock and uppermost Llandovery bentonites as stratigraphic markers in Estonia. *Latvia and Sweden. GFF 128*, 139–146.

Kiipli, T., Kallaste, T. & Nestor, V., 2010a: Composition and correlation of volcanic ash beds of Silurian age from the eastern Baltic. *Geological Magazine 147*, 895–909.

Kiipli, T., Kallaste, T., Nestor, V. & Loydell, D.K., 2010b: Integrated Telychian (Silurian) K-bentonite chemostratigraphy and biostratigraphy in Estonia and Latvia. *Lethaia 43*, 32–44.

Kiipli, T., Kiipli, E. & Kaljo, D., 2010c: Silurian sea level variations estimated using SiO_2/Al_2O_3 and K_2O/Al_2O_3 ratios in the Priekule drill core section, Latvia. *Bolletino della Societa Paleontologica Italiana 49*, 55–63.

Kiipli, E., Kiipli, T. & Kallaste, T., 2006: Identification of the O-bentonite in the deep shelf sections with implication on stratigraphy and lithofacies, East Baltic Silurian. *GFF 128*, 255–260.

Kiipli, T., Kiipli, E., Kallaste, T., Hints, R., Somelar, P. & Kirsimäe, K., 2007: Altered volcanic ash as an indicator of marine environment, reflecting pH and sedimentation rate – example from the Ordovician Kinnekulle bed of Baltoscandia. *Clays and Clay Minerals 55*, 177–188.

Kiipli, T., Orlova, K., Kiipli, E. & Kallaste, T., 2008b: Use of immobile trace elements for the correlation of Telychian bentonites on Saaremaa Island, Estonia, and mapping of volcanic ash clouds. *Estonian Journal of Earth Sciences 57*, 39–52.

Kiipli, T., Radzevičius, S., Kallaste, T., Motuza, V., Jeppsson, L. & Wicksröm, L., 2008c: Wenlock bentonites in Lithuania and correlation with bentonites from sections in Estonia, Sweden and Norway. *GFF 130*, 203–210.

Ray, D.C., 2007: The correlation of Lower Wenlock Series (Silurian) bentonites from the Lower Hill Farm and Eastnor Park boreholes, Midland Platform, England. *Proceedings of the Geologists' Association 118*, 175–185.

Ray, D.C., Collings, A.V.J., Worton, G.J. & Jones, G., 2011: Upper Wenlock bentonites from Wren's Nest Hill, Dudley; comparisons with prominent bentonites along Wenlock Edge, Shropshire, England. *Geological Magazine 148*, 670–681.

Sell, B.K. & Samson, S.D., 2011: Apatite phenocryst compositions demonstrate a miscorrelation between the Millbrig and Kinnekulle K-bentonites of North America and Scandinavia. *Geology 39*, 303–306.

Winchester, J.A. & Floyd, P.A., 1977: Geochemical discrimination of different magma series and their differentiation products using immobile elements. *Chemical Geology 20*, 325–343.

II – Kiipli, E.; Kiipli, T.; Kallaste, T.; **Siir, S**. 2012. Al_2O_3/TiO_2 ratio of the clay fraction of Late Ordovician–Silurian carbonate rocks as an indicator of paleoclimate of the Fennoscandian Shield. Elsevier. *Palaeogeography, Palaeoclimatology, Palaeoecology*, **365/366**, 312-320.

Palaeogeography, Palaeoclimatology, Palaeoecology 365–366 (2012) 312–320

Contents lists available at SciVerse ScienceDirect

Palaeogeography, Palaeoclimatology, Palaeoecology

journal homepage: www.elsevier.com/locate/palaeo

Al_2O_3/TiO_2 ratio of the clay fraction of Late Ordovician–Silurian carbonate rocks as an indicator of paleoclimate of the Fennoscandian Shield

Enli Kiipli *, Tarmo Kiipli, Toivo Kallaste, Sven Siir

Institute of Geology, Tallinn University of Technology, Ehitajate tee 5, 19086 Tallinn, Estonia

ARTICLE INFO

Article history:
Received 22 March 2012
Received in revised form 2 October 2012
Accepted 4 October 2012
Available online 11 October 2012

Keywords:
Ordovician
Silurian
Clay
Al/Ti ratio
Climate
Baltica

ABSTRACT

In the Fennoscandian Shield the fluctuations in arid–humid climate conditions are inferred from the Al_2O_3/TiO_2 ratio of the clay fraction of Estonian carbonate rocks of the Baltoscandian sedimentary Basin. The Late Ordovician climate of the Fennoscandian Shield was mainly semi-humid with several humid pulses in the Sandbian, mid-Katian and Hirnantian. The post-Hirnantian climate was fluctuating between humid and arid until stable humid conditions were established in the Middle and early Late Llandovery. Starting from the latest Llandovery, the climate turned semi-arid and arid. The Ordovician–Silurian long-term trend toward aridity was caused by the equator-ward drift of the Baltica plate. Shorter-term fluctuations of Al_2O_3/TiO_2 reflect climate changes of the global extent.

1. Introduction

The climate during the Ordovician and Silurian fluctuated strongly due to several glaciations. Besides the widely known Late Ordovician glaciations several Early and Middle Ordovician glaciations have been suggested (Turner et al., 2011, 2012). Paleotemperature, oceanic circulation, extinctions of fauna, variations in sea level and lithology have been used to describe the Ordovician and Silurian environmental changes (see Munnecke et al., 2010 for a review). The tropical temperatures (Trotter et al., 2008) and atmospheric pCO_2 (Berner and Kothavala, 2001) were high in the Early Ordovician, declining in the Middle Ordovician. Several numerical climate models suggest glaciation at south pole despite the high pCO_2 (Herrmann et al., 2004; Nardin et al., 2011). The present study is focused on fluctuations in arid–humid conditions during the transition into icehouse in the Late Ordovician, recovery in the post-Hirnantian and transition to glaciations in the Silurian. The study is based on geochemistry of the terrigenous clay fraction of Estonian sedimentary carbonate rocks. The Al_2O_3/TiO_2 (hereinafter referred to as Al/Ti) ratio of the clay fraction is used as a proxy for weathering and climate in the Fennoscandian Shield, the provenance of clay for the Estonian shelf situated in the NE part of the Baltoscandian carbonate Basin (Fig. 1).

The mineralogy and chemistry of a terrigenous sediment depend on the composition of parent rock and the weathering conditions related to the amount of rainfall, temperature and topography (Ronov and Migdisov, 1965; Singer and Galan, 1984; Curtis, 1990; Young and Nesbitt, 1998; Van de Kamp, 2010). The initially heterogeneous weathering products are mixed and homogenized during erosion and transport, and finally differentiated in the sedimentary basin according to the grain size. Studying the distribution of Al and Ti in Palaeozoic rocks of the East European Platform, Ronov and Migdisov (1965) concluded that the Al/Ti ratio of the clay fraction was preserved in sedimentary basins, as Ti and Al were bound together in the clay-forming process. Both Al and Ti are immobile elements in near-neutral conditions, but their migration diverges with pH of the environment. Aluminum goes into the solution at pH<4 and pH>10, whereas Ti is mobile at pH<2. In clays Ti can replace Al in the crystal lattice, depending on the intensity of chemical weathering (Akul'shina, 1976). Temperature and precipitation determine the intensity of chemical weathering being greater in humid climate and weaker in arid climate (Van de Kamp, 2010). Correspondingly lower or higher Al/Ti ratios have been recorded in recent marine sediments of the South China Sea (Wei et al., 2004) and Indian lake sediments (Warrier and Shankar, 2009).

Investigating different geological sections, including the formations with coal interbeds pointing to humid and evaporates assigned to arid climate, Akul'shina (1976) elaborated empirical relationship for the Al/Ti ratio and climate: Al_2O_3/TiO_2<20 for humid, 20–30 for semi-humid and semi-arid, and >30 for arid climate. This gradation is used in the present work as a reference for estimating paleoenvironmental conditions. We presume that during the studied time interval the Fennoscandian Shield had a stable average rock composition that was subjected to weathering. The parent rock may have had a local imprint on the chemical composition of the clay that formed, but during erosional mixing an average composition was achieved. When

* Corresponding author.
E-mail address: enli.kiipli@gi.ee (E. Kiipli).

0031-0182/$ – see front matter © 2012 Elsevier B.V. All rights reserved.
http://dx.doi.org/10.1016/j.palaeo.2012.10.001

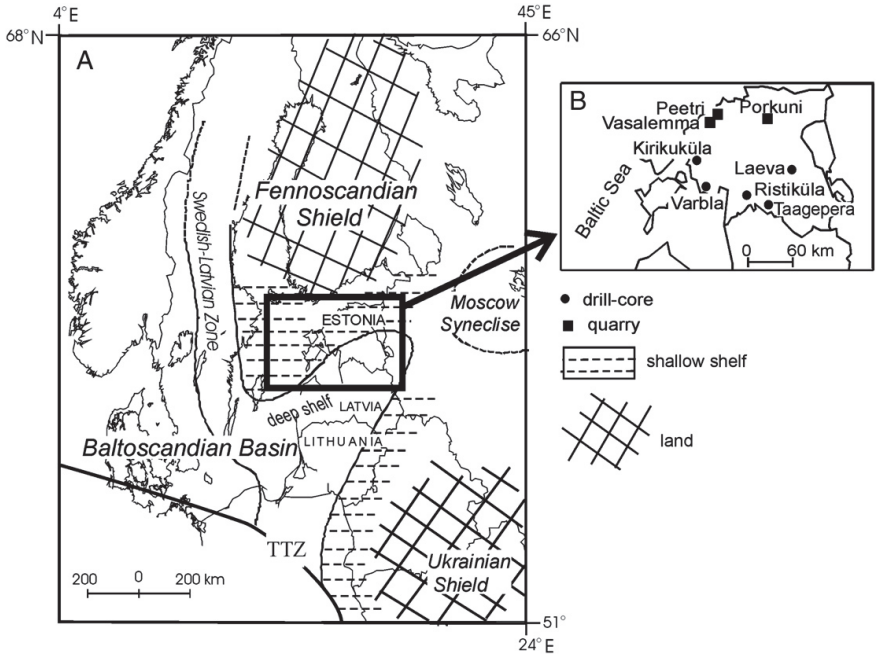

Fig. 1. Location map with paleogeographic setting (A) and sampled sections of Estonia (B).

climate changes, the local compositional differences in clay chemistry, particularly the Al/Ti ratio, change simultaneously in the same direction, resulting in a new average. The comparison between temporally different averages allows to state alterations in weathering conditions. As the weathering area was mainly the same through Ordovician–Silurian, the study gives comparable results.

The Al/Ti ratio of clay is juxtaposed with Baltica's drift from high to low latitudes, global glaciation events, and contemporaneous lithological features of the Estonian shelf to differentiate between regional and global climate changes.

2. Geological background and materials

During the Ordovician and Silurian the Baltica Plate drifted toward the equator, crossing southerly mid- and low-latitude climatic zones. The drift was temporarily interrupted due to the Baltica–Laurentia collision in the middle of Silurian (Torsvik et al., 1992, 1996; Cocks and Torsvik, 2005). Although the investigated clay fraction is extracted from the carbonate rock of sedimentary Baltoscandian Basin, it characterizes weathering in a wide area of the Fennoscandian Shield with conceivable center about thousand kilometers away from the Basin. The Finnish Precambrian area consists of Svecokarelian micaceous schists and gneisses, plutonic rocks such as gneissose granodiorites and quartz diorites with minor bodies of mafic peridotites, gabbros and quartz-gabbros, and Vyborg rapakivi granite at the SE border of the Shield (Simonen et al., 1997). These rocks were the main source of terrigenous sediments for the Estonian shelf. To the central part of the Baltoscandian Basin the terrigenous material may have reached from different directions by currents (Kiipli et al., 2009a) making it difficult to follow the climate development, thereby only shelf sediments were used for clay extraction. Limestone, marlstone and dolomite with admixture of siliciclastics are the main sedimentary rock types in the Estonian shelf. Limestone spreads in the shallowest area, marlstone in the transitional and claystone in the deep shelf. Coastal sand facies is absent, probably swept away. In late Silurian the amount of mica in the carbonate rocks gradually increased (Viiding et al., 1983) pointing to the influence of the rising Caledonian mountains. The existence of the Ordovician–Silurian Baltoscandian carbonate Basin ended in the latest Silurian.

The Estonian cores were chosen for study assuming that the main portion of terrigenous matter had a single provenance. The main part of the Ordovician and lower Silurian samples came from the Laeva-13 drill core (hereinafter referred to as Laeva), with additional samples from other cores and quarries (Fig. 1).

3. Methods

The samples were treated with 1 N HCl solution to remove the carbonate portion of the rock. The insoluble residue of the samples of the Laeva core was analyzed for grain size with laser sedigraph Horiba. The clay fraction < 1 μm was separated by settling the siliciclastic suspension for 24 h in a 10-cm water column. Material that did not settle to the bottom – the clay fraction – was centrifuged, dried and used for chemical and mineralogical analyses. Pressed clay powder pellets were subjected to XRF analysis using the Bruker AXS S-4 spectrometer. The grain size of the material, less than 1 μm, was favorable for XRF measurements, producing reliable reflections for all measured elements. Concentration of elements was calculated using the standard software "MultiRes" from Bruker AXS. The relative standard deviation of major components was 0.2–0.9% (calculated from 8 measurements of inhouse reference material Es-1), that of Al_2O_3/TiO_2 ratio was 0.8%. Clay minerals were determined in selected samples on the basis of XRD analysis. The proportion of clay and grain fraction in the studied samples varies significantly (Fig. 2). Titanium concentrates preferably in fine-grained silt fraction, while Al is most abundant in clay (Fig. 3). To retain fingerprints of chemical weathering and avoid grain size effects on the Al/Ti ratio only clay fraction was used in the present study.

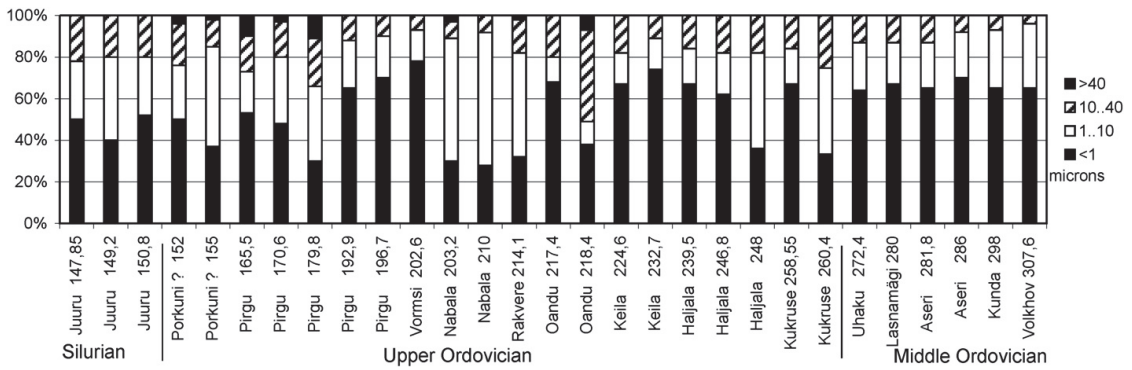

Fig. 2. Grain-size composition of insoluble residue of the Ordovician and Silurian samples from the Laeva-13 core, calculated according to the sedigraph grain-size analyses.

4. Results

Grain size analysis of the Laeva core revealed that most of the siliciclastic material in carbonates can be termed as 'mud', i.e. consisting of clay and silt. A small part of fine sand occurs in the Oandu, Pirgu and Porkuni stages. The content of clay in the insoluble residue varies from 27 to 77% (Fig. 2). Clay minerals are composed of terrigenous illite with some chlorite admixture. In Ordovician clays the content of chlorite is below 20%, in Silurian clays 20–25% (Viiding et al., 1983). Authigenic minerals, such as very fine-grained quartz (Fig. 4, indexes 1a and 1b), corrensite (Fig. 4, index 2) and hematite in association with goethite (Fig. 4, index 3), occur at some stratigraphic levels. Two intervals of extra high silica values were indicated at depths around 250 and 70 m, both caused by addition of dispersed fine-grained authigenic quartz. The lower excursion corresponds to the lower Haljala silica sponge *Pyritonema* occurrence found in wide areas from Estonia to Russia (Männil, 1966); the Aeronian increase corresponds to chert recorded in many geological sections of Estonia (Kiipli et al., 2004). The content of MgO reaches 11% in the Late Ordovician Pirgu Stage. XRD analyses reveal chlorite–smectite, corrensite, as a carrier of Mg. Corrensite occurs also in K-bentonites, the layers of altered volcanic ash, of the transitional zone between deep and shallow shelf (Hints et al., 2006). As the K-bentonitic clay forms *in situ*, the corrensite in the whole rock is of authigenic origin as well. The authigenic minerals do not affect Al/Ti ratio of the terrigenous clay component.

Terrigenous rather uniform illitic composition of clay is not very effective for tracking the climatic variations of the investigated time-span in the Fennoscandian Shield. The Al/Ti ratio of clay as a proxy for the weathering intensity is more sensitive indicator revealing fluctuations at several stratigraphic levels, which can be interpreted as changes in weathering conditions in the provenance region. These levels mostly do not coincide with those where authigenic minerals influence the chemical composition, showing that different processes drive the formation of authigenic minerals in the sedimentary basin and the Al/Ti ratio of terrigenous clays (Fig. 4).

The composite section (Fig. 5A) shows a long-term Al/Ti trend in average values from about 20–25 in the Ordovician to 25–32 in the Silurian. This trend is disrupted by four intervals with values below 20: in Sandbian, Katian, Hirnantian (Upper Ordovician) and lower Silurian. The Hirnantian sediments (Fig. 5 v) reveal Al/Ti values around 18. The post-Hirnantian values at first rise rapidly and decrease after that, reaching the lowest values in the Middle and lower Late Llandovery. The Al/Ti low of the Middle Llandovery occurs in thick deposits of cryptocrystalline limestone of the Raikküla Stage. A similar decrease in the ratio characterizes the mid-Katian with minimal Al/Ti values in the Rakvere Stage and Saunja Formation of the Nabala Stage, both represented by cryptocrystalline limestone as well. The uppermost Llandovery (Silurian) reveals an increase in Al/Ti up to 30, staying within the limits of 25–32 in the Wenlock and early Ludlow. In the Wenlock and Ludlow wide distribution of sedimentary-diagenetic

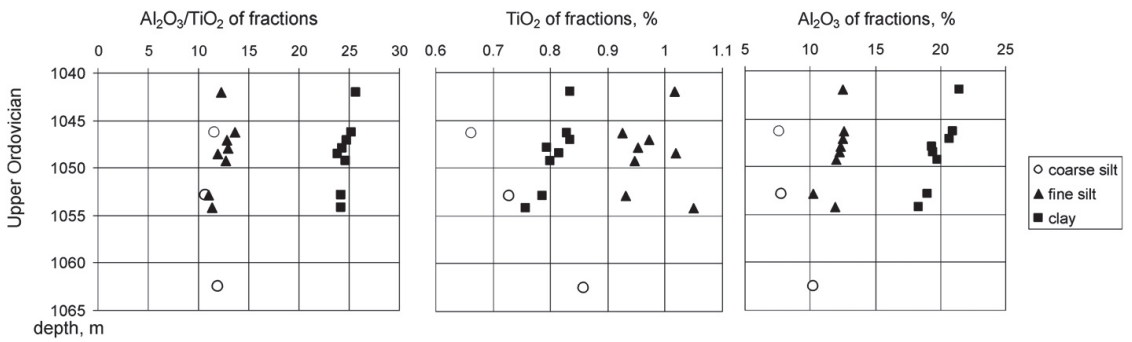

Fig. 3. Content of Al_2O_3 and TiO_2 and their ratio in coarse silt, fine silt and clay of the insoluble residue of the Aizpute-41 core (W Latvia) showing different distribution of the elements in fractions.

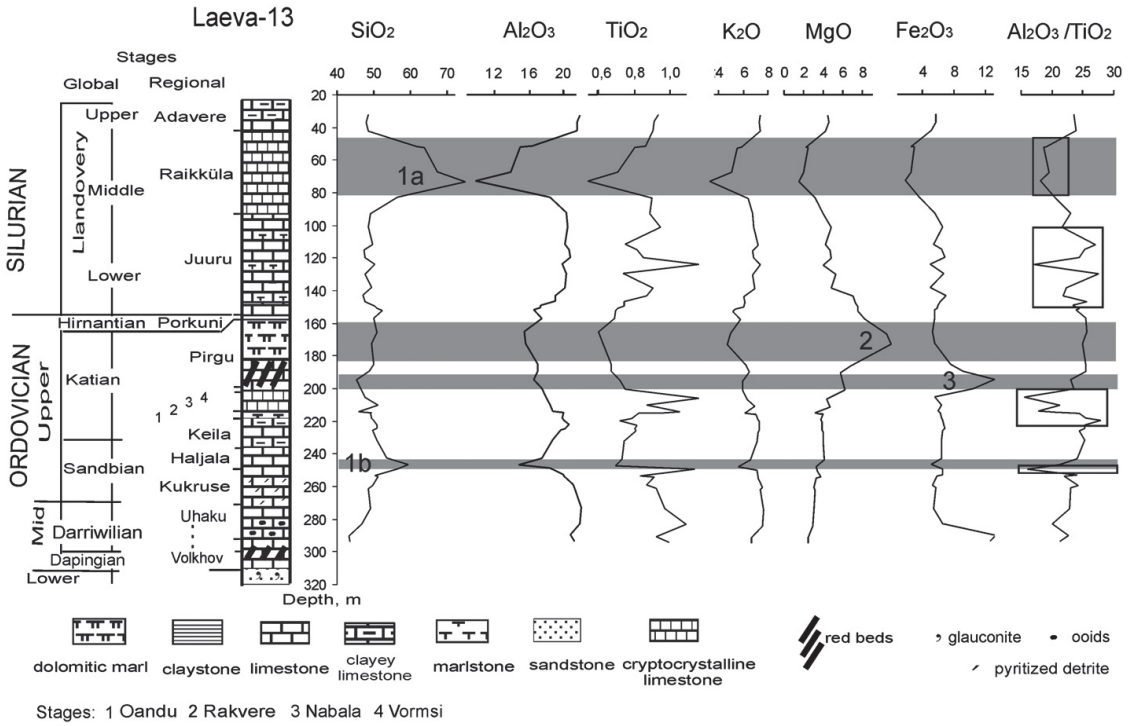

Fig. 4. Geological section of the Laeva-13 core and vertical distribution of major elements (%), and Al_2O_3/TiO_2 ratio of the clay fraction. Gray shadings show the intervals where admixture of authigenic minerals influences the chemical composition: 1a and 1b—quartz, 2—corrensite, 3—hematite. Boxes point to Al_2O_3/TiO_2 excursions.

dolostones on the Estonian shallow shelf (Kiipli et al., 2011) indicates arid climate being in good accordance with high Al/Ti ratios (Fig. 5 x).

5. Discussion

5.1. The basic lines of model

According to the moderately low Al/Ti values, the Ordovician climate of the Fennoscandian Shield was mainly semi-humid (Fig. 5A). Humid pulses in Late Ordovician and early Silurian, interrupting the semi-humid conditions, show intervals of relatively intense chemical weathering, though not intense enough to influence the clay mineralogy. The late Silurian climate was semi-arid and arid without humid pulses, indicating uniform weaker chemical weathering.

We tested the compatibility between the data on weathering intensity in the Fennoscandian Shield, most characteristic lithological features of adjacent sedimentary Baltoscandian Basin, Gondwana glaciations, and climate zones which Baltica crossed during its drift (Fig. 5). The movement of Baltic Craton is based on paleomagnetic data, with Oslo, Norway as the reference location (Torsvik et al., 1996). The uncertaince of the location varies from 5° to 25° latitude, mainly around 5°. The given track is reliable, although, based on the present investigation, the most equator-ward positions in the middle of Silurian seems too close to the equator. The lithology, mainly the illitic composition of clay within the carbonate rocks of Baltoscandian Basin, does not suit with the tropical wet climate characteristic of low latitudes. Kaolinite, the index of strong weathering, does not appear before the Devonian in the Estonian geological sections. Also, the great number of K-bentonites reached from the west with westerly winds do not support the position of Baltic shelf within the low-latitude belt of trade winds. In the Timan–Petchora Basin, NW from the Fennoscandian Shield, the Late Ordovician–Llandovery section consists of dolostones (Baarli et al., 2003; Antoshkina, 2004) indicating arid, not wet equatorial climate belt. We therefore shifted the mid-Silurian track of Baltoscandia's movement toward higher latitudes about 10° in comparison with the positions given by Torsvik et al. (1996) (Fig. 5B). The Baltica drifted from temperate to tropical climate, from the Ferrel to the Hadley cell. The stability of climate in this transitional zone depends on how constant the boundary between tropical and midlatitude belt is. The terminus of the tropical Hadley circulation is determined by planet radius and rotation rate, and many less stable variables, among which the temperature is the most important one (Seidel et al., 2008; Schneider et al., 2010). The temperature-dependent aquaplanet model by Levine and Schneider (2011) is therefore used to show the Hadley terminus (Fig. 5B). When dealing with geological past, different size and location of cratons, oceanic circulation *etc.* complicate the climate study. Nevertheless, some general considerations can be listed: proceeding from the Clausius–Clapeyron relation in which the water holding capacity of air is an exponentially increasing function of temperature, the zonally and annually average global precipitation increases in times of global warm climate and decreases in cold climate (Rind, 2000). During the rise of global temperatures the temperate and polar areas will get more precipitation, while the subtropical regions suffer from increased aridity. The model simulation of the present-day warming predicts that tropical wet regions should get wetter and dry regions dryer (Wentz et al., 2007). At the transition from warm to cold Earth the climate changes *vice versa*. The cold Earth, icehouse, means permanent ice in polar region, the cool Earth is without direct evidences of permanent ice (Royer, 2006), and the warm or hothouse world is without ice sheets. In highly cold and hot worlds temperature gradient between the pole and equator diminishes, the Hadley cell weakens

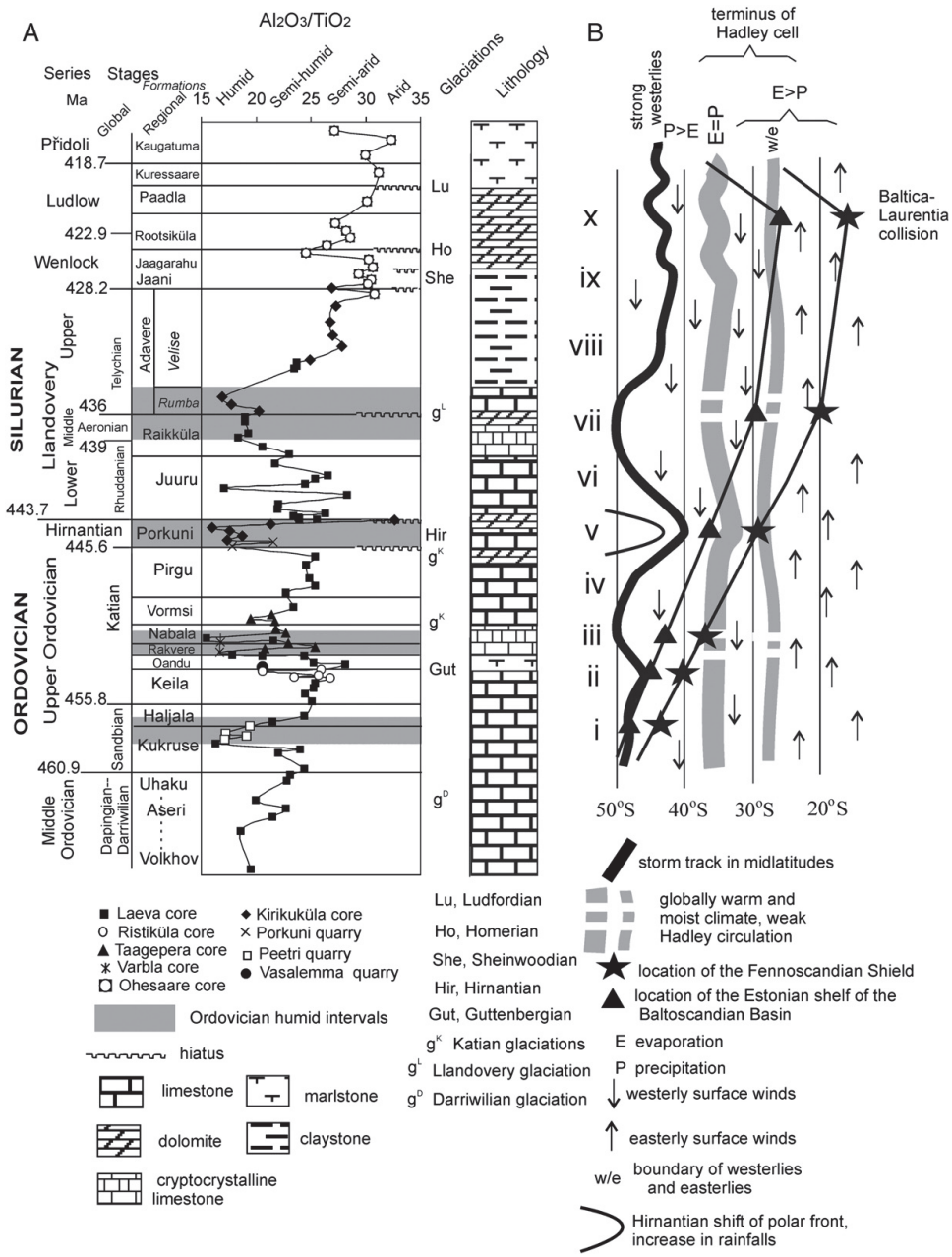

Fig. 5. (A): Ordovician–Silurian composite of Al_2O_3/TiO_2 ratio of the clay fraction of Estonian samples, and lithology in the Estonian shelf of the Baltoscandian Basin. (B): schematic movement of the Estonian shelf and Fennoscandian Shield in accordance with the drift of the Baltic Craton from mid- to low latitudes, the counter-clockwise rotation taken into account. Arid–humid gradation of Al_2O_3/TiO_2 from Akul'shina (1976). Correlation of regional and global stages by Nõlvak et al. (2006) and Nestor (1990). Drift of the Baltic Craton after Torsvik et al. (1996) with compiled 10° southward shift of the track in the late Silurian. 'g^{K}'—Katian ice-sheets in Gondwana by Loi et al. (2010); 'g^{D}'—Darriwilian glaciation by Turner et al. (2012); and 'g^{L}'—Llandovery glaciation (Azmy et al., 1998; Melchin and Holmden, 2006).

(Levine and Schneider, 2011) and weak winds occur in subtropics and tropics. In Fig. 5B the temperate Ferrel cell and two components of the Hadley terminus – the evaporation–precipitation equity and boundary between westerly winds and easterly trade winds – are shown, as they affected most the region under consideration during the Late Ordovician and Silurian. The temperature interval between 280 and 300 K was used. It incorporates the present-day average global temperature 288 K and the Late Ordovician and Silurian temperatures,

with highest values for the warm and lowest for the cold world. The Ordovician temperature is based on the study by Trotter et al. (2008) giving the average tropical temperatures near-modern for the Katian and 5 to 10 °C lower for the Hirnantian. Recently, Pucéat et al. (2010) questioned the methodology of Trotter et al. (2008), but did not give new temperatures for the Early Palaeozoic saying that a secular trend in oxygen isotope composition occurred. Both components of the Hadley cell terminus have rather conservative position at the range of 280 and 300 K, as the temperature-dependent shift is less than 5° latitude (Levine and Schneider, 2011) (Fig. 5B). The midlatitude storm track with the strongest westerlies and rainfalls oscillates in wider limits. It shifts equator-ward when the global climate is cold, and pole-ward when it is warm. Toggweiler and Russell (2008) give the storm track position at 45° to 50° S in the modern world, and 7–10° N during the last glacial maximum. Very wide shift of climate belts for the Late Triassic in the western Tethys margin is suggested by Berra et al. (2010). Their proposed oscillation of the arid belt of the Hadley cell was more than 10° of latitude between the cold and warm Earth. The present study reveals some particular times when the conservative estimates of climate boundaries according to the aquaplanet model of Levine and Schneider (2011) are not applicable. The intervals in the Katian, Hirnantian and Llandovery of lowest Al/Ti values point to rapid rearrangement of global climate and, probably, large shifts in climate belts (Fig. 5B).

5.2. The Sandbian–Katian

Midlatitude strong westerlies controlled the climate in the Sandbian and early Katian. At the Kukruse and Haljala times the Fennoscandian Shield and Baltoscandian Basin were situated at the storm track, which brought rainy weather to Fennoscandia and caused intense chemical weathering, as shown by the decreased Al/Ti ratio (Fig. 5 i). K-bentonites are numerous in the Baltoscandian geological sections indicating westerly winds typical for the temperate climate zone (Torsvik and Rehnström, 2003). In the mid-Katian a positive excursion of carbon (Saltzman and Young, 2005) and oxygen isotopes (Buggisch et al., 2010) has been considered as an indicator of glaciation at south pole (the Guttenbergian glaciation), corresponding to the end of the Keila Stage in the Baltoscandian region (Ainsaar et al., 1999) (Fig. 5 ii). The Al/Ti ratio shows minor oscillation responding to the Guttenbergian glaciation and a large decrease and variation of Al/Ti ratio following the glaciation event (Fig. 5 iii). Probably, the postglacial global warming caused world-wide humid conditions and increase in precipitation in the Fennoscandian Shield. Cryptocrystalline limestones of the Rakvere and Nabala stages in the Estonian shelf support the idea about climate warming, as the formation of large amount of lime mud needs warm waters. Global warmth caused the pole-ward retreat of the westerly storm track. Absence of volcanic ashes in the geological sections of the eastern part of the Baltoscandian Basin may evidence weakened winds, as K-bentonites present in Scania (Lashkovas, 2000) and Bornholm (Kiipli et al., 2009b) indicate volcanic activity, but ashes did not reach the eastern areas.

The Fennoscandian Shield entered the subtropics and climate turned more arid in the late Katian (Fig. 5 iv). Loi et al. (2010) suggest two glaciations, one at the *barbata* chitinozoan biozone in middle of the Katian corresponding to the Vormsi Stage, and the second at the end of the Katian, 447 Ma, corresponding to the upper Pirgu Stage and taking place after the Boda warming event. In the Pirgu time the dolomitization of the Yaroslavskaya Series in the adjacent Russian Platform, and sulfate accumulation in the Pechora Basin (Nikishin et al., 1996; Antoshkina, 2004) indicate arid climate. Scattered dolomite addition in limestones up to 30% is characteristic of carbonates in the Estonian and West-Latvian sections (Kiipli and Kiipli, 2006). In the Fennoscandian Shield the chemical weathering weakened shown by the rise of Al/Ti ratio. Views on the global temperatures for late Katian differ—cool climate (Cherns and Wheeley, 2007) and warm climate of the Boda event (Fortey and Cocks, 2005; Armstrong et al., 2009) have been suggested. The data of the present investigation do not allow to distinguish the late Katian glaciations and warming events. Gradual drying shown by Al/Ti increase suggests that weathering in the dry belt of the Hadley terminus near 30° S, where the Fennoscandian provenance was located, might have been stationary and independent of the short-term global climate warming or cooling. Though, Al/Ti rise during the Vormsi time, following the Rakvere and Nabala humid pulses, points to global climate change and may affirm the small-scale glaciation suggested by Loi et al. (2010).

5.3. The Hirnantian

A decrease in temperature lead to the Hirnantian glaciation, the most prominent climatic event in the end-Ordovician (Brenchley et al., 1994). Data from Canadian Anticosti Island show fluctuation of tropical temperatures in the latest Katian around 33–38 °C (Finnegan et al., 2011) and a 5–10° fall in the Hirnantian (Trotter et al., 2008; Finnegan et al., 2011). According to general considerations, the global climate of peak glaciation is cold and dry, but the Hirnantian Al/Ti data obtained from Estonian samples (Fig. 5 v) reveal humid conditions, despite the location of the Fennoscandian Shield at the dry subtropical latitude 30° S. In cold global climate the midlatitude precipitation maximum is farther equatorward than the storm track (O'Gorman and Schneider, 2008)—a shift of cold polar front toward low latitudes has been inferred from cool-water faunal migration toward tropics in the Hirnantian (Vandenbroucke et al., 2009, 2010). Approach of the storm track suggests increase in precipitation in the Fennoscandian Shield. Also, the Hirnantian ice-age consisted of several waxing and wanings of ice sheets in Gondwana (Ghienne, 2003; Loi et al., 2010). Unconformities bound and intersect the Porkuni Stage in the Baltoscandian Basin (Hints et al., 2010) corresponding to eustatic regressions and, probably, more severe climate conditions in the south pole. The preserved sediments of the Porkuni Stage correspond to modest transgressions and temporary warmings within longer glaciation period and thereby reflect oscillating, not steady state cold and dry climate. Mineralogical investigation also supports the idea about intense weathering in the Hirnantian. The study has revealed an Upper Ordovician more mature composition of the sand fraction extracted from the Estonian carbonate rock (Viiding et al., 1983). The Sandbian K-feldspar/quartz ratio 2:1 decreases to 1:4 in the Hirnantian, which can be considered as an indication of increase in weathering intensity. Nevertheless, the dolomitic interlayers in Estonian geological sections reveal temporary aridity, and small coral reefs point to warm waters. Better understanding of the Hirnantian climate needs further investigations.

5.4. The early Silurian

Following the Hirnantian glaciation, the beginning of Silurian reveals large-scale and rapid climatic variations in the Fennoscandian Shield, as the Al/Ti ratio oscillates largely (Fig. 5 vi). By the Middle and early Late Llandovery (Fig. 5 vii) the Al/Ti ratios stabilize and show humid climate in the Shield. For the Aeronian, Middle Llandovery, the ice-free world is considered on the ground of $\delta^{18}O$ value −1‰ of the ocean water, inferred from 'clumped isotopes' (Finnegan et al., 2011). A short-term return of the glaciation took place in late Aeronian shown by a sedimentary gap and regression in most Estonian geological sections, and about 1‰ positive excursion in $\delta^{18}O$ of brachiopods indicating cooling (Azmy et al., 1998). In the early Telychian corresponding to the Rumba Formation the moist conditions returned to the Fennoscandian Shield together with high sea level in the Baltoscandian Basin (Johnson, 2006; Kiipli et al., 2010b). The Aeronian and early Telychian humid pulses may have the same reason as for the Katian humid interval—moisture increase at all latitudes due to global warming. At globally warm climate the

Hadley cell weakens. In the Middle Llandovery the sluggish seawater and air movement is shown by cryptocrystalline limestones in the Estonian–Latvian shelf, and black shales in the deep part of the Baltoscandian Basin. The humidity and warm temperatures together caused intense weathering in the Fennoscandian Shield, but the lack of kaolinite among terrigenous clay minerals points that chemical weathering was not the strongest.

5.5. The Late Llandovery

In the Late Llandovery Al/Ti ratio reveals semi-humid and later semi-arid climate in the Fennoscandian Shield (Fig. 5 viii). Global climate change was responsible for the abrupt end of humid conditions, corresponding to the Rumba/Velise Formation boundary. The Late Llandovery was transitional between the Aeronian warm and Sheinwoodian cold global states. The Hadley circulation, being weak in hothouse and icehouse climates, strengthened and weakened in accordance with temperature changes during the Telychian. The oscillation of warmer and cooler temperatures, persisting in subtropics until the Wenlock, is inferred from $\delta^{18}O$ of Estonian conodonts (Lehnert et al., 2010). The oscillation probably indicates temporary increase in temperature gradient between the pole and equator, corresponding strengthening of the Hadley circulation, activation of wind and subtropical drying. Numerous clouds of volcanic ashes came from the Scandinavian side to the eastern Baltoscandian Basin with westerly winds (Kiipli et al., 2008a,b, 2010a) whereas in the previous Aeronian only rare K-bentonite layers are recorded in the Estonian and Latvian geological sections. The sea-level stand was high in the Telychian at the beginning of the Velise time (Johnson, 2006; Kiipli et al., 2010b) suggesting mainly ice-free world. Later on, the high sea-level turned into gradually regressive trend evidenced by increasing Si/Al ratio in the Priekule drill core (Kiipli et al., 2010b), and ended with a hiatus comprising the upper *lapworthi–centrifugus* biozones of the latest Telychian (Loydell et al., 2003) speaking about formation of small ice sheets at the pole. Two superimposed processes – the shift of Fennoscandian Shield deeper into the desert zone and increased dryness due to temporary Hadley intensification – caused rearrangement of climate toward aridity during the Telychian, the increase in Al/Ti ratio being in compliance with this change (Fig. 5A viii).

5.6. The Wenlock and later Silurian

In the early Wenlock, at the beginning of Sheinwoodian glaciation (Fig. 5 ix), the temperatures in the Baltoscandian Basin decreased (Wenzel and Joachimski, 1996; Heath et al., 1998; Lehnert et al., 2010). The drift of Baltica toward the equator ended in the middle of Silurian as the Baltica and Laurentia cratons collided (Fig. 5 x) (Torsvik et al., 1996). The maximum dolomite occurrence of the Rootsiküla Stage, and the following replacement of dolomites by marlstones in the Kuressaare Stage and Přidoli Series, shows that in the latest Silurian the Baltoscandian Basin was back in temperate climate. The collision finished in the Ludlow and thereafter the merged Baltica–Laurentia drifted back toward higher latitudes (Torsvik et al., 1996). Though the Baltoscandian Basin shifted to the zone of westerly winds, the K-bentonites disappeared upward from the Rootsiküla Stage. Probably, the volcanism ended due to the thickening of the lithosphere in collision process.

The Sheinwoodian, Homerian and Ludfordian glaciations (Wenzel and Joachimski, 1996; Kaljo et al., 1997; Saltzman, 2005; Kiipli et al., 2010b; Lehnert et al., 2010; Cramer et al., 2011) caused oscillation of lithology, climate and sea level in the Baltoscandian Basin and elsewhere (Jeppsson, 1990; Jeppsson et al., 2006; Johnson, 2006). On the contrary, Al/Ti ratios during the Wenlock-to-Přidoli indicate more stable conditions than in the Late Ordovician–early Silurian, as humid pulses are not recorded in the Fennoscandian Shield. The Sheinwoodian to mid-Ludfordian sea was characterized by long-term moderate low stand with shorter-range sea level falls corresponding to peak glaciations (Kiipli et al., 2010b). The long-lasting low sea stand points to permanent smaller ice sheets at south pole responsible for cool global climate without warm humid intervals.

6. Conclusion

Two superimposed processes influenced the climate in the Fennoscandian Shield—long-term drift of the Baltic Craton from mid-latitudes toward the equator, and shorter-term global or regional climate changes. The Al/Ti of terrigenous clay reflects the overall trend toward weaker chemical weathering and dryer conditions in accordance with the drift of Baltica, thereby justifying the use of the ratio as an indicator of climate. The short-term climate changes are reflected in Al/Ti rapid fluctuations, mainly coinciding with or converging around climatically unstable periods of Ordovician glaciations. The midlatitude storm track influenced the climatic changes in the Sandbian and Hirnantian. In the Silurian the subtropical Hadley circulation governed the Fennoscandian Shield and Baltoscandian Basin. The humid pulses of middle Katian and Middle Llandovery show that climatic belts changed considerably at globally warm periods. Lithology of sedimentary rocks of the Baltoscandian Basin is compatible with climate in general. Several lithological features, *e.g.* K-bentonites, deposits of cryptocrystalline limestone, black shale in the deep shelf, or widespread dolomite, correspond to climatic peculiarities, such as lack or presence of wind, warmth, or aridity. A lot of new information about global and regional climate has been inferred from the Al/Ti ratio, and yet additional data from the Baltic region and other continents would be necessary to support or deny the given suggestions.

Acknowledgments

The work was financially supported by the Estonian Ministry of Education and Science grant SF0140016s09, and is a contribution to the International Geoscience Programme (IGCP) no. 591. Sampled cores come from the collection of the Institute of Geology at Tallinn University of Technology; Dr. L. Ainsaar is thanked for the Ristiküla core samples. Ms. S. Peetermann is thanked for the help with English. We are grateful to two anonymous reviewers.

References

Ainsaar, L., Meidla, T., Martma, T., 1999. Evidence for a widespread carbon isotopic event associated with late Middle Ordovician sedimentological and faunal changes in Estonia. Geological Magazine 136, 49–62.

Akul'shina, E.P., 1976. Methods for determining weathering conditions, sedimentation and post-sedimentary transformations according to clay minerals. In: Akul'shina, E.P. (Ed.), Glinistye mineraly kak pokazateli litogeneza (Clay Minerals as Indicators of Rock Forming Conditions). Nauka, Novosibirsk, pp. 9–37 (in Russian).

Antoshkina, A.I., 2004. Upper Ordovician in the Chernyshev Swell, Timan–northern Ural region. In: Hints, O., Ainsaar, L. (Eds.), 8th Meeting of the Working Group on the Ordovician Geology of Baltoscandia, May 13–18, 2004, Tallinn and Tartu, Estonia, WOGOGOB-2004 Conference Materials, Abstracts and Field Guidebook, Tartu, pp. 13–14.

Armstrong, H.A., Baldini, J., Challands, T.J., Gröcke, D.R., Owen, A.W., 2009. Response of the Inter-tropical Convergence Zone to Southern Hemisphere cooling during Upper Ordovician glaciation. Palaeogeography, Palaeoclimatology, Palaeoecology 284, 227–236.

Azmy, K., Veizer, J., Bassett, M.G., Copper, P., 1998. Oxygen and carbon isotopic composition of Silurian brachiopods: implications for coeval seawater and glaciations. Geological Society of America Bulletin 110, 1499–1512.

Baarli, B.G., Johnson, M.E., Antoshkina, A.I., 2003. Silurian stratigraphy and paleogeography of Baltica. In: Landing, E., Johnson, M.E. (Eds.), Silurian Lands and Seas: New York State Museum Bulletin, 493, pp. 3–34.

Berner, R.A., Kothavala, Z., 2001. GEOCARB III: a revised model of atmospheric CO_2 over Phanerozoic time. American Journal of Science 301, 182–204.

Berra, F., Jadoul, F., Anelli, A., 2010. Environmental control on the end of the Dolomia Principale/Hauptdolomit depositional system in the central Alps: coupling sea-level and climate changes. Palaeogeography, Palaeoclimatology, Palaeoecology 290, 138–150.

Brenchley, P.J., Marshall, J.D., Carden, G.A.F., Robertson, D.B.R., Long, D.G.F., Meidla, T., Hints, L., Anderson, T.F., 1994. Bathymetric and isotopic evidence for a short-lived Late Ordovician glaciation in a greenhouse period. Geology 22, 295–298.
Buggisch, W., Joachimski, M.M., Lehnert, O., Bergström, S.M., Repetski, J.E., Webers, G.F., 2010. Did intense volcanism trigger the first Late Ordovician icehouse? Geology 38, 327–330.
Cherns, L., Wheeley, J.R., 2007. A pre-Hirnantian (Late Ordovician) interval of global cooling — the Boda event re-assessed. Palaeogeography, Palaeoclimatology, Palaeoecology 251, 449–460.
Cocks, L.R.M., Torsvik, T.H., 2005. Baltica from the Late Precambrian to Mid-Palaeozoic times: the gain and loss of a terrane's identity. Earth-Science Reviews 72, 39–66.
Cramer, B.D., Brett, C.E., Melchin, M.J., Männik, P., Kleffner, M.A., McLaughlin, P.J., Loydell, D.K., Munnecke, A., Jeppsson, L., Corradini, C., Bruton, F.R., Saltzman, M.R., 2011. Revised correlation of Silurian provincial series of North America with global and regional chronostratigraphic units and $\delta^{13}C_{carb}$ chemostratigraphy. Lethaia 44, 185–202.
Curtis, C.D., 1990. Aspects of climatic influence on the clay mineralogy and geochemistry of soils, palaeosols and clastic sedimentary rocks. Journal of the Geological Society of London 147, 351–357.
Finnegan, S., Bergmann, K., Eiler, J.M., Jones, D.S., Fike, D.A., Eisenman, I., Hughes, N.C., Tripati, A.K., Fischer, W.W., 2011. The magnitude and duration of Late Ordovician–Early Silurian glaciation. Science 331, 903–906.
Fortey, R.A., Cocks, L.R.M., 2005. Late Ordovician global warming—the Boda event. Geology 33, 405–408.
Ghienne, J., 2003. Late Ordovician sedimentary environments, glacial cycles, and post-glacial transgression in the Taoudeni Basin, West Africa. Palaeogeography, Palaeoclimatology, Palaeoecology 189, 117–145.
Heath, R.J., Brenchley, P.J., Marshall, J.D., 1998. Early Silurian carbon and oxygen stable-isotope stratigraphy of Estonia: implications for climate change. In: Landing, E., Johnson, M.E. (Eds.), Silurian Cycles. Linkages of Dynamic Stratigraphy with Atmospheric, Oceanic and Tectonic Changes: New York State Museum Bulletin, 491, pp. 313–326.
Herrmann, A.D., Patzkowsky, M.E., Pollard, D., 2004. The impact of paleogeography, pCO_2, poleward ocean heat transport and sea level change on global cooling during the Late Ordovician. Palaeogeography, Palaeoclimatology, Palaeoecology 206, 59–74.
Hints, R., Kirsimäe, K., Somelar, P., Kallaste, T., Kiipli, T., 2006. Chloritization of Late Ordovician K-bentonites from the northern Baltic Palaeobasin—influence from source material or diagenetic environment. Sedimentary Geology 191, 55–66.
Hints, L., Hints, O., Kaljo, D., Kiipli, T., Männik, P., Nõlvak, J., Pärnaste, H., 2010. Hirnantian (latest Ordovician) bio- and chemostratigraphy of the Stirnas-18 core, western Latvia. Estonian Journal of Earth Sciences 59, 1–24.
Jeppsson, L., 1990. An oceanic model for lithological and faunal changes tested on the Silurian record. Journal of the Geological Society of London 147, 663–674.
Jeppsson, L., Eriksson, M.E., Calner, M., 2006. A latest Llandovery to latest Ludlow high-resolution biostratigraphy based on the Silurian of Gotland—a summary. GFF 128, 109–114.
Johnson, M.E., 2006. Relationship of Silurian sea-level fluctuations to oceanic episodes and events. GFF 128, 115–121.
Kaljo, D., Kiipli, T., Martma, T., 1997. Carbon isotope event markers through the Wenlock–Přidoli sequence at Ohesaare (Estonia) and Priekule (Latvia). Palaeogeography, Palaeoclimatology, Palaeoecology 132, 211–223.
Kiipli, E., Kiipli, T., 2006. Carbonate distribution in the East Baltic deep shelf in the Late Ordovician–Early Silurian. GFF 128, 147–152.
Kiipli, E., Kiipli, T., Kallaste, T., 2004. Bioproductivity rise in the East Baltic epicontinental sea in the Aeronian (Early Silurian). Palaeogeography, Palaeoclimatology, Palaeoecology 205, 255–272.
Kiipli, T., Orlova, K., Kiipli, E., Kallaste, T., 2008a. Use of immobile trace elements for the correlation of Telychian bentonites on Saaremaa Island, Estonia, and mapping of volcanic ash clouds. Estonian Journal of Earth Sciences 57, 39–52.
Kiipli, T., Soesoo, A., Kallaste, T., Kiipli, E., 2008b. Geochemistry of Telychian (Silurian) K-bentonites in Estonia and Latvia. Journal of Volcanology and Geothermal Research 171, 45–58.
Kiipli, E., Kiipli, T., Kallaste, T., 2009a. Reconstruction of currents in the Mid-Ordovician–Early Silurian central Baltic Basin using geochemical and mineralogical indicators. Geology 37, 271–274.
Kiipli, T., Kallaste, T., Kleesment, A., Nielsen, A., 2009b. Corroded hydrothermal quartz in Ordovician altered volcanic ash beds of the Baltoscandian Region. Estonian Journal of Earth Sciences 58, 268–272.
Kiipli, T., Kallaste, T., Nestor, V., Loydell, D.K., 2010a. Integrated Telychian (Silurian) K-bentonite chemostratigraphy and biostratigraphy in Estonia and Latvia. Lethaia 43, 32–44.
Kiipli, T., Kiipli, E., Kaljo, D., 2010b. Silurian sea level variations estimated using SiO_2/Al_2O_3 and K_2O/Al_2O_3 ratios in the Priekule drill core section, Latvia. Bolletino della Societa Paleontologica Italiana 49, 55–63.
Kiipli, T., Einasto, R., Kallaste, T., Nestor, V., Siir, S., Perens, H., 2011. Geochemistry and correlation of volcanic ash beds from Rootsiküla Stage (Wenlock–Ludlow) in the eastern Baltic. Estonian Journal of Earth Sciences 60, 207–219.
Lashkovas, J., 2000. The Sedimentation Environments of the Ordovician Basin in the South-western Margin of the East European Platform and Lithogenesis of Deposits. Institute of Geology, Vilnius . (314 pp.).
Lehnert, O., Männik, P., Joachimski, M.M., Calner, M., Frýda, J., 2010. Palaeoclimate perturbations before the Sheinwoodian glaciation: a trigger for extinctions during the 'Ireviken Event'. Palaeogeography, Palaeoclimatology, Palaeoecology 296, 320–331.
Levine, X.J., Schneider, T., 2011. Response of the Hadley circulation to climate change in an aquaplanet GCM coupled to a simple representation of ocean heat transport. Journal of the Atmospheric Sciences 68, 769–783.
Loi, A., Ghienne, J.-F., Dabard, M.P., Paris, F., Botquelen, A., Christ, N., Elaouad-Debbaj, Z., Gorini, A., Vidal, M., Videt, B., Destombes, J., 2010. The Late Ordovician glacio-eustatic record from a high-latitude storm-dominated shelf succession: the Bou Ingarf section (Anti-Atlas, Southern Morocco). Palaeogeography, Palaeoclimatology, Palaeoecology 296, 332–358.
Loydell, D.K., Männik, P., Nestor, V., 2003. Integrated biostratigraphy of the lower Silurian of the Aizpute-41 core, Latvia. Geological Magazine 140, 205–229.
Männil, R., 1966. Evolution of the Baltic Basin during the Ordovician. Valgus, Tallinn . (201 pp. (in Russian with English summary)).
Melchin, M.J., Holmden, C., 2006. Carbon isotope chemostratigraphy of the Llandovery in Arctic Canada: implications for global correlation and sea-level change. GFF 128, 173–180.
Munnecke, A., Calner, M., Harper, D.A.T., Servais, T., 2010. Ordovician and Silurian sea-water chemistry, sea level, and climate: a synopsis. Palaeogeography, Palaeoclimatology, Palaeoecology 296, 389–413.
Nardin, E., Goddéris, Y., Donnadieu, Y., Le Hir, G., Blakey, R.C., Pucéat, E., Markus Aretz, M., 2011. Modeling the Early Paleozoic long-term climatic trend. GSA Bulletin 123, 1181–1192.
Nestor, H., 1990. Table 2. Silurian stratigraphy of Estonia. In: Kaljo, D., Nestor, H. (Eds.), Field Meeting Estonia 1990, An Excursion Guidebook. Tallinn, pp. 24–25.
Nikishin, A.M., Ziegler, P.A., Stephenson, R.A., Cloething, S.A.P.L., Furne, A.V., Fokin, P.A., Ershov, A.V., Bolotov, S.N., Korotaev, M.V., Alekseev, A.S., Gorbachev, V.I., Shipilov, E.V., Lankreijer, A., Bembinova, E.Yu., Shalimov, I.V., 1996. Late Precambrian to Triassic history of the East European Craton: dynamics of sedimentary basin evolution. Tectonophysics 268, 23–63.
Nõlvak, J., Hints, O., Männik, P., 2006. Ordovician time-scale in Estonia: recent developments. Proceedings of the Estonian Academy of Sciences Geology 55, 95–108.
O'Gorman, P.A., Schneider, T., 2008. The hydrological cycle over a wide range of climates simulated with an idealized GCM. Journal of Climate 21, 3815–3832.
Pucéat, E., Joachimski, M.M., Bouilloux, A., Monna, F., Bonin, A., Motreuil, S., Morinière, P., Hénard, S., Mourin, J., Dera, G., Quesne, D., 2010. Revised phosphate–water fractionation equation reassessing paleotemperatures derived from biogenic apatite. Earth and Planetary Science Letters 298, 135–142.
Rind, D., 2000. Relating paleoclimate data and past temperature gradients: some suggestive rules. Quaternary Science Reviews 19, 381–390.
Ronov, A.B., Migdisov, A.A., 1965. Main features of the geochemistry of elements-hydrolysates in processes of weathering and sedimentation. Geochimiya 2, 131–157 (in Russian).
Royer, D.L., 2006. CO_2-forced climate thresholds during the Phanerozoic. Geochimica et Cosmochimica Acta 70, 5665–5675.
Saltzman, M.R., 2005. Phosphorus, nitrogen, and the redox evolution of the Paleozoic oceans. Geology 33, 573–576.
Saltzman, M.R., Young, S.A., 2005. Long-lived glaciation in the Late Ordovician? Isotopic and sequence-stratigraphic evidence from western Laurentia. Geology 33, 109–112.
Schneider, T., O'Gorman, P., Levine, X.J., 2010. Water vapor and the dynamics of climate changes. Reviews of Geophysics 48 (article Nr. RG3001).
Seidel, D.J., Fu, Q., Randel, W.J., Reichler, T.J., 2008. Widening of the tropical belt in a changing climate. Nature Geoscience 1, 21–24.
Simonen, A., Donner, J.J., Laikakari, I., 1997. Finland. In: Moore, E.M., Fairbridge, R.W. (Eds.), Encyclopedia of Europe and Asian Regional Geology. Chapman and Hall, London, pp. 230–236.
Singer, A., Galan, E. (Eds.), 1984. Palygorskite–sepiolite; Occurrences, Genesis and Uses. : Developments in Sedimentology, 37. Elsevier, Amsterdam (352 pp.).
Toggweiler, J.R., Russell, J., 2008. Ocean Circulation in a Warming Climate. Nature 451, 286–288.
Torsvik, T.H., Rehnström, E.F., 2003. The Tornquist Sea and Baltica–Avalonia docking. Tectonophysics 362, 67–82.
Torsvik, T.H., Smethurst, M.A., Van der Voo, R., Trench, A., Abrahamsen, N., Halvorsen, E., 1992. Baltica. A synopsis of Vendian–Permian palaeomagnetic data and their palaeotectonic implications. Earth-Science Reviews 33, 133–152.
Torsvik, T.H., Smethurst, M.A., Meert, J.G., Van der Voo, R., McKerrow, W.S., Brasier, M.D., Sturt, B.A., Walderhaug, H.J., 1996. Continental break-up and collision in the Neoproterozoic and Palaeozoic—a tale of Baltica and Laurentia. Earth-Science Reviews 40, 229–258.
Trotter, J.A., Williams, I.S., Barnes, C.R., Lécuyer, C., Nicoll, R.S., 2008. Did cooling oceans trigger Ordovician biodiversification? Evidence from conodont thermometry. Science 321, 550–554.
Turner, B.R., Armstrong, H.A., Holt, P., 2011. Visions of ice sheets in the Early Ordovician greenhouse world: evidence from the Peninsula Formation, Cape Peninsula, South Africa. Sedimentary Geology 236, 226–238.
Turner, B.R., Armstrong, H.A., Wilson, C.R., Makhlouf, I.M., 2012. High frequency eustatic sea-level changes during the Middle to early Late Ordovician of southern Jordan: indirect evidence for a Darriwilian Ice Age in Gondwana. Sedimentary Geology 251–252, 34–48.
Van de Kamp, P., 2010. Arkose, subarkose, quartz sand, and associated muds derived from felsic plutonic rocks in glacial to tropical humid climates. Journal of Sedimentary Research 80, 895–918.
Vandenbroucke, T.R., Armstrong, H.A., William, M., Zalasiewicz, J.A., Sabbe, K., 2009. Ground-truthing Late Ordovician climate models using the paleobiogeography of graptolites. Paleoceanography 24, PA 4202.
Vandenbroucke, T.R.A., Armstrong, H.A., Williams, M., Paris, F., Zalasiewicz, J.A., Sabbe, K., Nõlvak, J., Challands, T.J., Verniers, J., Servais, T., 2010. Polar front shift and atmospheric CO_2 during the glacial maximum of the Early Paleozoic Icehouse. Proceeding of the National Academy of Sciences of the United States of America 107, 14983–14986.
Viiding, H.A., Kleesment, A.E., Konsa, M., Heinsalu, H., Jürgenson, E., 1983. Evolution of the terrigenous component of sedimentary rocks of the southern slope of the Baltic

Shield. In: Viiding, H.A. (Ed.), Terrigenous Minerals of the Baltic Sedimentary Rocks. Academy of Sciences of Estonia, Tallinn, pp. 7–22 (in Russian).
Warrier, A.K., Shankar, R., 2009. Geochemical evidence for the use of magnetic susceptibility as a paleorainfall proxy in the tropics. Chemical Geology 265, 553–562.
Wei, G., Liu, Y., Li, X., Shao, L., Fang, D., 2004. Major and trace element variations of the sediments at ODP Site 1144, South China Sea, during the last 230 ka and their paleoclimate implications. Palaeogeography, Palaeoclimatology, Palaeoecology 212, 331–342.
Wentz, F.J., Ricciardulli, L., Hilburn, K., Mears, C., 2007. How much more rain will global warming bring? Science 317, 233–235.
Wenzel, B., Joachimski, M.M., 1996. Carbon and oxygen isotopic composition of Silurian brachiopods (Gotland/Sweden): palaeoceanographic implications. Palaeogeography, Palaeoclimatology, Palaeoecology 122, 143–166.
Young, G.M., Nesbitt, H.W., 1998. Processes controlling the distribution of Ti and Al in weathering profiles, siliciclastic sediments and sedimentary rocks. Journal of Sedimentary Research 68, 448–455.

III – Kiipli, T.; Kallaste, T.; Nielsen, A.; Schovsbo, N.; **Siir, S**. 2014. Geochemical discrimination of the Upper Ordovician Kinnekulle Bentonite in the Billegrav-2 drill core section, Bornholm, Denmark. *Estonian Journal of Earth Sciences*, **63**, 264–270.

Estonian Journal of Earth Sciences, 2014, **63**, 4, 264–270 doi: 10.3176/earth.2014.29

Geochemical discrimination of the Upper Ordovician Kinnekulle Bentonite in the Billegrav-2 drill core section, Bornholm, Denmark

Tarmo Kiipli[a], Toivo Kallaste[a], Arne T. Nielsen[b], Niels H. Schovsbo[c] and Sven Siir[a]

[a] Institute of Geology at Tallinn University of Technology, Ehitajate tee 5, 19086 Tallinn, Estonia; tarmo.kiipli@ttu.ee
[b] Natural History Museum of Denmark, University of Copenhagen, Øster Voldgade 5-7, DK-1350 Copenhagen, Denmark; arnet@snm.ku.dk
[c] Geological Survey of Denmark and Greenland, Øster Voldgade 10, DK-1350 Copenhagen, Denmark; nsc@geus.dk

Received 30 June 2014, accepted 16 September 2014

Abstract. The content of the trace elements Ti, Nb, Zr and Th has been analysed in 34 Upper Ordovician bentonites from the Billegrav-2 drill core, Bornholm, Denmark. The section contains two 80–90 cm thick bentonites, which potentially may represent the Kinnekulle Bentonite, as well as several rather thick but composite bentonite layers with thin terrigenous shale interbeds. Comparison of the four immobile trace elements with data from the Kinnekulle Bentonite reported from other locations in Baltoscandia indicate that the 80 cm thick bentonite between 88.30 and 89.10 m in the Billegrav-2 core represents this marker bed. The other thick (90 cm) bentonite in the Billegrav-2 core, exceeding the thickness of the Kinnekulle Bentonite, belongs to the Sinsen or uppermost Grefsen Series bentonites. Bentonites in the Grefsen Series frequently contain much higher concentrations of trace elements than the Kinnekulle Bentonite.

Key words: bentonites, Ordovician, Denmark, Kinnekulle.

INTRODUCTION

The lower part of the Upper Ordovician contains numerous altered volcanic ash layers in the Baltoscandian area, amongst them the unusually thick so-called Kinnekulle Bentonite, which represents one of the largest eruptions that has ever taken place during the Phanerozoic (Huff et al. 1992, 1996). After recognition of the volcanic origin of the clay-rich interbeds in the Ordovician of Scandinavia by Thorslund (1945), Hagemann & Spjeldnaes (1955) first applied these layers, in particular the thickest one (XXII), to correlation of sections. In North Estonia Jürgenson (1958) correlated five bentonite layers, including the thickest one (d) at the base of the Keila Stage. Männil (1966) correlated the thickest bentonite (XXII) in Scandinavia with the thickest one (d) in the East Baltic. Using these correlations, Vingisaar (1972) published the first distribution and thickness map of the 'main metabentonite' layer across the entire Baltoscandian area. Bergström et al. (1995) applied trace element geochemistry to correlation in combination with palaeontological data and thickness of the beds. Bergström et al. (1995) also named the thickest bed the 'Kinnekulle' K-bentonite.

In the Oslo Region, south-central Sweden and Estonia one of the bentonites in the Sandbian Stage (Upper Ordovician) is significantly thicker than the others, supporting correlation, whereas in Latvia and Lithuania all bentonites are thin and, hence, recognition of the Kinnekulle Bentonite is not possible without using chemical or mineralogical fingerprinting. In Scania, southernmost Sweden, the same problem was encountered by Bergström et al. (1997), as more than one thick bentonite occur in Kyrkbäcken and other sections, and identification of the Kinnekulle Bentonite is not straightforward.

In order to identify individual eruption layers, researchers have used phenocryst compositions of apatite (Batchelor 2009; Ray et al. 2011; Sell & Samson 2011), biotite (Batchelor 2003) and sanidine (Kiipli et al. 2007, 2010, 2011, 2012, 2014a; Männik et al. 2014). Separation of phenocrysts for analyses is, however, time-consuming and often phenocrysts are absent or altered to an extent that they cannot be properly identified. Therefore a series of immobile trace elements have been used for correlations (Huff et al. 1998; Inanli et al. 2009; Hetherington et al. 2011; Kiipli et al. 2013; Kaljo et al. 2014).

The aim of the present contribution is to demonstrate the possibilities and problems of geochemical identification of individual volcanic eruption layers and, if possible, to identify the Kinnekulle Bentonite in the Billegrav-2 drill core section on Bornholm, Denmark.

MATERIAL

Seventy-six geochemical samples were collected from the ca 12 m thick Sandbian part of the Billegrav-2 drill core (Figs 1, 2), Bornholm, Denmark. The Sandbian strata are resting unconformably on a thin Komstad Limestone (basal Dapingian) and are in turn overlain by grey and black shales of Katian age; these strata are locally on Bornholm assigned to the *Dicellograptus* Shale. The conspicuous feature of the Sandbian section is that ca 50% of the section is formed by volcanogenic sediment altered to clay, i.e. bentonite. The other 50% of the section is formed by grey, often silicified mudstone. The bentonites contain also much chert. The section includes two thick bentonites (80 and 90 cm) and also thick intervals where bentonite material dominates. These intervals are separated by only thin terrigenous mudstone interbeds.

The Billegrav-2 well (DGU 248.61) was drilled as part of a shallow drilling campaign conducted by the Geological Survey of Denmark and Greenland (GEUS) on southern Bornholm in August 2010. The well was fully cored and subsequently subjected to an extensive logging programme by GEUS in order to characterize the lithology, the water composition and the flow capacity of the fracture systems (Schovsbo et al. 2011).

LOGSTRATIGRAPHICAL UNITS IN BILLEGRAV-2

Pedersen & Klitten (1990) discerned 6 units (A–F) and 16 subunits based on the gamma-ray log pattern in water wells and scientific wells drilled on southern Bornholm. The log signature of the logstratigraphical units was expanded to also include the formation resistivity and the sonic velocity by Schovsbo et al. (2011). The bentonite-rich interval occurs within log unit D that corresponds to the *Dicellograptus* Shale of traditional Danish terminology (Fig. 2). The log zone is divided into subunits D1–D3 of which the D3/D2 boundary approximates the *Dicellograptus foliaceus*/*D. clingani* zonal boundary and the D2/D1 boundary approximates the top of the bentonite-rich interval (= Sularp Shale according to the terminology proposed by Lindström 1953; Bergström et al. 1999). This level corresponds to log unit D1 of Pedersen & Klitten (1990). Bergström & Nilsson (1974) correlated this part of the shale with the *D. multidens* [now *foliaceus*] Zone. This unit is much thicker in the Billegrav-2 core (ca 12 m) than at Læså (2.9 m, cf. Funkquist 1919). It is apparently about 1 m thinner in the Sømarken-2 well (see Pedersen & Klitten 1990, fig. 5).

LOG RESPONSE OF BENTONITE BEDS

The log readings of the formation resistivity and gamma ray in the bentonite-rich shale interval clearly indicate that the thick bentonite beds in the mid to upper part are characterized by low formation resistivity and high Gr values (Fig. 2). No clear log signature is seen in the lower part of the interval. This probably reflects that the bentonite–shale intercalations are thin and below logging resolution. The low resistivity of the bentonites probably reflects different clay

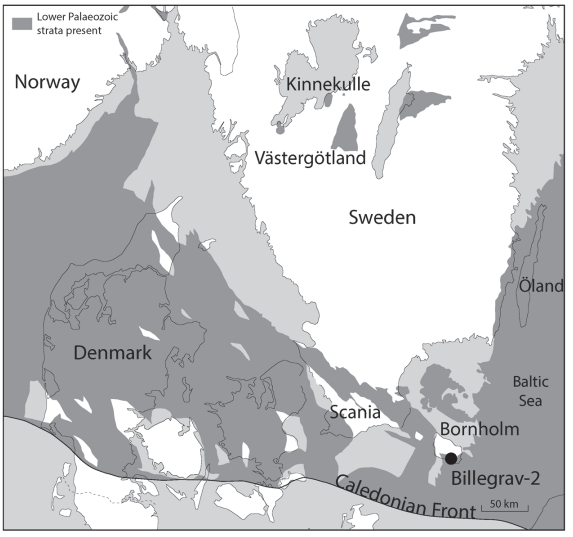

Fig. 1. Location of the Billegrav-2 drilling site and distribution of Lower Palaeozoic sediments in southern Scandinavia. Modified from Nielsen & Schovsbo (2011)

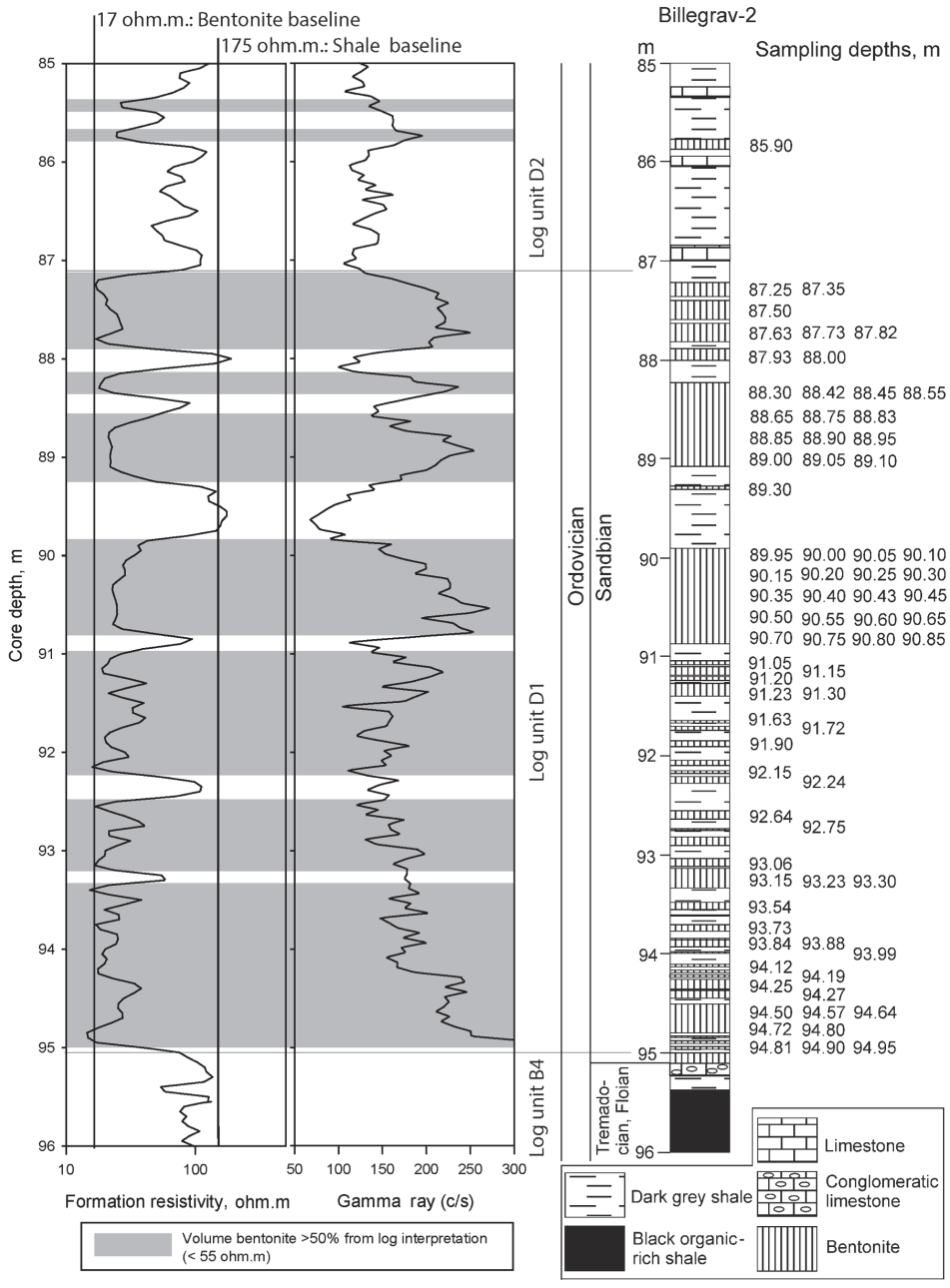

Fig. 2. Log data, lithology and sampling depths of the Billegrav-2 core section.

minerals with high cation exchange capacity, such as mix-layer clays compared with the inter-bedded shale that in part is silicified. The formation resistivity appears to be about 17 ohm.m for relatively pure bentonite and 175 ohm.m. for relatively pure shale.

LABORATORY METHOD

X-ray fluorescence analyses for determination of major chemical components and trace elements were made on a Bruker S4 Pioneer spectrometer. The X-ray tube with Rh-anode and maximum working power of 3 kW was used. Eight grams of fine powder (grains not larger than 50 μm) per sample were mixed with eight drops of 5% Mowiol solution and pressed. Pellets were dried for 2 h at 105 °C. The samples were measured and preliminary results were calculated by using the manufacture's standard methods MultiRes and GeoQuant. Ten international and in-house reference materials were used to refine analytical results by up to a few per cent of the concentration. The results are available in an electronic attachment at http://dx.doi.org/10.15152/GEO.6.

The results were compared with published geochemical compositions of the Kinnekulle Bentonite from Scandinavia and the East Baltic (Bergström et al. 1997; Kiipli et al. 2011; Batchelor 2014; Siir et al. 2015).

Four elements, Ti, Nb, Zr and Th, were used in searching for the Kinnekulle Bentonite as these have been shown to be immobile during conversion of volcanic ash to authigenic silicates (Kiipli et al. 2008, 2014b). Element ratios vs Al_2O_3 are used for comparison in order to eliminate the effects of different residual enrichment of immobile elements during conversion of volcanic ash to authigenic silicates (Kiipli et al. 2013).

HOMOGENEITY OF THE KINNEKULLE BENTONITE COMPOSITION

The most reliable average composition of the Kinnekulle Bentonite, based on analytical results from 13 laboratories worldwide (reference sample Es-15), is published by Kiipli et al. (2000). Sample Es-15 originates from the upper part of the Kinnekulle Bentonite in the Pääsküla exposure, North Estonia. There the Kinnekulle Bentonite contains abundant authigenic K-feldspar and 18–19% Al_2O_3. More frequently the Kinnekulle Bentonite consists predominantly of illite–smectite and contains 20–26% Al_2O_3, even up to 31% in a kaolinite-rich variety from the Valga core (Kiipli et al. 2007). In Scandinavia bentonites often contain some carbonate or chert diluting the immobile elements and in these cases the Al_2O_3 content may be as low as 14–17% (Batchelor 2014).

Average immobile element/Al_2O_3 ratios in the Kinnekulle Bentonite, calculated on the basis of 46 analyses from the East Baltic and Scandinavia, are as follows:

$$TiO_2 \times 10^4/Al_2O_3 = 122,$$
$$Nb \times 10^4/Al_2O_3 = 0.595,$$
$$Zr \times 10^4/Al_2O_3 = 8.26,$$
$$Th \times 10^4/Al_2O_3 = 0.648.$$

Data from the Fjäcka and Vasagård exposures are excluded from these calculations because they are deviating from the main data cluster (Fig. 3). These average values are used for comparison in Fig. 3. All element ratios in particular samples are divided by the average values for the Kinnekulle Bentonite. Figure 3A shows that the composition of particular samples of the Kinnekulle Bentonite in the East Baltic mostly does not differ from the average more than 1.2 times. In Scandinavian sections the deviation from the average can reach 1.4 times and in the Fjäcka and Vasagård sections the differences are 1.6–2.6 times.

IDENTIFICATION OF THE KINNEKULLE BENTONITE IN THE BILLEGRAV-2 SECTION

The comparison of Sandbian bentonites with the Kinnekulle Bentonite shows that other bentonites mostly have higher concentrations of Ti, Nb, Zr and Th (Fig. 3B). Zr concentrations are often especially high in the lower part of the Sandbian section in the Billegrav-2 core, showing up to 3.5 times higher values than in the Kinnekulle Bentonite. High contents of Zr characterize many bentonites of the Grefsen Series (Batchelor 2014), so the lower bentonites in the Billegrav-2 core likely belong to this series. Lower concentrations of elements compared with the Kinnekulle Bentonite are less frequent.

Eight of a total of 34 separate bentonite layers show geochemical similarity with the Kinnekulle Bentonite. Starting from below, the depths of these samples are: 93.88, 93.84, 92.75 and 91.90 m, inside the lower 90 cm thick bentonite at 90.0 and 90.45–90.60 m, inside the upper 80 cm thick bentonite at 88.55–88.95, 89.05–89.10, 87.5 and 87.25–87.35 m (Fig. 3B). Four layers in the lower part of the section are thin (1–4 cm) and alternate with high Zr layers and, hence, likely belong to the Grefsen Series. A relatively small part of the overlying thick bentonite between 89.95 and 90.85 m (25% e.g. five samples of a total of 20) is similar to the Kinnekulle Bentonite. The most likely candidate for the Kinnekulle Bentonite is the 80 cm thick bentonite between 88.30 and 89.10 m, revealing in nine of 13 samples closely similar compositions with the Kinnekulle Bentonite. Higher up the upper part of the thick composite bentonite layer between 87.25 and 88.00 m also exhibits some similarity with the Kinnekulle Bentonite.

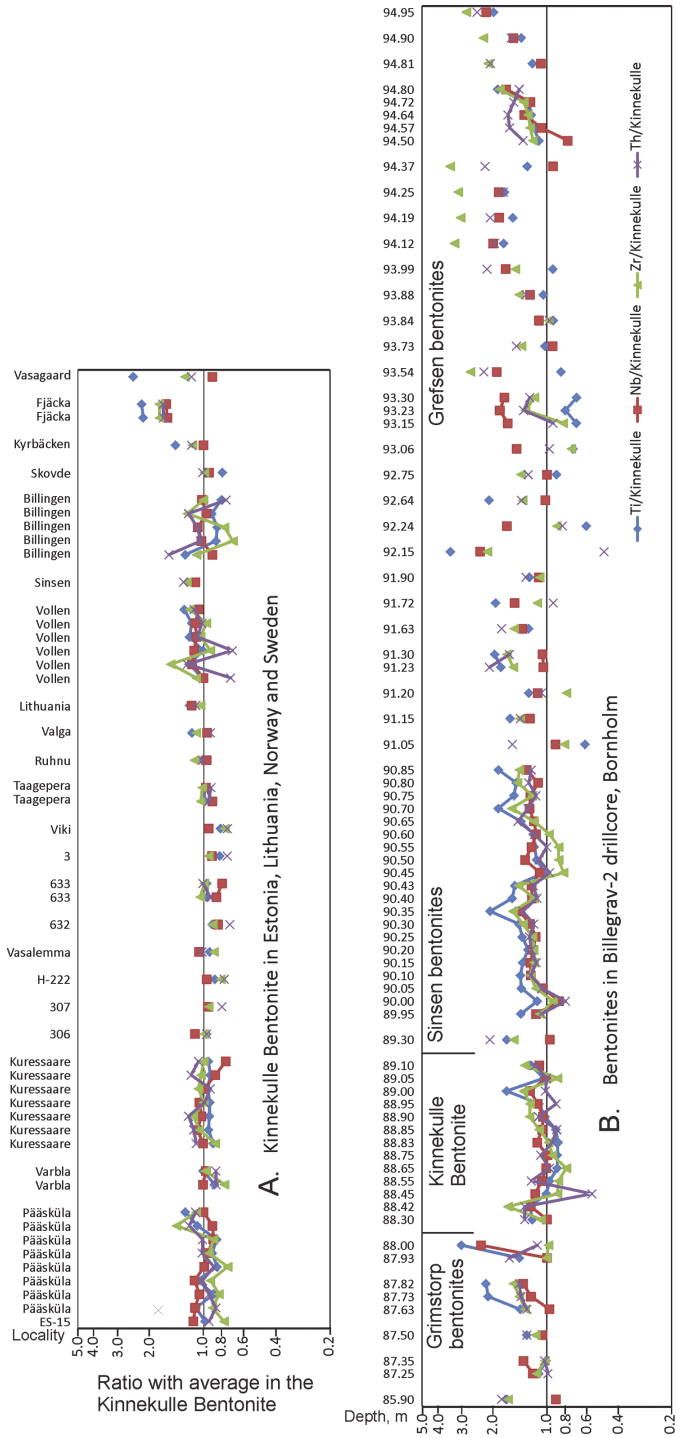

Fig. 3. Geochemical comparison of Ti, Nb, Zr and Th immobile element concentrations in the Kinnekulle Bentonite in the East Baltic and Scandinavia. **A**, reference data of the Kinnekulle Bentonite (Bergström et al. 1997; Kiipli et al. 2009, 2011; Batchelor 2014); **B**, comparison with bentonites from the Billegrav-2 section. All element/Al_2O_3 ratios are divided by the average of the Kinnekulle Bentonite. In the vertical scale 1 is the average value of the Kinnekulle Bentonite. Samples from the same bentonite bed are connected with a line.

DISCUSSION

Possibilities and problems of using immobile elements for proving correlations

Immobile trace elements, analysed easily by the X-ray fluorescence method (Ti, Nb, Zr, Th and major element Al_2O_3), can be confidently used for the correlation of bentonites. However, volcanic ash compositions from repetitive eruptions from the same volcanic source may exhibit similar compositions. A favourable situation for volcanic stratigraphy is when ashes from different volcanoes alternate regularly (Kiipli et al. 2010). Using the thickness of bentonites for correlation is unreliable as a thick eruption layer can be thin in other areas.

Bentonites from single eruptions and composite layers from several eruptions

Internal compositional variations of two thick bentonite layers in the Billegrav-2 core indicate that the composition of magma can vary during long-lasting eruptions. The absence of terrigenous shale interbeds suggests that it was the same continuous eruption. Compositional variations can be caused by involving the lower layers from a stratified magma chamber during the eruption or differentiation of ash material during air transport or redeposition. Somewhat larger variations in the composition of the Kinnekulle Bentonite in Scandinavia (Fig. 3) compared to the East Baltic may indicate a change in wind directions during the eruption. The maximum power of the eruption is likely represented by the middle part of the Kinnekulle Bentonite in the Billegrav-2 core and at this time the ash cloud reached the most distant areas including the East Baltic. Initial and final stages of the eruption reached mostly Scandinavia, creating different compositions in the lower and upper parts of the bentonite layer. Thin shale interbeds in the interval between 87.25 and 87.82 m in the Billegrav-2 core indicate that this thick bentonite formed from several volcanic eruptions.

Causes of geochemical differences of the Fjäcka and Vasagård bentonites compared with the Kinnekulle Bentonite

The bentonites from these two localities were not used for calculating the average composition of the Kinnekulle Bentonite due to large deviation from the other data at hand, although these sections were previously believed to represent this bed. The compositional difference of the Fjäcka bentonite (Batchelor 2014) may be caused by mixing with terrigenous material as indirectly indicated by the high carbonate content. Terrigenous material commonly contains significantly higher contents of trace elements than is typical of the Kinnekulle Bentonite. The bentonite from Vasagård has only a significantly higher content of Ti, whereas the other immobile elements occur at low levels. This may indicate that bentonite from Vasagård (or at least the sample taken in 2003 from the poor outcrop and analysed by Kiipli et al. 2009) does not belong to the Kinnekulle Bentonite.

CONCLUSIONS

The study suggests with high probability that the 80 cm thick bentonite in the Billegrav-2 core section between 88.30 and 89.10 m represents the Kinnekulle Bentonite. Bentonites above it belong to the Grimstorp Series and those below to the Sinsen and Grefsen series. One of the Sinsen or uppermost Grefsen Series bentonites is 90 cm thick, thus exceeding the thickness of the Kinnekulle Bentonite. Bentonites in the Grefsen Series frequently show much higher concentrations of trace elements than the Kinnekulle Bentonite.

Acknowledgements. This work is a contribution to IGCP 591 project and target-financed project SF0140016s09 and ETF8963 of the Estonian Ministry of Education and Research. The authors thank Donatas Kaminskas and Warren Huff for helpful reviews.

REFERENCES

Batchelor, R. A. 2003. Geochemistry of biotite in meta-bentonites as an age discriminant indicator of regional magma sources and potential correlating tool. *Mineralogical Magazine*, **67**, 807–817.

Batchelor, R. A. 2009 (for 2008). Geochemical 'Golden Spike' for Lower Palaeozoic metabentonites. *Earth and Environmental Science Transactions of the Royal Society of Edinburgh*, **99**, 177–187.

Batchelor, R. A. 2014. Geochemistry of Upper Ordovician metabentonites and their cognate apatite microphenocrysts from Norway and Sweden. *GFF*, **136**, 387–397.

Bergström, S. M. & Nilsson, R. 1974. Age and correlation of the Middle Ordovician bentonites on Bornholm. *Bulletin of the Geological Society of Denmark*, **23**, 27–48.

Bergström, S. M., Huff, W. D., Kolata, D. R. & Bauert, H. 1995. Nomenclature, stratigraphy, chemical fingerprinting, and areal distribution of some Middle Ordovician K-bentonites in Baltoscandia. *Geologiska Föreningens i Stockholm Förhandlingar (GFF)*, **117**, 1–13.

Bergström, S. M., Huff, W. D., Kolata, D. R., Yost, D. A. & Hart, C. 1997. A unique Middle Ordovician K-bentonite bed succession at Röstånga, S. Sweden. *GFF*, **119**, 231–244.

Bergström, S. M., Huff, W. D., Koren, T., Larsson, K., Ahlberg, P. & Kolata, D. R. 1999. The 1997 core drilling through Ordovician and Silurian strata at Röstånga, S. Sweden: preliminary stratigraphic assessment and regional comparison. *GFF*, **121**, 127–135.

Funkquist, H. P. A. 1919. Asaphusregionens omfattning i sydöstra Skåne och på Bornholm. *Lunds Universitets Årsskrift* N. F. Avd. 2, **16**, 56 pp.

Hagemann, F. & Spjeldnaes, N. 1955. The Middle Ordovician of the Oslo Region, Norway, 6, Notes on bentonites (K-bentonites) from the Oslo-Asker District. *Norsk Geologisk Tidsskrift*, **35**, 29–52.

Hetherington, C. J., Nakrem, H. A. & Potel, S. 2011. Note on the composition and mineralogy of upper Silurian bentonites from the Ringerike District: implications for local and regional stratigraphic correlation and sedimentation. *Norwegian Journal of Geology*, **91**, 181–192.

Huff, W. D., Bergström, S. M. & Kolata, D. R. 1992. Gigantic Ordovician volcanic ash fall in North America and Europe: biological, tectonomagmatic, and event-stratigraphic significance. *Geology*, **20**, 875–878.

Huff, W. D., Kolata, D. R., Bergström, S. M. & Zhang, Y. S. 1996. Large-magnitude Middle Ordovician volcanic ash falls in North America and Europe: dimensions, emplacement and post emplacement characteristics. *Journal of Volcanology and Geothermal Research*, **73**, 285–301.

Huff, W. D., Bergström, S. M., Kolata, D. R. & Sun, H. 1998. The Lower Silurian Osmundsberg K-bentonite. Part II: mineralogy, geochemistry, chemostratigraphy and tectonomagmatic significance. *Geological Magazine*, **135**, 15–26.

Inanli, F. Ö., Huff, W. D. & Bergström, S. M. 2009. The Lower Silurian (Llandovery) Osmundsberg K-bentonite in Baltoscandia and the British Isles: chemical fingerprinting and regional correlation. *GFF*, **131**, 269–279.

Jürgenson, E. 1958. Metabentonites in Estonian SSR. *Trudy Instituta Geologii AN ÉSSR*, 2, 73–85 [in Russian].

Kaljo, D., Grytsenko, V., Kallaste, T., Kiipli, T. & Martma, T. 2014. Upper Silurian stratigraphy of Podolia revisited: carbon isotopes, bentonites and biostratigraphy. *GFF*, **136**, 136–141.

Kiipli, T., Batchelor, R. A., Bernal, J. P., Cowing, C., Hagel-Brunnstrom, M., Ingham, M. N., Johnson, D., Kivisilla, J., Knaack, C., Kump, P., Lozano, R., Michiels, D., Orlova, K., Pirrus, E., Rousseau, R. M., Ruzicka, J., Sandstrom, H. & Willis, J. P. 2000. Seven sedimentary rock reference samples from Estonia. *Oil Shale*, **17**, 215–223.

Kiipli, T., Kiipli, E., Kallaste, T., Hints, R., Somelar, P. & Kirsimäe, K. 2007. Altered volcanic ash as an indicator of marine environment, reflecting pH and sedimentation rate – example from the Ordovician Kinnekulle bed of Baltoscandia. *Clays and Clay Minerals*, **55**, 177–188.

Kiipli, T., Soesoo, A., Kallaste, T. & Kiipli, E. 2008. Geochemistry of Telychian (Silurian) K-bentonites in Estonia and Latvia. *Journal of Volcanology and Geothermal Research*, **171**, 45–58.

Kiipli, T., Kallaste, T., Kleesment, A. & Nielsen, A. T. 2009. Corroded hydrothermal quartz in Ordovician altered volcanic ash beds of the Baltoscandian Region. *Estonian Journal of Earth Sciences*, **58**, 268–272.

Kiipli, T., Kallaste, T. & Nestor, V. 2010. Composition and correlation of volcanic ash beds of Silurian age from the eastern Baltic. *Geological Magazine*, **147**, 895–909.

Kiipli, T., Einasto, R., Kallaste, T., Nestor, V., Perens, H. & Siir, S. 2011. Geochemistry and correlation of volcanic ash beds from the Rootsiküla Stage (Wenlock–Ludlow) in the eastern Baltic. *Estonian Journal of Earth Sciences*, **60**, 207–219.

Kiipli, T., Kallaste, T. & Nestor, V. 2012. Correlation of upper Llandovery–lower Wenlock bentonites in the När (Gotland, Sweden) and Ventspils (Latvia) drill cores: role of volcanic ash clouds and shelf sea currents in determining areal distribution of bentonites. *Estonian Journal of Earth Sciences*, **61**, 295–306.

Kiipli, T., Kallaste, T., Kiipli, E. & Radzevičius, S. 2013. Correlation of Silurian bentonites based on the immobile elements in the East Baltic and Scandinavia. *GFF*, **135**, 152–161.

Kiipli, T., Radzevičius, S. & Kallaste, T. 2014a. Silurian bentonites in Lithuania: correlations based on sanidine phenocryst composition and graptolite biozonation – interpretation of volcanic source regions. *Estonian Journal of Earth Sciences*, **63**, 18–29.

Kiipli, T., Soesoo, A. & Kallaste, T. 2014b. Geochemical evolution of Caledonian volcanism recorded in the sedimentary rocks of the eastern Baltic region. In *New Perspectives on the Caledonides of Scandinavia and Related Areas* (Corfu, F., Gasser, D. & Chew, D. M., eds), *Geological Society of London Special Publications*, **390**, 177–192.

Lindström, M. 1953. On the Lower Chasmops beds in the Fågelsång district (Scania). *Geologiska Föreningens i Stockholm Förhandlingar*, **75**, 125–148.

Männik, P., Põldvere, A., Nestor, V., Kallaste, T., Kiipli, T. & Martma, T. 2014. The Llandovery–Wenlock boundary interval in west-central continental Estonia: an example from the Suigu (S-3) core section. *Estonian Journal of Earth Sciences*, **63**, 1–17.

Männil, R. 1966. *Evolution of the Baltic Basin during the Ordovician*. Valgus, Tallinn, 200 pp. [in Russian, with English summary].

Nielsen, A. T. & Schovsbo, N. H. 2011. The Lower Cambrian of Scandinavia: depositional environment, sequence stratigraphy and palaeogeography. *Earth Science Reviews*, **107**, 207–310.

Pedersen, G. K. & Klitten, K. 1990. Anvendelse af gamma-logs ved correlation af marine skifre i vandforsyningsboringer på Bornholm. *Danmarks Geologisk Forening Årskrift 1987–89*, 21–35.

Ray, D. C., Collings, A. V. J., Worton, G. J. & Jones, G. 2011. Upper Wenlock bentonites from Wren's Nest Hill, Dudley: comparisons with prominent bentonites along Wenlock Edge, Shropshire, England. *Geological Magazine*, **148**, 670–681.

Schovsbo, N. H., Nielsen, A. T., Klitten, K., Mathiesen, A. & Rasmussen, P. 2011. Shale gas investigations in Denmark: Lower Palaeozoic shales on Bornholm. *Geological Survey of Denmark and Greenland Bulletin*, **23**, 9–14.

Sell, B. K. & Samson, S. D. 2011. Apatite phenocryst compositions demonstrate a miscorrelation between the Millbrig and Kinnekulle K-bentonites of North America and Scandinavia. *Geology*, **39**, 303–306.

Siir, S., Kallaste, T., Kiipli, T. & Hints, R. 2015. Internal stratification of two thick Ordovician bentonites of Estonia: deciphering primary magmatic, sedimentary, environmental and diagenetic signatures. *Estonian Journal of Earth Sciences*, **64** [accepted].

Thorslund, P. 1945. Om bentonitlager i Sveriges kambrosilur. *Geologiska Föreningens i Stockholm Förhandlingar*, **67**, 286–288 [in Swedish].

Vingisaar, P. 1972. On the distribution of the main metabentonite stratum (d; XXII) in the Middle Ordovician of Baltoscandia. *Eesti NSV Teaduste Akadeemia Toimetised, Keemia, Geoloogia*, **21**, 62–70 [in Russian, with English summary].

IV – **Siir, S**., Kallaste, T., Kiipli, T. & Hints, R. 2015. Internal stratification of two thick Ordovician bentonites of Estonia: deciphering primary magmatic, sedimentary, environmental and diagenetic signatures. *Estonian Journal of Earth Sciences*, **64**, 2, 140-158.

Estonian Journal of Earth Sciences, 2015, **64**, 2, 140–158 doi: 10.3176/earth.2015.23

Internal stratification of two thick Ordovician bentonites of Estonia: deciphering primary magmatic, sedimentary, environmental and diagenetic signatures

Sven Siir, Toivo Kallaste, Tarmo Kiipli and Rutt Hints

Institute of Geology at Tallinn University of Technology, Ehitajate tee 5, 19086 Tallinn, Estonia; sven.siir@ttu.ee

Received 2 June 2014, accepted 10 September 2014

Abstract. Twenty-six samples from two major altered volcanic ash beds, Kinnekulle and BII Bentonite of the Kuressaare core section (K-3), Saaremaa Island, were explored to record the geochemical and mineralogical heterogeneity of beds. Signs of ash transport fractionation, redeposition of volcanic ash and diagenetic redistribution of material are described and interpreted. In authigenic mineralogy of the Kinnekulle Bentonite illite–smectite dominates with addition of K-feldspar at the margins. The BII Bentonite is composed of chlorite–smectite and illite–smectite. The stability of phenocryst compositions, including that of sanidine and biotite, indicates that both bentonites originate from a single eruption. The observed rather stable pyroclastic sanidine compositions in the cross section of bentonites confirm the reliability of sanidine-based fingerprinting of altered volcanic ash beds. Trace element distribution in bentonites and host rocks indicates that Zr, Ga, Rb, Nb, Ti and Th stayed largely immobile during volcanic ash alteration and reflect primary ash composition. However, some redistribution of Nb and Ti as well as Y has probably occurred near the contacts of bentonite with the host rock. More scattered grain size distribution and immobile element patterns of the Kinnekulle Bentonite support the idea that the primary ash bed had a heterogeneous composition and it was one of the biggest bentonites of the Phanerozoic and most likely records an extended volcanic event. Significant geochemical variations, including a high S content, near the upper and lower contacts of the Kinnekulle Bentonite and elevated Ca and P in host rocks of both bentonites suggest that the studied large ash-falls caused notable perturbations in shallow marine and early post-sedimentary environment.

Key words: K-bentonite, Mg-bentonite, Ordovician, Estonia.

INTRODUCTION

Volcanic ash fallout is an ‘instantaneous’ event compared to geological time and can be used for precise regional correlation of sedimentary sections (Kolata et al. 1987; Bergström et al. 1995; T. Kiipli et al. 2008a, 2010a, 2010b, 2012, 2014a, 2014b, 2015; Ray et al. 2011; Kaljo et al. 2014; Männik et al. 2014). Volcanic ashes carry also information for the reconstruction of tectonomagmatic environments in volcanic source areas (Batchelor 2009; Hetherington et al. 2011; Kiipli et al. 2013, 2014c). Super-eruptions, ejecting more than 1000 km^3 of dense rock equivalent, transport huge amounts of magmatic material from the Earth’s interior to the surface, some of which freezes immediately as surface rocks, but much of ejected fine material enters the atmosphere as aerosol creating a ‘dark rug’ cover in the upper layers. Aerosols from major blowouts may remain in the atmosphere for up to five years (Rampino et al. 1988) and during this time the influx of solar radiation to the Earth’s surface is impeded, causing global cooling. Lower temperature exerts stress on life and sometimes even causes its extinction after the largest eruptions (Hints et al. 2003; Perrier et al. 2012). Volcanic ash fallouts can also directly affect marine geochemistry, triggering transient acidification of sea water, and quick release of different metals which can either act as nutrients supporting primary production or toxify the marine environment, the latter leading to a possible mass mortality event (e.g. Jones & Gislason 2008; Duggen et al. 2010). Thus, the interaction of primary volcanic ash with different environmental and biotic factors can vary case by case and the signals of these variations may be preserved in the cumulative composition of old volcanic ash beds.

Amorphous glassy material of volcanic ash in sediments alters to clay minerals (commonly smectite) and other authigenic silicates (Grim & Güven 1978), forming bentonites. The primary vertical chemical and mineralogical composition of individual ash beds is not homogeneous (Dahlqvist et al. 2012), but varies due to a successive change in magma composition during long-lasting eruptions and physical fractionation (possibly also chemical alteration) of ash in air transport and settling

in water basins (Fisher & Schmincke 1984). Bergström et al. (1997) and Huff et al. (2010) suggested that in the conditions of an overall slow sedimentation rate and intense volcanism visually homogeneous bentonite layers can accumulate from several volcanic eruptions providing ashes of different compositions. Further, in the course of burial, volcanic ashes are altered by various diagenetic processes (Altaner et al. 1984; Brusewitz 1988; Kiipli et al. 2007; R. Hints et al. 2008).

The aim of this study is to test, describe and interpret the internal heterogeneity of different origins of two major Upper Ordovician bentonite beds in Baltoscandia: the Sandbian Kinnekulle Bentonite of the Keila Regional Stage (Bergström et al. 1995; L. Hints et al. 2008) and the Katian BII Bentonite of the Pirgu Regional Stage (Kiipli et al. 2004, 2015; Hints et al. 2006).

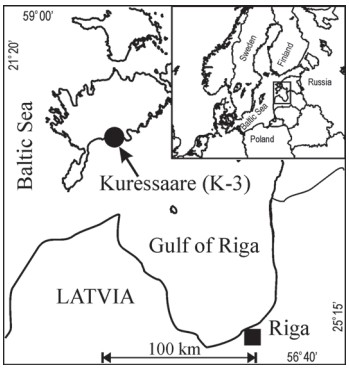

Fig. 1. Location of the Kuressaare (K-3) drill hole in the southern part of Saaremaa Island, Estonia.

MATERIAL AND METHODS

The Kinnekulle Bentonite is the thickest (up to 2 m in the Östergotland area in Sweden and up to 70 cm on Hiiumaa Island in Estonia) and most widely distributed altered volcanic ash bed in the Ordovician of Baltoscandia and the BII Bentonite is the thickest (up to 30 cm) in the Pirgu Stage of Estonia. The ash for both bentonites originated from tectonically active margins of the Iapetus Palaeo-Ocean at a distance of more than 1000–2000 km (Torsvik & Rehnström 2003) from the study site and accordingly both eruptions are considered as very large volcanic events. During their burial and alteration history, the Early Palaeozoic bentonites of the region never reached considerable burial depth and are characterized by low thermal maturity (Somelar et al. 2010).

The material for the current study was collected from the Kuressaare (K-3) drill core from southern Saaremaa Island (Fig. 1), stored at the Keila core depository of the Geological Survey of Estonia. The Kinnekulle Bentonite, marking the boundary of the Haljala and Keila stages, is 40 cm thick and the BII Bentonite in the middle of the Pirgu Stage is 30 cm thick (Figs 2, 3). Host rocks of the Kinnekulle Bentonite are limestones and those of the BII Bentonite, argillaceous marlstones. Based on the facies framework of the Baltic Palaeobasin, the Ordovician sedimentary section of the Kuressaare core belongs to the transition zone between the proximal shallow and deeper shelf sea areas (Põlma 1967).

During sampling both bentonites were divided into eight equal parts, therefore BII samples are 3.75 cm and Kinnekulle samples 5 cm thick. The amount of the study material was about 15–20 g per sample. Host rock samples were taken for comparison at 5 and 30 cm below and at 5 and 15 cm above of the Kinnekulle Bentonite, and at 3, 10 and 20 cm below and above the BII Bentonite layer.

Major chemical components and trace elements were determined by X-ray fluorescence (XRF) methods using a Bruker S4 Pioneer spectrometer. The X-ray tube with the Rh-anode and maximum working power 3 kW was used. Eight grams of fine powder (grains not larger than 50 μm) of samples was mixed with eight drops of 5% Mowiol solution in distilled water and pressed. The pellets were dried for 2 h at 105 °C. The samples were measured and preliminary results were calculated by using the manufacturer's standard methods software MultiRes and GeoQuant. The XRF data in the present study represent the average of these two measurements. Ten international and in-house reference materials were used to refine analytical results by up to a few per cent of the concentration.

Grain material for X-ray diffraction (XRD) and micro-analyses was separated using the following procedure: about 2 g of bentonite samples were dispersed ultrasonically during 2 min in 50 mL of 0.1% Na-pyrophosphate solution. The remaining Na-pyrophosphate suspension was slowly poured away. The pouring must be done very carefully so that the separated grains would not be lost with the suspension of the material. This procedure was performed twice. The next step was adding 25 mL of 1 : 4 HCl solution to the separated grain material for dissolving carbonate minerals and treated with ultrasound until the acid solution became warm and started to steam slightly; the process took about 3 min. According to our experience, this procedure extracts most of the grains larger than 0.04 mm from the bentonite sample.

The XRD measurements of the bulk sample and grain fraction were performed on a D-8 Advance

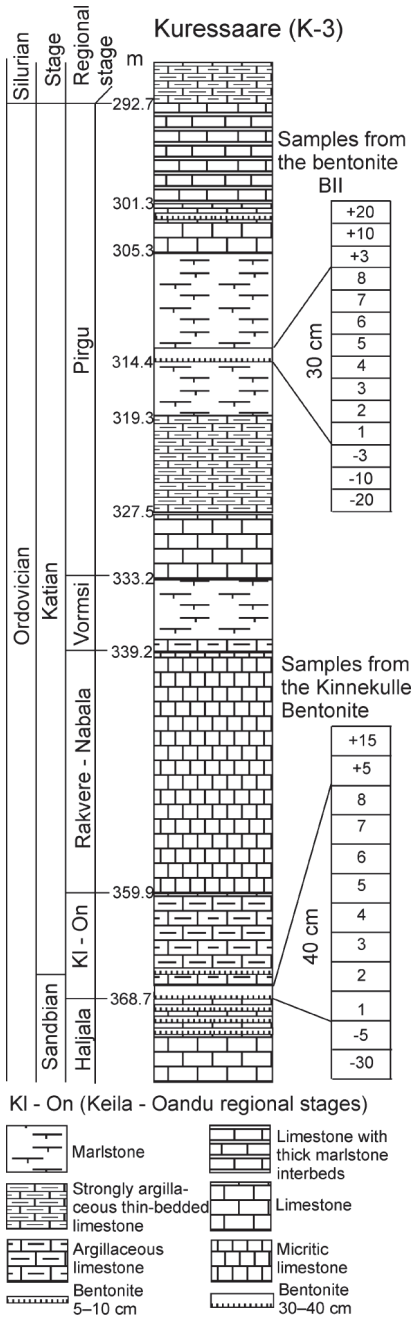

Fig. 2. The lithology and stratigraphy of the Kuressaare (K-3) drill core.

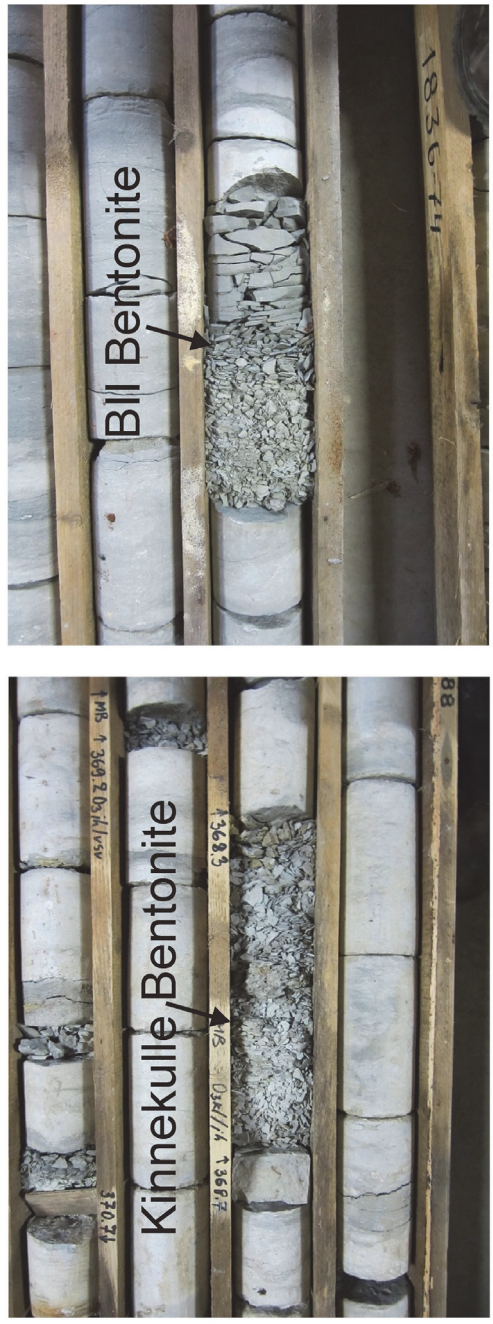

Fig. 3. Drill core photos of the BII and Kinnekulle bentonites.

instrument from Bruker AXS. The measured diffraction patterns were analysed with the TOPAS and EVA software and Microsoft Excel.

Microanalyses of grains were performed with an energy-dispersive X-ray instrument (EDXRF), connected to the scanning electron microscope, under low vacuum (30 Pa) conditions. The electron beam was generated by 20 kV and 650 pA. The basaltic glass BBM-1G, distributed by the International Association of Geoanalysts, was measured together with the studied grains and used as a reference. On the basis of these measurements, Al, Si and Fe concentrations were corrected linearly by a few per cent of the concentration. According to repetitive measurements of BBM-1G, the precision of measurements was better than 0.4%.

RESULTS

XRD analysis of bulk bentonite

Main components of the BII Bentonite detected through the layer are illite–smectite, chlorite–smectite and K-feldspar plus quartz and dolomite (Fig. 4). From these minerals, chlorite–smectite (corrensite) is known only from the bentonites of the Pirgu Stage in Estonia (Hints et al. 2006).

Lower samples of the BII Bentonite are mineralogically quite similar, having a minor amount of calcite and pyrite in sample 1. Small portions of quartz and dolomite appear in sample 3 and these phases consistently increase towards the upper boundary of the bentonite layer. In the upper part of the bentonite (samples 7 and 8) traces of calcite could be observed again. The content of illitic layers in illite–smectite in bentonites of the Pirgu Stage in the East Baltic has been previously reported to vary between 71% and 74% (Hints et al. 2006).

Lower host rock of the BII Bentonite is mostly composed of calcite and dolomite, together with smaller amounts of quartz, illite, K-feldspar, chlorite and traces of pyrite. The host rock just above the bentonite consists mainly of calcite but there are also traces of K-feldspar, quartz and dolomite. The dolomitization and quartz component increase 10 cm above the bentonite, however, this sample is still highly calcitic. This trend continues until 20 cm higher and the rock composition gradually becomes similar to the rock below the bentonite.

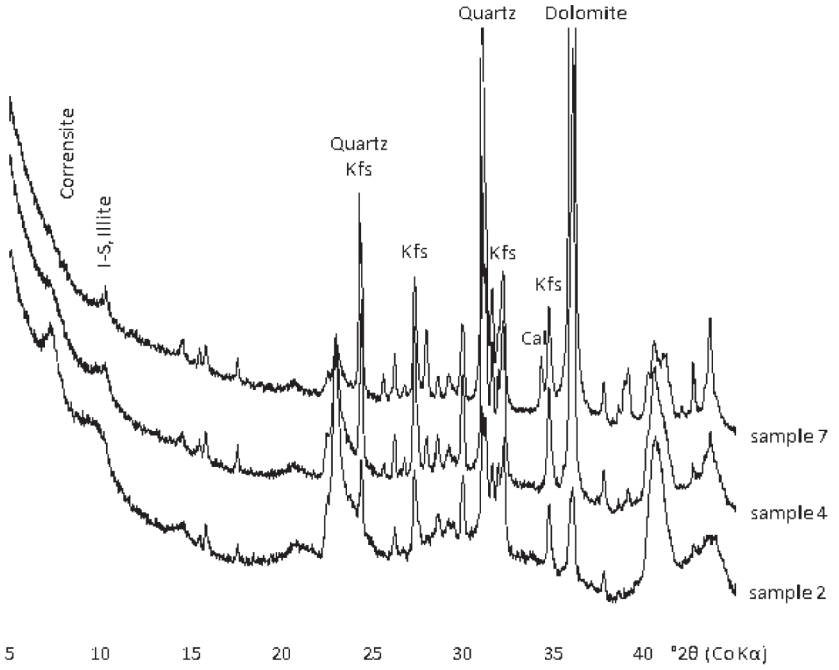

Fig. 4. Examples of XRD patterns from the BII Bentonite. Patterns demonstrate an increase in quartz and dolomite content upwards in the bed. Clay minerals are most abundant in the lower part of the bentonite. I–S, illite–smectite; Kfs, potassium feldspar; Cal, calcite.

Similarly to bentonites, the clay fraction of the host rocks of the Pirgu Stage in the transition zone also contains abundant chlorite–smectite (E. Kiipli et al. 2012).

The mineral composition of the Kinnekulle Bentonite has previously been studied in the Pääsküla exposure, northern Estonia (Hints et al. 1997), where the mineral assemblage of the bentonite was reported to be composed of potassium feldspar and illite–smectite. The same minerals occur in the Kinnekulle Bentonite over the entire northern and central region of Estonia (Kiipli et al. 2007). The content of illitic layers in illite–smectite in the East Baltic area varies between 71% and 87%.

In the Kinnekulle Bentonite of the Kuressaare drill core, illite–smectite occurs as the dominant mineral phase with the highest concentrations in the middle of the bentonite layer. The K-feldspar content is lower than in North Estonian settings, but similarly to those sections the content of K-feldspar reaches the maximum at the upper and lower boundaries of the layer (samples 1, 2 and 8) (Fig. 5).

Major components revealed by XRF analysis

The chemical composition of the two targeted bentonites differs significantly. The most outstanding feature of the compositional variations can be illustrated on the MgO–K_2O chart (Fig. 6). The Kinnekulle Bentonite has a typical K-bentonite composition with the K_2O content around 7% in the middle part. The BII Bentonite has a lower K_2O content (around 5%) and a high content of MgO between 9% and 13%. It suggests that Mg-bentonite could be a more appropriate name for this lithological variety of bentonite. It is distinctive that the host rocks near the BII Bentonite are also enriched in MgO compared with the host rocks of the Kinnekulle Bentonite.

Furthermore, the internal chemical variability patterns of major elements of the BII Bentonite and the Kinnekulle Bentonite possess distinct individual features (Fig. 5). The BII Bentonite shows big differences in geochemistry between the upper and lower parts of the bentonite. SiO_2, Al_2O_3, Fe_2O_3 and MgO follow a similar upward decreasing trend and the differences between the upper and lower parts of bentonite are obvious, whereas the CaO level changes in the opposite direction. Based on the distribution of a number of major components, the Kinnekulle Bentonite is rather uniform throughout the layer. However, it exhibits notably higher K_2O and S contents near both the lower and upper contacts with the host rock. A conspicuous increase in P_2O_5 associated with some rise in CaO occurs in host rocks directly above both bentonites. The host rocks of the bentonites have significantly lower concentrations of all typical elements of silicate minerals and higher contents of CaO than the bentonite beds.

The comparison of the major element composition of bentonites with that of the silicate part of host rocks shows that bentonites contain significantly more Al_2O_3 and less SiO_2 and TiO_2 (Fig. 7). Distinctive is a higher SiO_2 content below the Kinnekulle Bentonite compared with other host rock samples (Fig. 7).

Trace elements revealed by XRF analysis

The studied bentonites have significantly lower concentrations of Ti, Cr and V than the silicate part of host rocks. These elements are therefore good discriminators for recognizing the volcanic origin of clay-rich layers. Higher concentrations of Ti were also recorded in the silicate fraction of host rocks.

The contents of trace elements such as Zr, Th and Nb are higher in the BII Bentonite than in the silicate part of host rocks, but in case of the Kinnekulle Bentonite do not show much difference. Compared to the BII Bentonite, the Kinnekulle Bentonite exhibits notably higher contents of Rb and Ba.

Trace elements vary considerably in the upper and lower parts of the BII Bentonite. Zr reaches 300 ppm in a lower sample and decreases steadily to 100 ppm in the upper part. Ga, Nb, Th, and Rb follow mostly the same pattern and show positive correlation with each other, indicating that these elements stayed largely immobile during the alteration (Fig. 7, Table 1). However, the maximum content of Nb in the silicate fraction of the host rock was recorded directly below the BII Bentonite.

Variations in the trace element content throughout the vertical section of the Kinnekulle Bentonite tend to be smaller but somewhat more irregular than those observed in the BII Bentonite. The most remarkable concentration shifts occur in the uppermost (sample 8) and lowermost (samples 1, 2) parts of the bed. Thus, Ga, Rb and Zr concentrations decrease near the lower and upper contacts (Fig. 7, Table 2). Samples from near the lower and upper contacts of the bentonite bed show also a significant rise in the content of chalcophile elements such as As and Pb, simultaneously with peak S and Fe concentrations. The trace element patterns from the middle part of the bed exhibit small-scale but still notable scattering of immobile trace elements, e.g. of Zr (Table 2, Fig. 8). The higher values of Nb in the silicate fraction of the host rock of the Kinnekulle Bentonite compared to the bentonite values suggest, similarly to the BII Bentonite, mobilization of Nb near the contacts of bentonite with the host rock. The Y values in the bentonite lack good correlation with other typical immobile elements. Its highest concentrations appear in the two

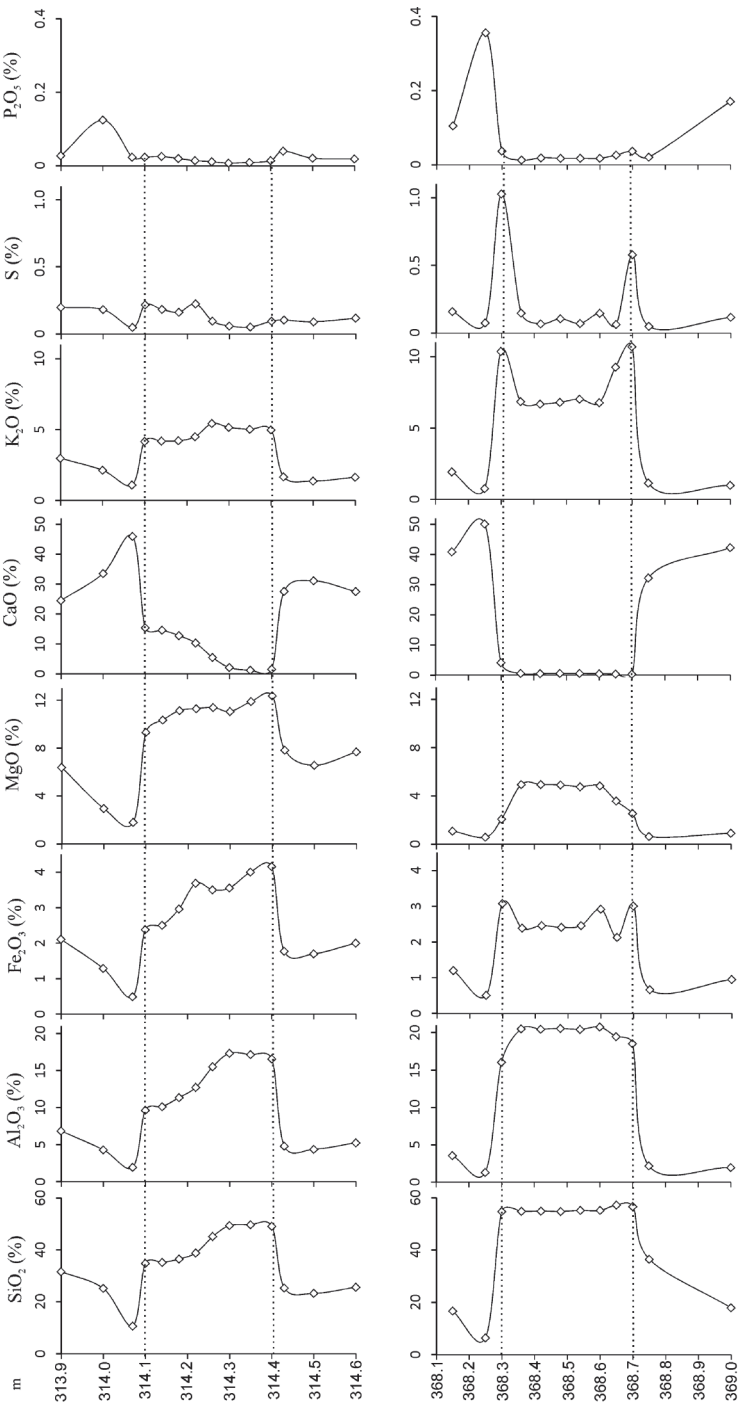

Fig. 5. The distribution of major components in the BII Bentonite (upper panel) and the Kinnekulle Bentonite (lower panel) and host limestones.

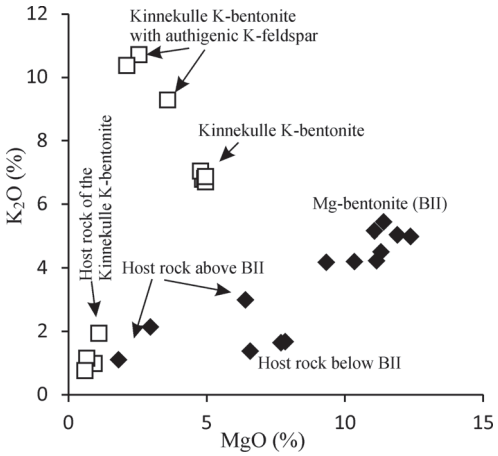

Fig. 6. The composition of two bentonites and host rocks illustrated on the MgO–K_2O chart. The Kinnekulle Bentonite has typical K-bentonite composition but the BII Bentonite shows high contents of MgO.

lowermost samples of the bentonite containing also slightly more P_2O_5 than the rest of samples. Peak concentrations of Y appear directly above the Kinnekulle Bentonite, together with peak values of CaO and P_2O_5.

The composition of grain material and pyroclastic sanidine

Grain material larger than 0.04 mm forms 2–10% of both bentonites. Higher concentrations are found in the lower parts of bentonites with a secondary peak in the third sample from below in the Kinnekulle bed and in the middle of the BII bed. The composition of minerals in grain fraction is presented in Table 3 and pyroclastic material is characterized in Table 4. According to XRD analysis, the authigenic K-feldspar component (end-member orthoclase_313 and K-sanidine, Kastner 1971) forms the major part of grains, varying between 70% and 85% in the Kinnekulle Bentonite. Microanalysis of grains revealed a number of clay aggregates in grain fractions of the BII Bentonite. Conversely, the samples of the Kinnekulle Bentonite were more efficiently purified and did not contain clay. Authigenic pyrite occurs mostly in concentration of 0.5–3.5% in grain fraction, except in the lower and upper samples of the Kinnekulle Bentonite where much higher contents were recorded.

The allogenic (terrigenous + pyroclastic) part (mostly 15–30%) of grains is formed predominantly of K–Na-sanidine (Kastner 1971), quartz and biotite. The quartz component remains at the same level (nearly 6%) within the four lower samples in the BII Bentonite and is followed by an increasing trend upwards. The volcanic sanidine (Na–K-sanidine) component is about 12% within the first six samples (except sample 3 where it reaches 19%), decreasing to nearly 5% in samples 7 and 8. The Kinnekulle Bentonite is rich in biotite (38% of grains measured by microanalysis), while authigenic sanidine forms 48% and Na–K-sanidine only 4% of measurements. Minor phenocrysts are quartz (5%) and apatite (4%).

Among pyroclastic grains the quartz content remains stable, being close to 50% of pyroclasts in the Kinnekulle Bentonite and 24–28% in the BII Bentonite (Table 4). The content of biotite in the Kinnekulle Bentonite decreases upwards and correspondingly the sanidine content rises. The composition of pyroclastic material was not calculated for the upper samples as these contain much terrigenous quartz, indistinguishable from pyroclastic one by XRD. According to XRD, K–Na–Ca-sanidine has a constant composition throughout both bentonite sections, averaging at 25.2 ± 0.6 mol% $(Na,Ca)AlSi_3O_8$ for the Kinnekulle Bentonite and 43.8 ± 0.4 mol% for the BII bed. Measurements of grain compositions by the energy-dispersive XRF (EDXRF) microanalyser confirm the XRD measurements. The composition of biotite detected from the Mg/(Mg + Fe) ratio is also stable throughout the section of the Kinnekulle Bentonite.

The distribution of maximum pyroclastic grain sizes (observed visually under microscope) is homogeneous in the BII Bentonite, staying around 180 μm. On the contrary, the maximum pyroclastic grain size distribution is rather variable in the Kinnekulle Bentonite, being remarkably high (300 μm) in samples 2 and 3, compared to the lowermost and uppermost parts of the bentonite (Table 4, Fig. 9).

DISCUSSION

Multiple- versus single-eruption hypothesis for the source of bentonite-forming material

To explain the origin of some of the major Early Palaeozoic bentonites, a multiple-eruption hypothesis has been put forward (Huff et al. 2010). Nevertheless, the vertical sections of both of the studied bentonites have a stable composition of primary magmatic phenocrysts, as evidenced by the high-precision XRD data of volcanic sanidine (Table 4). Furthermore, sanidine compositional data exhibit good correspondence between XRD and EDXRF data. The Mg/(Mg + Fe) atom ratio in biotite in the Kinnekulle Bentonite was also found to be stable. The observed stability of the composition of primary phenocrysts provides evidence that the magmatic

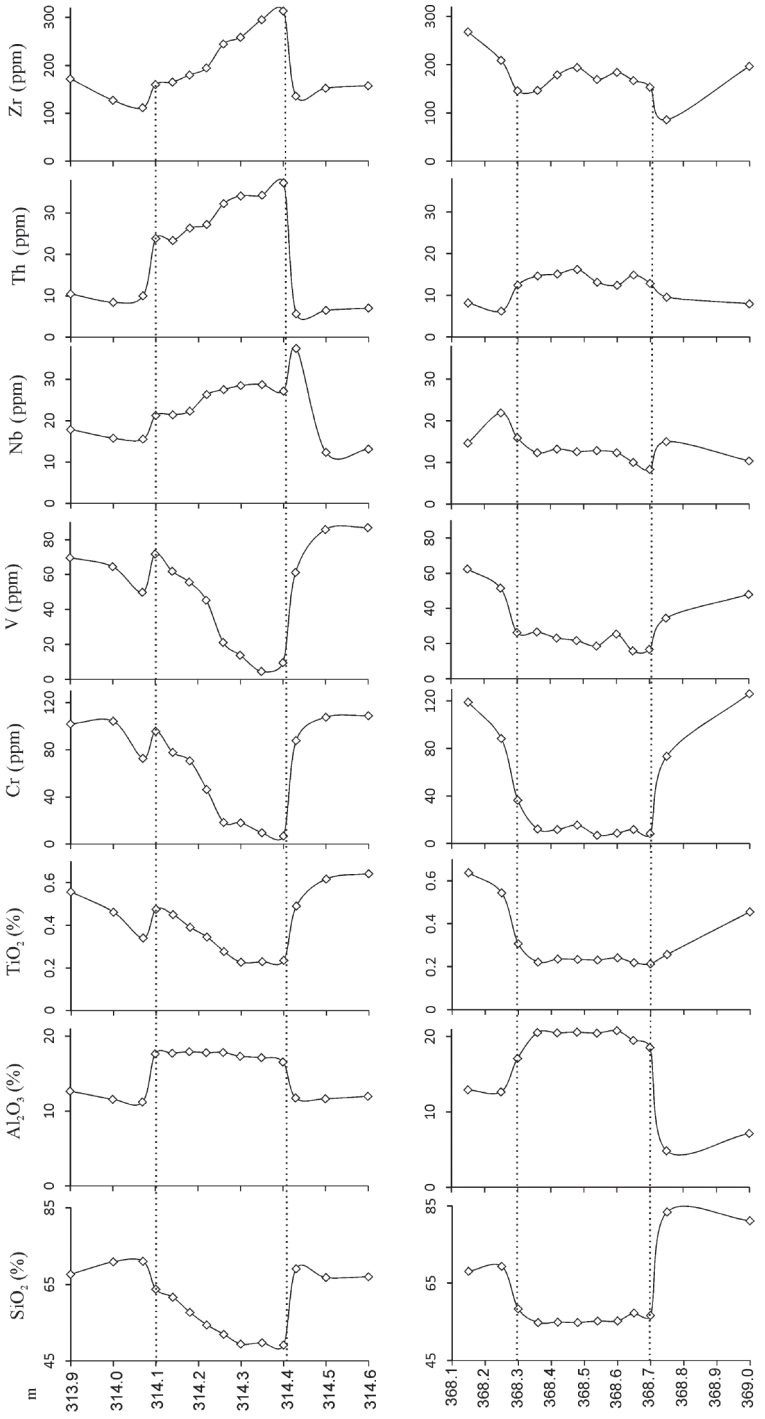

Fig. 7. The distribution of major and trace elements in the silicate fraction of rocks (upper panel – BII Bentonite, lower panel – Kinnekulle Bentonite). The carbonate material from host rock was removed by dissolving in the HCl solution before XRF analyses. For the upper part of the BII Bentonite concentrations were recalculated to the contents within the silicate part of samples.

Table 1. Major and trace element contents in the BII Bentonite and host rock

	Sample/depth (m)/lithology													
	BII –20/ 314.60/ limestone	BII –10/ 314.50/ limestone	BII –3/ 314.43/ limestone	BII_1/ 314.40/ bentonite	BII_2/ 314.35/ bentonite	BII_3/ 314.30/ bentonite	BII_4/ 314.26/ bentonite	BII_5/ 314.22/ bentonite	BII_6/ 314.18/ bentonite	BII_7/ 314.14/ bentonite	BII_8/ 314.10/ bentonite	BII +3/ 314.07/ limestone	BII +10/ 314.00/ limestone	BII +20/ 313.90/ limestone
Major elements (%)														
LOI 920°	31.0	32.3	31.4	9.1	8.9	10.1	13.6	19.2	22.2	24.1	24.4	37.1	29.6	25.6
SiO_2	25.7	23.3	25.4	49.2	49.8	49.4	45.2	38.9	36.5	35.2	34.8	10.7	25.2	31.7
TiO_2	0.216	0.185	0.191	0.236	0.230	0.227	0.241	0.247	0.248	0.258	0.260	0.051	0.154	0.240
Al_2O_3	5.3	4.4	4.8	16.6	17.2	17.3	15.5	12.7	11.4	10.1	9.7	2.0	4.3	6.9
Fe_2O_3	2.0	1.7	1.8	4.2	4.0	3.6	3.5	3.7	3.0	2.5	2.4	0.5	1.3	2.1
MnO	0.053	0.047	0.054	0.007	0.006	0.008	0.018	0.032	0.038	0.040	0.039	0.028	0.039	0.043
MgO	7.7	6.6	7.8	12.4	11.9	11.1	11.4	11.3	11.1	10.4	9.3	1.8	3.0	6.4
CaO	27.5	31.1	27.6	1.6	1.3	2.2	5.5	10.3	12.9	14.6	15.5	45.9	33.6	24.6
Na_2O	0.07	0.06	0.06	0.24	0.24	0.27	0.25	0.25	0.20	0.16	0.15	0.03	0.08	0.11
K_2O	1.6	1.4	1.7	5.0	5.0	5.2	5.4	4.5	4.2	4.2	4.2	1.1	2.1	3.0
P_2O_5	0.019	0.021	0.040	0.014	0.010	0.008	0.011	0.014	0.020	0.026	0.024	0.024	0.124	0.028
Cl	0.022	0.021	0.021	0.010	0.009	0.008	0.010	0.013	0.016	0.018	0.024	0.023	0.028	0.023
S	0.12	0.09	0.10	0.10	0.05	0.06	0.10	0.23	0.16	0.18	0.22	0.05	0.18	0.20
F	0.12	0.10	0.10	0.54	0.54	0.56	0.44	0.51	0.42	0.28	0.27	0.03	0.05	0.17
Trace elements (ppm)														
As	2	2	1	4	3	3	3	6	5	4	4	0	0	3
Ba	138	121	117	29	50	61	78	83	53	69	116	20	94	137
Cr	44	35	37	7	10	18	16	33	45	45	52	16	40	53
Cu	8	11	7	5	3	4	2	7	6	6	6	8	5	7
Ga	5	3	5	17	18	18	15	12	10	10	8	<5	3	6
La	17	19	26	8	8	16	19	15	12	1	11	37	<20	14
Nb	5	4	9	27	29	28	24	19	14	12	12	4	7	7
Ni	16	14	17	34	34	30	35	41	31	25	22	6	13	23
Pb	6	11	13	8	9	7	9	14	10	9	12	9	13	8
Rb	48	42	43	97	100	100	87	69	64	64	64	14	36	52
Sc	<20	<20	<20	0	<20	19	18	<20	<20	<20	13	<20	9	<20
Sn	<10	<10	<10	7	6	7	5	5	4	3	2	<10	<10	<10
Sr	221	275	192	72	77	77	70	74	79	86	96	474	361	290
Th	5	4	6	37	34	34	28	19	17	13	13	0	6	9
U	<5	0	2	6	7	4	5	5	3	3	4	<5	<5	<5
V	39	35	33	10	5	14	18	32	35	35	39	18	23	34
Y	15	13	14	29	26	20	17	12	13	14	14	10	17	17
Zn	19	17	18	18	16	18	20	25	24	24	22	6	15	22
Zr	51	46	49	314	296	259	213	139	114	94	87	26	45	73

Table 2. Major and trace element contents in the Kinnekulle Bentonite and host rock

	Sample/depth (m)/lithology											
	Kin –30/ 369.00/ limestone	Kin –5/ 368.75/ limestone	Kin 1/ 368.70/ bentonite	Kin 2/ 368.65/ bentonite	Kin 3/ 368.60/ bentonite	Kin 4/ 368.54/ bentonite	Kin 5/ 368.48/ bentonite	Kin 6/ 368.42/ bentonite	Kin 7/ 368.36/ bentonite	Kin 8/ 368.30/ bentonite	Kin +5/ 368.25/ limestone	Kin +15/ 368.15/ limestone
Major elements (%)												
LOI 920°	32.9	24.3	5.0	5.3	7.1	6.9	7.4	7.3	7.5	6.1	38.6	31.9
SiO_2	18.0	36.6	56.7	57.3	55.3	55.2	54.9	55.0	54.9	54.8	6.5	16.8
TiO_2	0.122	0.124	0.214	0.219	0.241	0.231	0.234	0.236	0.222	0.289	0.053	0.183
Al_2O_3	2.0	2.2	18.6	19.5	20.8	20.5	20.6	20.5	20.5	16.1	1.3	3.6
Fe_2O_3	1.0	0.7	3.0	2.1	2.9	2.5	2.4	2.5	2.4	3.1	0.5	1.2
MnO	0.040	0.036	0.008	0.008	0.008	0.009	0.008	0.009	0.007	0.009	0.046	0.042
MgO	0.9	0.7	2.5	3.6	4.8	4.8	4.9	5.0	5.0	2.1	0.6	1.1
CaO	42.3	32.2	0.4	0.4	0.5	0.6	0.6	0.6	0.6	4.2	50.2	40.9
Na_2O	0.04	0.04	0.18	0.26	0.37	0.37	0.37	0.39	0.43	0.21	0.04	0.09
K_2O	1.0	1.2	10.7	9.3	6.8	7.0	6.8	6.7	6.9	10.4	0.8	1.9
P_2O_5	0.171	0.021	0.037	0.027	0.018	0.018	0.018	0.019	0.013	0.037	0.356	0.105
Cl	0.031	0.028	0.016	0.022	0.029	0.032	0.032	0.031	0.042	0.036	0.031	0.038
S	0.12	0.05	0.58	0.06	0.15	0.07	0.11	0.07	0.15	1.03	0.08	0.16
F	0.02	0.03	0.20	0.34	0.40	0.39	0.38	0.41	0.42	0.15	0.04	0.02
Trace elements (ppm)												
As	4	1	13	3	4	3	3	1	6	35	2	1
Ba	33	30	195	156	175	158	147	185	129	116	5	51
Cr	34	43	9	12	9	7	16	12	12	34	14	38
Cu	10	5	5	3	3	4	3	1	2	10	7	7
Ga	1	2	12	17	22	23	22	23	22	13	<5	3
La	26	20	8	8	6	8	<20	<20	10	9	36	24
Nb	4	8	8	10	12	13	13	13	12	15	3	6
Ni	9	7	12	17	16	9	7	7	6	20	2	7
Pb	5	9	10	6	8	7	7	8	9	26	13	11
Rb	25	27	98	113	130	126	127	128	122	85	16	37
Sc	<20	14	5	17	10	28	9	0	<20	2	2	<20
Sn	<10	<10	8	8	10	8	7	10	8	7	<20	<10
Sr	191	141	38	58	78	79	77	79	80	74	198	264
Th	4	4	13	15	12	13	16	15	15	12	7	8
U	<5	3	4	3	3	4	6	3	2	4	5	3
V	17	25	17	16	25	19	22	23	27	25	8	24
Y	21	13	22	24	20	21	18	20	14	16	49	23
Zn	6	7	10	10	12	12	11	12	11	11	5	11
Zr	49	42	154	167	184	170	194	179	147	137	21	77

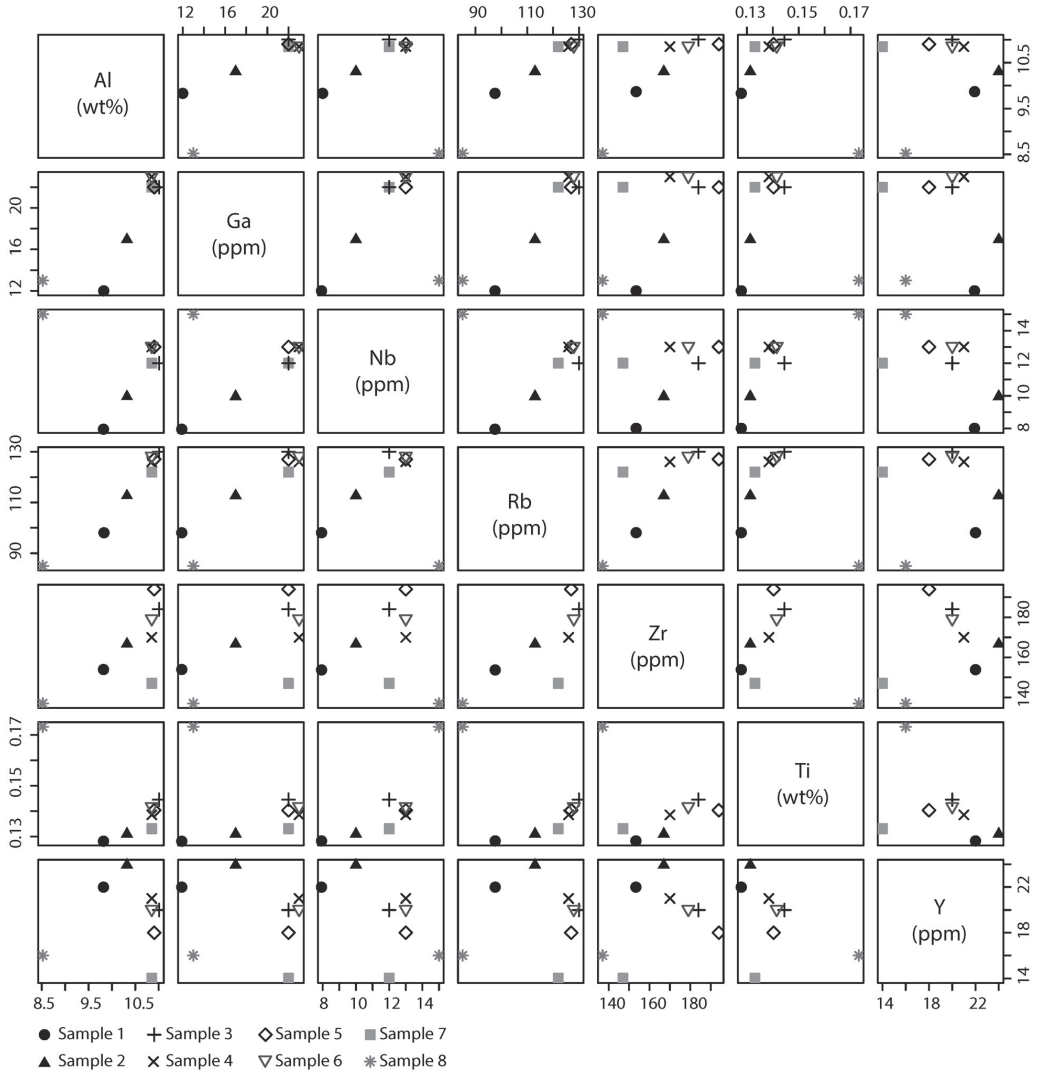

Fig. 8. Scatterplot matrix showing immobile element distribution in the cross section of the Kinnekulle Bentonite. The graphic presents pairwise relations of Al, Ti, Ga, Nb, Rb, Zr and Y. In case of homogeneous source material the ratios of immobile elements are expected to remain constant during ash alteration. However, for the Kinnekulle Bentonite the trace element scatterplots reveal notable variations between different samples, which might suggest either primary geochemical inhomogeneity of source material or diagenetic redistribution. Samples close to the upper and lower contacts of the bentonite (samples 1, 2 and 8) are characterized by a somewhat different immobile trace metal behaviour than the samples from the middle part of the bentonite. Those samples also have the lowest Al content. Samples 3–6 are characterized by a considerably homogeneous trace element composition. The distribution of Zr in the middle part of the Kinnekulle Bentonite, however, does not show good correlation with that of Al and with other immobile trace elements. Y demonstrates a rather different behaviour with respect to other immobile elements in the upper and lower parts of the bentonite.

Table 3. The composition of major minerals in the grain fraction

	Kinnekulle Bentonite						BII Bentonite							
	Biotite		Magmatic sanidine		Authigenic sanidine		Authigenic sanidine		Magmatic sanidine		Authigenic aggregates			
											Mostly illite–smectite		Mostly chlorite–smectite	
	n = 51		*n* = 5		*n* = 53		*n* = 47		*n* = 16		*n* = 7		*n* = 7	
	%	STD	%	STD	%	STD	%	STD	%	STD	%	STD	%	STD
Na_2O	0.37	0.07	2.51	0.09	0.06	0.04	0.10	0.05	4.35	0.22	0.10	0.06	0.04	0.02
MgO	6.97	0.46	0.06	0.03	0.11	0.15	0.29	0.14	0.24	0.17	7.99	0.65	14.96	0.77
Al_2O_3	16.44	0.36	18.36	0.09	17.82	0.18	17.67	0.21	18.61	0.39	17.53	1.13	15.09	0.93
SiO_2	39.06	1.16	62.83	0.51	62.55	0.59	63.07	0.48	63.83	1.03	60.56	0.62	57.13	0.96
S	0.15	0.19	0.12	0.09	0.08	0.08	0.10	0.13	0.09	0.07	0.21	0.09	0.38	0.26
K_2O	9.23	0.25	11.72	0.08	15.59	0.26	15.41	0.23	9.01	0.30	6.70	0.49	3.52	0.17
CaO	0.16	0.09	0.32	0.06	0.15	0.11	0.09	0.05	0.47	0.22	0.57	0.06	0.63	0.11
TiO_2	4.44	0.33	0.11	0.10	0.09	0.10	0.02	0.06	0.01	0.04	0.31	0.25	0.10	0.10
MnO	0.23	0.04	0.05	0.02	0.01	0.03	0.00	0.03	0.00	0.04	0.01	0.04	0.02	0.03
FeO	22.49	1.35	0.55	0.21	0.63	0.50	0.27	0.17	0.32	0.12	2.84	0.86	4.57	0.38
BaO	0.38	0.11	0.40	0.17	0.06	0.08	0.02	0.07	0.27	0.56	0.04	0.05	0.02	0.07
Index in the chemical formula														
Na	0.06	0.01	0.24	0.01	0.01	0.00	0.01	0.00	0.41	0.02				
K	0.94	0.01	0.74	0.01	0.99	0.01	0.99	0.01	0.56	0.02				
Ca	0.02	0.01	0.02	0.00	0.01	0.01	0.01	0.00	0.02	0.01				
Ba	0.01	0.00	0.01	0.00	0.00	0.00	0.00	0.00	0.01	0.01				
Mg	0.95	0.06	nc	nc	nc	nc	nc	nc	nc	nc				
Fe	1.70	0.06	0.02	0.01	0.02	0.02	0.01	0.00	0.01	0.00				
Ti	0.30	0.02	nc	nc	nc	nc	nc	nc	nc	nc				
Mn	0.02	0.00	nc	nc	nc	nc	nc	nc	nc	nc				
Al	1.32	0.03	1.02	0.01	1.00	0.01	0.99	0.01	1.02	0.03				
Si	2.67	0.03	2.96	0.02	2.98	0.02	3.00	0.01	2.97	0.03				
Biotite:	(K,Na)1(Mg,Fe,Ti,Ca)3(Al,Si)4O10(OH,F)2						Feldspars:		(K,Na,Ca,Ba)1(Si,Al,Fe)4O8					

n, number of measurements; nc, not calculated.

Table 4. Characterization of the pyroclastic material

Depth (m)	XRD results				EDXRF microanalyses results			Micoscope
	Quartz in pyroclasts (%)	Biotite in pyroclasts (%)	Sanidine in pyroclasts (%)	Na + Ca in sanidine (mol%)	Na + Ca in sanidine (mol%)	Mg/(Mg + Fe) atom ratio in biotite	Other minerals	Maximum size of pyroclastic grains (μm)
BII Bentonite								
314.10	nd	0.0	nd	44.0	nd			nd
314.14	nd	0.0	nd	44.0	43.8		Quartz	170
314.18	nd	0.0	nd	43.6	nd			180
314.22	nd	0.0	nd	44.1	43.1		Quartz	180
314.26	nd	0.0	nd	44.0	nd			170
314.30	23.9	0.0	76.1	43.7	43.2		Quartz	180
314.35	27.0	0.0	73.0	43.5	43.3		Quartz	180
314.40	27.7	0.0	72.3	43.5	43.9		Quartz, TiO_2	190
Kinnekulle Bentonite								
368.30	nd	nd	nd	nd	nd	nd		180
368.36	49.4	6.1	44.6	25.2	26.4	0.36	Quartz	200
368.42	52.2	7.9	39.9	25.3	nd	nd		210
368.48	52.7	7.0	40.3	25.0	nd	0.35	Quartz	200
368.54	52.0	12.4	35.6	25.1	nd	nd		220
368.60	55.1	16.9	27.9	24.9	25.7	0.35	Quartz, apatite	300
368.65	52.9	16.2	30.9	25.2	24.7	0.37	Quartz, apatite	300
368.70	48.2	21.4	30.5	26.0	25.6	0.37	Quartz, apatite	230

nd, not determined.

material most likely originated from a single volcanic eruption for both bentonites.

On the other hand, notable grain size difference of pyroclastic minerals was documented across the section of the Kinnekulle Bentonite. As a rule, coarser grain material falls first from volcanic ash clouds and consequently the lower part of the bentonite must contain larger grains than the upper part. However, while the grain size in the BII Bentonite perfectly follows this rule, in the Kinnekulle Bentonite the maximum primary grain size was found in the second and third samples from below. This may indicate relatively long duration of the Kinnekulle eruption. The deposition of larger grains in the middle of an eruption can be caused by a temporary rise in the power of the eruption or change in wind direction. The pyroclastic grain distribution of the BII Bentonite shows no obvious signatures of primary volcanogenic or air-transport-induced heterogeneity and this bentonite probably originates from a shorter eruption. The recorded immobile trace element distribution patterns in the studied sections do not contradict the concept of the single-eruption origin of both bentonites. However, variations in the contents of some minor elements (e.g. Zr, Rb, P_2O_5) in the Kinnekulle bed could reflect notable variations in pyroclastic minerals input during sedimentation.

Role of the mixing of material during transport and emplacement

The Zr content in the BII Bentonite is the highest in the lower sample and decreases upwards. As this trend occurs already in lower samples, it cannot be explained by redeposition and points to the fractionation of material already during air transport. Obviously the phenocrysts larger and heavier (e.g. zircon) than vitric particles deposited faster and accumulated in the lower part of the ash bed. In case of the Kinnekulle Bentonite the heterogeneity of the primary ash layer is signalled by somewhat irregular distribution of Zr content across the section, with the highest concentrations in sample 5.

Ash deposition in shallow-water marine environments might be accompanied by considerable redeposition and mixing of primary ash with regular marine sediments. Terrigenous and calcareous admixture in the Kinnekulle Bentonite is noticeable only in the upper sample, as indicated by slightly elevated values of CaO and Cr. Data for the BII Bentonite, however, suggest that the upper part of the bentonite layer was mixed with marine calcareous mud and terrigenous material (Fig. 7). Judging from the absence of carbonate material and low content of Ti, Cr and V, the 3–4 lower samples represent pure bentonite. The admixture of terrigenous and carbonate

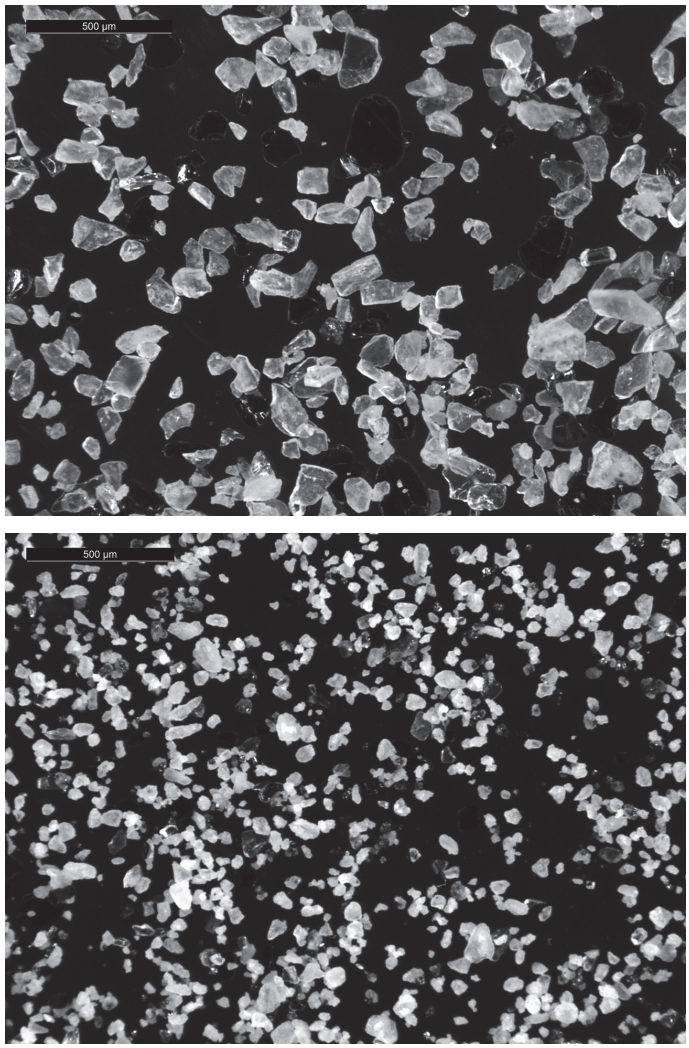

Fig. 9. Photographs of the grain fraction of the Kinnekulle Bentonite showing much larger grains in sample 3 (upper image) than in the lowermost sample 1 (lower image).

sedimentary material increases upwards starting from sample 4, as seen from the content of dolomite in bulk samples (Fig. 4) and an increase in Ti, Cr and V. Thus, geochemical trends indicate that the full section of the primary ash layer of the BII Bentonite formed under a combination of two physical processes: (1) direct fall-out of ash from the atmosphere and (2) reworking and redeposition of ash during transport from shallow- to deeper-marine environments.

Diagenetic alteration

While SiO_2 contents are high in evolved source magmas (e.g. between 60% and 80%), the concentrations in bentonites are typically significantly lower (e.g. between 40% and 60%), indicating the dissolution and removal of silica during the transformation of volcanic ash to authigenic minerals. The source magma composition of the Kinnekulle Bentonite has been determined from

glass inclusions in quartz phenocrysts (Huff et al. 1996). These analyses showed approximately 78% SiO_2 and 13% Al_2O_3. After diagenetic alteration the SiO_2 contents of bentonite are much lower – around 55%. The removal of SiO_2 from ash beds could be indicated by the accumulation of authigenic chert below thick ash beds (Grim & Güven 1978) and less frequently above them. In our case unusually high SiO_2 contents reaching 80% (Fig. 7) in the silicate part of host rock below the Kinnekulle Bentonite most likely indicate silica leaching from the bentonite. The process is similar to the silicification of conodonts (Laufeld & Jeppson 1976). The absence of elevated SiO_2 contents above the BII Bentonite suggests that either (1) early release of silica was mostly completed before the deposition of layers above, or that (2) the system was open enough to support effective migration of dissolved silica. Among other major components Na_2O, common in source magmas, has been almost completely dissolved and removed. Only small amounts of Na_2O are preserved within sanidine phenocrysts in both bentonites.

The rest of less soluble residual material has altered into clay minerals and authigenic potassium feldspar. During authigenic mineral formation, ash assimilated some elements from the surrounding environment, whereas the set of assimilated elements has been considerably different in the Kinnekulle and BII bentonites. The most obvious difference is the incorporation of Mg during the alteration of primary ash of the BII Bentonite. The content of Mg is low in the evolved source magmas (for example 0.07% in the source magma of the Kinnekulle ash, Huff et al. 1996), i.e. the observed 11–12% of MgO in the BII Bentonite and 5% in the Kinnekulle Bentonite should be predominantly of authigenic origin. Hints et al. (2006) explained the formation of high-Mg chlorite–smectite-rich bentonites under the influence of saline evaporitic waters from sabkhas of the Pirgu Age. Although hypersaline sediments of the Pirgu Age are not known in Estonia, sedimentary diagenetic dolomites occur in younger Hirnantian sediments. So it is possible that initially lagoonal environments existed also in the Pirgu Age and these primary sediments have been eroded later. The outflow of lagoonal waters along the seafloor to the open sea of the transition zone may explain both: partial dolomitization of host rocks of Pirgu age and the occurrence of chlorite–smectite in host rocks (Kiipli et al. 2012). Higher temperature in Pirgu time, possibly favouring the development of evaporitic settings, is supported by Fortey & Cocks (2005). On the basis on the movement of tropical fauna to lower latitudes, they showed a global warming in Katian time. In contrast, the limestones around the Kinnekulle Bentonite are considered to have been deposited in cold water conditions as the Baltica plate was located at that time in intermediate latitudes in the southern hemisphere (Torsvik & Rehnström 2003). Being deposited under normal marine conditions, the ash of the Kinnekulle Bentonite converted mostly to illite–smectite during alteration, the illitization process controlled by external K-flux.

Similarly to illite–smectite, the formation of authigenic K-feldspar in bentonites needs an external source of K. High potassium contents reaching 10% at the margins of the Kinnekulle Bentonite cannot be supplied from volcanic ash where the initial K_2O content was 4% (Huff et al. 1996). The K_2O content can exceed 15% in other sections (Kiipli et al. 2007). A number of hypotheses have been put forward to explain the formation of K-feldspar and incorporation of additional potassium into bentonites. Kiipli et al. (2007) suggested that high pH in shallow-sea environments enables incorporation of cations from sea water, favouring the formation of feldspars instead of H^+ in low-pH conditions, which leads to the formation of clay minerals. R. Hints et al. (2008) suggested that authigenic feldspar in Estonian bentonites might be a product of recrystallization of early diagenetic metastable zeolites, formed due to the interaction of ash and juxtaposed highly alkaline calcareous muds. Somelar et al. (2010) concluded that significant influx of potassium controlling illitization of smectite in Early Silurian bentonites was caused by regional saline fluids flowing into sedimentary rocks significantly later than the deposition time.

Late diagenetic formation of K-feldspar (or its precursor phase) in bentonites is, however, problematic because of frequent alternation of bentonites of different composition in sections. For example, the Kuressaare drill core contains the following bentonites: 368.7 m – illite–smectite with K-feldspar addition at margins, 314.4 m – chlorite–smectite with illite–smectite (present study), 215.7 m – 7 cm of pure K-feldspar, 214–158 m – 16 thin bentonite layers consisting of illite–smectite including a K-feldspar layer at 184.8 m (Kallaste & Kiipli 2006; Kiipli et al. 2006). According to R. Hints et al. (2008), the upper part of the Kinnekulle Bentonite in the Põõsaspea exposure (Northwest Estonia), includes a layer of sedimentary breccia where angular grains consist of pure K-feldspar, while the fine-grained mass of breccia contains terrigenous clay and carbonates. This indicates that the hardened layer in the upper part of the bentonite had already formed before a storm event brecciated it, strongly supporting an early start of the recrystallization of primary ash.

Supposing that Al_2O_3 was immobile (13% in source magma and 20% in bentonite) during the conversion of

volcanic ash to clay and feldspar, we see that concentrations of immobile elements in the Kinnekulle Bentonite have risen 1.5 times compared with source magma. In our previous analyses on the East Baltic materials we have considered Ti, Zr, Th and Nb as immobile (Kiipli et al. 2008b, 2013). The present data from the BII Bentonite, where the maximum Nb content significantly exceeding common values in the silicate parts of the host rock occurs directly below the bentonite, indicate small-scale mobility of this element during the conversion of volcanic ash in lime sediment. Although small-scale mobility to a distance of a few centimetres may not exclude the use of Nb in the interpretation of source magma, still, care should be taken when using this element in particular cases. In the samples of the Kinnekulle Bentonite, for example, the Nb/Y ratio, commonly used for discriminating magma series (Winchester & Floyd 1977), was found to vary from 0.4 to 0.9. However, this considerably large variation is largely dependent on the irregular distribution of Y, whose content in beds was likely controlled by combined factors such as the input of pyroclastic apatite and leaching of elements near the upper contact of the ash bed.

Environmental effects of ash-falls and interaction of the ash–water–sediment system

Some previous works have reported a marked decrease in the diversity of marine life after the deposition of the thick Kinnekulle Bentonite (Hints et al. 2003; Perrier et al. 2012) and interpreted those variations as consequences of environmental perturbations caused by volcanic eruptions. The geochemical signatures recorded in bentonites and their host rocks by the current study demonstrate that both studied large ash-falls, but more notably the Kinnekulle ash-fall, triggered environmental changes in marine settings where they were deposited. The direct effect of the ash-fall can be read from the peaks of sulphur below and above the Kinnekulle Bentonite. Sulphur fixation in sediments occurs when organic material is decayed in an anoxic environment via microbial sulphate reduction. Life forms on the sea bottom possibly died at the lower contact of the primary ash layer as a result of abrupt burial under the ash, which initially could be up to 1 m thick, and thus promoted the development of anoxia below. Water-soluble ash leachates could additionally provide an extra source of sulphate for sulphate reduction near a freshly deposited ash layer. It is also possible that ash-fall was accompanied by toxification of the water column and mass mortality. The deposition of dead organic matter on the sea floor could have been slower than of volcanic dust due to its better flotation properties. Consequently the organic matter could accumulate in the upper layers of the ash bed, thus explaining sulphur accumulation in the upper layer of bentonite. Alternatively, an ash-fall could trigger an increase in primary production through fertilizing the water column with essential macro- and micronutrients (e.g. Duggen et al. 2010). The resultant rise in organic matter flux to the shallow sea bottom could promote quick consumption of free oxygen and sulphate reduction.

The absence of sulphur peaks at the margins of the BII Bentonite may be caused by a shorter duration of the eruption and a smaller amount of ash which reached the sedimentation area. Violet patches in host rock also indicate an environment with better oxygenated sediments and probably with lower bioproductivity during the deposition of the bentonite. The lower sulphur content of this bentonite could as well reflect more suppressed microbial sulphate reduction in a marine environment with increased salinity.

An outstanding feature of both studied bentonites is P and Ca peaks (Fig. 5) in the host rock directly above the bentonites. This effect is greater after the thicker Kinnekulle Bentonite and less significant after the smaller BII Bentonite. Note that the previously discussed sulphur peak occurs in the Kinnekulle bed just below the Ca- and P-rich host rock. Increased productivity after the ash-fall, bottom oxygen deficit, enhanced sulphate reduction and raised alkalinity near the sediment–water interface could possibly favour precipitation of calcium carbonate from the dissolved Ca-hydrocarbonate. The enrichment of P, which is a fundamental limiting nutrient for marine life (Filippelli 2002; E. Kiipli et al. 2010), is more controversial. Phosphorus mostly remineralized in the course of organic matter breakdown on the seafloor and most of it externally recycled in shallow marine environments. Studies of modern volcanic ashes indicate that some ash-falls might provide a considerable extra source of P for marine environments through rapid release of the element from ash (Jones & Gislason 2008). The recorded P_2O_5 values in the Kinnekulle and BII bentonites are rather low; however, it does not exclude the possibility that some of P was released during very early stages of ash transformation. We suppose that P-enrichment above the studied bentonites could have been induced either (1) by the release of P during anoxic breakdown of organic matter under increased flux of organic matter to the seafloor or (2) by the desorption of phosphorous species or leaching of P from ash particles, and thereafter fixation in alkaline mud above the ash beds.

CONCLUSIONS

1. Both the Kinnekulle and BII bentonites in the Kuressaare section were formed from a single volcanic eruption as evidenced by the stability of the composition of phenocrysts through the entire section of the bentonite. In Norway and Sweden a multiple eruption deposit has been interpreted in the Kinnekulle Bentonite (Batchelor 2014), thus our study area received only some of the ash events. Sanidine phenocryst compositions that have been used in many previous studies for proving the correlations of volcanic ash beds are stable throughout the vertical section and therefore serve as a good discrimination criterion. Phenocrysts from the redeposited parts of bentonites can also be used for correlation. Sanidine composition can be analysed very precisely (±0.5 mol%) with advanced XRD technologies.
2. The Kinnekulle Bentonite, one of the major volcanic ash beds of the Phanerozoic, was formed from the eruption of longer duration, with a maximum power of the eruption in the middle. Pyroclastic mineral grain size distribution and immobile trace element composition point to the layered and heterogeneous nature of the primary ash bed.
3. The BII Bentonite formed from a less voluminous eruption of shorter duration. Its full thickness was accumulated from the redeposition of volcanic material in shallow-sea areas.
4. For reliable trace-element-based correlation of thick bentonites the bulk chemical composition of several samples covering the whole section should be studied. Lower parts of the bentonites originating from direct ash-falls are of correlative value. However, the mobility of trace elements should be checked in advance.
5. The Kinnekulle ash-fall and to a lesser extent the BII ash-fall had a notable effect on the chemistry of juxtaposed marine sediments. Peak concentrations of Ca and P directly above both bentonites and the increased S content near bentonite contacts show that the ash-falls triggered significant fluctuations in biotic and geochemical cycles in shallow marine settings.

Acknowledgements. We greatly appreciate constructive criticism and numerous helpful comments of the reviewer Richard A. Batchelor and an anonymous referee. This study was supported by the Estonian Ministry of Education and Research through the target research project No. SF0140016s09.

REFERENCES

Altaner, S. P., Hower, J. & Whitney, G. 1984. Model for K-bentonite formation – evidence from zoned K-bentonites in the disturbed belt, Montana. *Geology*, **12**, 412–415.

Batchelor, R. A. 2009. Geochemical "Golden Spike" for Lower Palaeozoic metabentonites. *Earth and Environmental Science Transactions of the Royal Society of Edinburgh*, **99**, 177–187.

Batchelor, R. A. 2014. Geochemistry of Upper Ordovician metabentonites and their cognate apatite microphenocrysts from Norway and Sweden. *GFF*, **136**, 387–397.

Bergström, S. M., Huff, W. D., Kolata, D. R. & Bauert, H. 1995. Nomenclature, stratigraphy, chemical fingerprinting, and areal distribution of some Middle Ordovician K-bentonites in Baltoscandia. *Geologiska Föreningens i Stockholm Förhandlingar (GFF)*, **117**, 1–13.

Bergström, S. M., Huff, W. D., Kolata, D. R., Yost, D. A. & Hart, C. 1997. A unique Middle Ordovician K-bentonite bed succession at Röstånga, S. Sweden. *GFF*, **119**, 231–244.

Brusewitz, A. M. 1988. Asymmetric zonation of a thick Ordovician K-bentonite bed at Kinnekulle, Sweden. *Clays and Clay Minerals*, **36**, 349–353.

Dahlqvist, P., Calner, M., Kallaste, T., Kiipli, T. & Siir, S. 2012. Geochemical variations within the mid-Silurian Grötlingbo Bentonite (Gotland, Sweden): discriminating between magmatic composition, ash transport fractionation and diagenetic effects. *GFF*, **134**, 273–282.

Duggen, S., Olgun, N., Croot, P., Hoffmann, L., Dietze, H., Delmelle, P. & Teschner, C. 2010. The role of airborne volcanic ash for the surface ocean biogeochemical iron-cycle. *Biogeosciences*, **7**, 827–844.

Filippelli, G. M. 2002. The global phosphorus cycle. In *Phosphates: Geochemical, Geobiological, and Materials Importance* (Kohn, M., Rakovan, J. & Hughes, J., eds), *Mineralogy & Geochemistry*, **48**, 391–425.

Fisher, R. V. & Schmincke, H. U. 1984. *Pyroclastic Rocks*. Springer-Verlag, Berlin, Heidelberg, New York, Tokyo, 472 pp.

Fortey, R. A. & Cocks, L. R. M. 2005. Late Ordovician global warming – The Boda event. *Geology*, **33**, 405–408.

Grim, R. E. & Güven, N. 1978. Bentonites, geology, mineralogy, properties and uses. *Developments in Sedimentology*, **24**, 1–256.

Hetherington, C. J., Nakrem, H. A. & Potel, S. 2011. Note on the composition and mineralogy of upper Silurian bentonites from the Ringerike District: implications for local and regional stratigraphic correlation and sedimentation. *Norwegian Journal of Geology*, **91**, 181–192.

Hints, L., Männik, P., Hints, O. & Hints, R. 2008. Discovery of the Ordovician Kinnekulle K-bentonite at the Põõsaspea cliff, NW Estonia. *Estonian Journal of Earth Sciences*, **57**, 192–196.

Hints, O., Kallaste, T. & Kiipli, T. 1997. Mineralogy and micropalaeontology of the Kinnekulle altered volcanic ash bed (Ordovician) at Pääsküla, North Estonia. *Proceedings of the Estonian Academy of Sciences, Geology*, **46**, 107–118.

Hints, O., Hints, L. & Meidla, T. 2003. Effects of the Ordovician Kinnekulle ash-fall recorded in northern Estonia. *Bulletin of the Geological Society of Denmark*, **50**, 115–123.

Hints, R., Kirsimäe, K., Somelar, P., Kallaste, T. & Kiipli, T. 2006. Chloritization of Late Ordovician K-bentonites from the northern Baltic Palaeobasin – influence from source material or diagenetic environment? *Sedimentary Geology*, **191**, 55–66.

Hints, R., Kirsimäe, K., Somelar, P., Kallaste, T. & Kiipli, T. 2008. Multiphase Silurian bentonites in the Baltic Palaeobasin. *Sedimentary Geology*, **209**, 69–79.

Huff, W. D., Kolata, D. R., Bergström, S. M. & Zhang, Y.-S. 1996. Large-magnitude Middle Ordovician volcanic ash falls in North America and Europe: dimensions, emplacement and post-emplacement characteristics. *Journal of Volcanology and Geothermal Research*, **73**, 285–301.

Huff, W. D., Bergström, S. M. & Kolata, D. R. 2010. Ordovician explosive volcanism. In *The Ordovician Earth System* (Finney, S. C. & Berry, W. B. N., eds), *The Geological Society of America Special Paper*, **466**, 13–28.

Jones, M. T. & Gislason, S. R. 2008. Rapid releases of metal salts and nutrients following the deposition of volcanic ash into aqueous environments. *Geochimica et Cosmochimica Acta*, **72**, 3661–3680.

Kaljo, D., Grytsenko, V., Kallaste, T., Kiipli, T. & Martma, T. 2014. Upper Silurian stratigraphy of Podolia revisited: carbon isotopes, bentonites and biostratigraphy. *GFF*, **136**, 136–141.

Kallaste, T. & Kiipli, T. 2006. New correlations of Telychian (Silurian) bentonites in Estonia. *Proceedings of the Estonian Academy of Sciences, Geology*, **55**, 241–251.

Kastner, M. 1971. Authigenic feldspars in carbonate rocks. *American Mineralogist*, **56**, 1403–1442.

Kiipli, E., Kallaste, T. & Kiipli, T. 2004. Metabentonites of the Pirgu Stage (Ashgill, Upper Ordovician) of the East Baltic. In *WOGOGOB-2004, 8th Meeting of the Working Group on the Ordovician Geology of Baltoscandia, May 13–18, Tallinn and Tartu, Estonia, Abstracts and Field Guidebook* (Hints, O. & Ainsaar, L., eds), pp. 53–54. Institute of Geology, University of Tartu.

Kiipli, E., Kiipli, T., Kallaste, T. & Ainsaar, L. 2010. Distribution of phosphorus in the Middle and Upper Ordovician Baltoscandian carbonate palaeobasin. *Estonian Journal of Earth Sciences*, **59**, 247–255.

Kiipli, E., Kiipli, T., Kallaste, T. & Siir, S. 2012. Al_2O_3/TiO_2 ratio of the clay fraction of Late Ordovician–Silurian carbonate rocks as an indicator of paleoclimate of the Fennoscandian Shield. *Palaeogeography, Palaeoclimatology, Palaeoecology*, **365–366**, 312–320.

Kiipli, T., Kallaste, T., Kiipli, E. & Orlova, K. 2006. Upper Ordovician volcanic ash beds. In *Kerguta (565) Drill Core* (Põldvere, A., ed.), *Estonian Geological Sections*, 7, 15–18.

Kiipli, T., Kiipli, E., Kallaste, T., Hints, R., Somelar, P. & Kirsimäe, K. 2007. Altered volcanic ash as an indicator of marine environment, reflecting pH and sedimentation rate – example from the Ordovician Kinnekulle bed of Baltoscandia. *Clays and Clay Minerals*, **55**, 177–188.

Kiipli, T., Jeppsson, L., Kallaste, T. & Söderlund, U. 2008a. Correlation of Silurian bentonites from Gotland and the East Baltic using sanidine phenocryst composition, and biostratigraphical consequences. *Journal of the Geological Society*, **165**, 211–220.

Kiipli, T., Orlova, K., Kiipli, E. & Kallaste, T. 2008b. Use of immobile trace elements for the correlation of Telychian bentonites on Saaremaa Island, Estonia, and mapping of volcanic ash clouds. *Estonian Journal of Earth Sciences*, **57**, 39–52.

Kiipli, T., Kallaste, T. & Nestor, V. 2010a. Composition and correlation of volcanic ash beds of Silurian age from the eastern Baltic. *Geological Magazine*, **147**, 895–909.

Kiipli, T., Kallaste, T., Nestor, V. & Loydell, D. K. 2010b. Integrated Telychian (Silurian) K-bentonite chemostratigraphy and biostratigraphy in Estonia and Latvia. *Lethaia*, **43**, 32–44.

Kiipli, T., Radzevičius, S., Kallaste, T., Kiipli, E., Siir, S., Soesoo, A. & Voolma, M. 2012. The Geniai Tuff in the southern East Baltic area – a new correlation tool near the Aeronian/Telychian stage boundary, Llandovery, Silurian. *Bulletin of Geosciences*, **87**, 695–704.

Kiipli, T., Kallaste, T., Kiipli, E. & Radzevičius, S. 2013. Correlation of Silurian bentonites based on the immobile elements in the East Baltic and Scandinavia. *GFF*, **135**, 152–161.

Kiipli, T., Kallaste, T., Nielsen, A., Schovsbo, N. & Siir, S. 2014a. Geochemical discrimination of the Upper Ordovician Kinnekulle Bentonite in the Billegrav-2 drill core section, Bornholm, Denmark. *Estonian Journal of Earth Sciences*, **63**, 264–270.

Kiipli, T., Radzevičius, S. & Kallaste, T. 2014b. Silurian bentonites in Lithuania: correlations based on sanidine phenocryst composition and graptolite biozonation – interpretation of volcanic source regions. *Estonian Journal of Earth Sciences*, **63**, 18–29.

Kiipli, T., Soesoo, A. & Kallaste, T. 2014c. Geochemical evolution of Caledonian volcanism recorded in the sedimentary rocks of the eastern Baltic region. In *New perspectives on the Caledonides of Scandinavia and Related areas* (Corfu, F., Gasser, D. & Chew, D. M., eds), *Geological Society Special Publications*, **390**, 177–192.

Kiipli, T., Dahlquist, P., Kallaste, T., Kiipli, E. & Nõlvak, J. 2015. Upper Katian (Ordovician) bentonites in the East Baltic, Scandinavia and Scotland: geochemical correlation and volcanic source interpretation. *Geological Magazine*, dx.doi.org/10.1017/S001675681400051X.

Kolata, D. R., Frost, J. K. & Huff, W. D. 1987. Chemical correlation of K-bentonite beds in the Middle Ordovician Decorah Subgroup, upper Mississippi Valley. *Geology*, **15**, 208–211.

Laufeld, S. & Jeppsson, L. 1976. Silicification and bentonites in the Silurian of Gotland. *GFF*, **98**, 31–44.

Männik, P., Põldvere, A., Nestor, V., Kallaste, T., Kiipli, T. & Martma, T. 2014. The Llandovery–Wenlock boundary interval in west-central continental Estonia: an example from the Suigu (S-3) core section. *Estonian Journal of Earth Sciences*, **63**, 1–17.

Perrier, V., Meidla, T., Tinn, O. & Ainsaar, L. 2012. Biotic response to explosive volcanism: ostracod recovery

after Ordovician ash-falls. *Palaeogeography, Palaeoclimatology, Palaeoecology*, **365–366**, 166–183.

Põlma, L. 1967. On the transitional area between the northern and axial lithofacies zones of the East Baltic Ordovician. *Proceedings of the Estonian Academy of Sciences, Chemistry, Geology*, **16**, 272–275 [in Russian].

Rampino, M. R., Self, S. & Stothers, R. B. 1988. Volcanic winters. *Annual Review of Earth and Planetary Science*, **16**, 73–99.

Ray, D. C., Collings, A. V. J., Worton, G. J. & Jones, G. 2011. Upper Wenlock bentonites from Wren's Nest Hill, Dudley: comparisons with prominent bentonites along Wenlock Edge, Shropshire, England. *Geological Magazine*, **148**, 670–681.

Somelar, P., Kirsimäe, K., Hints, R. & Kirs, J. 2010. Illitization of Early Paleozoic K-bentonites in the Baltic Basin: decoupling of burial- and fluid-driven processes. *Clays and Clay Minerals*, **58**, 388–398.

Torsvik, T. H. & Rehnström, E. F. 2003. The Tornquist Sea and Baltic Avalonia docking. *Tectonophysics*, **362**, 67–82.

Winchester, J. A. & Floyd, P. A. 1977. Geochemical discrimination of different magma series and their differentiation products using immobile elements. *Chemical Geology*, **20**, 325–343.

Kahe paksu Ordoviitsiumi bentoniidi sisemine stratifikatsioon: magmaliste, setteliste, keskkonna ja diageneetiliste tunnuste dešifreerimine

Sven Siir, Toivo Kallaste, Tarmo Kiipli ja Rutt Hints

Uuriti 26 proovi kahest suurest vulkaanilise tuha kihist, Kinnekulle ja BII Bentoniidist Kuressaare K-3 puuraugust Saaremaalt, eesmärgiga välja selgitada kihtide sisemine geokeemiline ning mineraloogiline heterogeensus. On kirjeldatud ja interpreteeritud märke materjali fraktsioneerumisest vulkaanituha transpordil ning ümbersettimisel merebasseinis ja tunnuseid elementide diageneetilisest ümberjaotumisest. Valdavaks autigeenseks mineraaliks Kinnekulle Bentoniidis on illiit-smektiit vähesema kaaliumpäevakivi lisandiga kihi äärtel. BII Bentoniit koosneb kloriit-smektiidist ja illiit-smektiidist. Magmaliste fenokristallide sanidiini ja biotiidi koostise stabiilsus mõlema kihi vertikaalläbilõikes tõendab, et mõlema bentoniidi lähtematerjal kuhjus ühest vulkaanipurskest. Sanidiini koostise stabiilsus (±0,5 mol%) mõlema bentoniidi läbilõikes kinnitab, et see on usaldusväärne kriteerium bentoniidikihtide identifitseerimiseks ja korrelatsiooniks. Mikroelementide jaotus osutab, et Zr, Ga, Rb, Nb, Ti ja Th püsisid immobiilsena vulkaanilise tuha muutumisel bentoniidiks, peegeldades hästi vulkaanilise tuha algset koostist. Siiski on märgata väikest Nb, Ti ja Y liikuvust kihtide kontaktil ümbriskivimiga. Märkimisväärsed S, Ca ja P akumulatsioonid kihtide kontaktidel ümbriskivimiga on tunnuseks, et vulkaanituha kuhjumine põhjustas märgatavaid hälbeid madalmere ning settelises keskkonnas.

DISSERTATIONS DEFENDED AT
TALLINN UNIVERSITY OF TECHNOLOGY ON
NATURAL AND EXACT SCIENCES

1. **Olav Kongas**. Nonlinear Dynamics in Modeling Cardiac Arrhytmias. 1998.

2. **Kalju Vanatalu**. Optimization of Processes of Microbial Biosynthesis of Isotopically Labeled Biomolecules and Their Complexes. 1999.

3. **Ahto Buldas**. An Algebraic Approach to the Structure of Graphs. 1999.

4. **Monika Drews**. A Metabolic Study of Insect Cells in Batch and Continuous Culture: Application of Chemostat and Turbidostat to the Production of Recombinant Proteins. 1999.

5. **Eola Valdre**. Endothelial-Specific Regulation of Vessel Formation: Role of Receptor Tyrosine Kinases. 2000.

6. **Kalju Lott**. Doping and Defect Thermodynamic Equilibrium in ZnS. 2000.

7. **Reet Koljak**. Novel Fatty Acid Dioxygenases from the Corals *Plexaura homomalla* and *Gersemia fruticosa.* 2001.

8. **Anne Paju**. Asymmetric oxidation of Prochiral and Racemic Ketones by Using Sharpless Catalyst. 2001.

9. **Marko Vendelin**. Cardiac Mechanoenergetics *in silico*. 2001.

10. **Pearu Peterson**. Multi-Soliton Interactions and the Inverse Problem of Wave Crest. 2001.

11. **Anne Menert**. Microcalorimetry of Anaerobic Digestion. 2001.

12. **Toomas Tiivel**. The Role of the Mitochondrial Outer Membrane in *in vivo* Regulation of Respiration in Normal Heart and Skeletal Muscle Cell. 2002.

13. **Olle Hints**. Ordovician Scolecodonts of Estonia and Neighbouring Areas: Taxonomy, Distribution, Palaeoecology, and Application. 2002.

14. **Jaak Nõlvak**. Chitinozoan Biostratigrapy in the Ordovician of Baltoscandia. 2002.

15. **Liivi Kluge**. On Algebraic Structure of Pre-Operad. 2002.

16. **Jaanus Lass**. Biosignal Interpretation: Study of Cardiac Arrhytmias and Electromagnetic Field Effects on Human Nervous System. 2002.

17. **Janek Peterson**. Synthesis, Structural Characterization and Modification of PAMAM Dendrimers. 2002.

18. **Merike Vaher**. Room Temperature Ionic Liquids as Background Electrolyte Additives in Capillary Electrophoresis. 2002.

19. **Valdek Mikli**. Electron Microscopy and Image Analysis Study of Powdered Hardmetal Materials and Optoelectronic Thin Films. 2003.

20. **Mart Viljus**. The Microstructure and Properties of Fine-Grained Cermets. 2003.

21. **Signe Kask**. Identification and Characterization of Dairy-Related *Lactobacillus.* 2003

22. **Tiiu-Mai Laht**. Influence of Microstructure of the Curd on Enzymatic and Microbiological Processes in Swiss-Type Cheese. 2003.

23. **Anne Kuusksalu**. 2–5A Synthetase in the Marine Sponge *Geodia cydonium*. 2003.

24. **Sergei Bereznev**. Solar Cells Based on Polycristalline Copper-Indium Chalcogenides and Conductive Polymers. 2003.

25. **Kadri Kriis**. Asymmetric Synthesis of C_2-Symmetric Bimorpholines and Their Application as Chiral Ligands in the Transfer Hydrogenation of Aromatic Ketones. 2004.

26. **Jekaterina Reut**. Polypyrrole Coatings on Conducting and Insulating Substracts. 2004.

27. **Sven Nõmm**. Realization and Identification of Discrete-Time Nonlinear Systems. 2004.

28. **Olga Kijatkina**. Deposition of Copper Indium Disulphide Films by Chemical Spray Pyrolysis. 2004.

29. **Gert Tamberg**. On Sampling Operators Defined by Rogosinski, Hann and Blackman Windows. 2004.

30. **Monika Übner**. Interaction of Humic Substances with Metal Cations. 2004.

31. **Kaarel Adamberg**. Growth Characteristics of Non-Starter Lactic Acid Bacteria from Cheese. 2004.

32. **Imre Vallikivi**. Lipase-Catalysed Reactions of Prostaglandins. 2004.

33. **Merike Peld**. Substituted Apatites as Sorbents for Heavy Metals. 2005.

34. **Vitali Syritski**. Study of Synthesis and Redox Switching of Polypyrrole and Poly(3,4-ethylenedioxythiophene) by Using *in-situ* Techniques. 2004.

35. **Lee Põllumaa**. Evaluation of Ecotoxicological Effects Related to Oil Shale Industry. 2004.

36. **Riina Aav**. Synthesis of 9,11-Secosterols Intermediates. 2005.

37. **Andres Braunbrück**. Wave Interaction in Weakly Inhomogeneous Materials. 2005.

38. **Robert Kitt**. Generalised Scale-Invariance in Financial Time Series. 2005.

39. **Juss Pavelson**. Mesoscale Physical Processes and the Related Impact on the Summer Nutrient Fields and Phytoplankton Blooms in the Western Gulf of Finland. 2005.

40. **Olari Ilison**. Solitons and Solitary Waves in Media with Higher Order Dispersive and Nonlinear Effects. 2005.

41. **Maksim Säkki**. Intermittency and Long-Range Structurization of Heart Rate. 2005.

42. **Enli Kiipli**. Modelling Seawater Chemistry of the East Baltic Basin in the Late Ordovician–Early Silurian. 2005.

43. **Igor Golovtsov**. Modification of Conductive Properties and Processability of Polyparaphenylene, Polypyrrole and polyaniline. 2005.

44. **Katrin Laos**. Interaction Between Furcellaran and the Globular Proteins (Bovine Serum Albumin β-Lactoglobulin). 2005.

45. **Arvo Mere**. Structural and Electrical Properties of Spray Deposited Copper Indium Disulphide Films for Solar Cells. 2006.

46. **Sille Ehala**. Development and Application of Various On- and Off-Line Analytical Methods for the Analysis of Bioactive Compounds. 2006.

47. **Maria Kulp**. Capillary Electrophoretic Monitoring of Biochemical Reaction Kinetics. 2006.

48. **Anu Aaspõllu.** Proteinases from *Vipera lebetina* Snake Venom Affecting Hemostasis. 2006.

49. **Lyudmila Chekulayeva**. Photosensitized Inactivation of Tumor Cells by Porphyrins and Chlorins. 2006.

50. **Merle Uudsemaa**. Quantum-Chemical Modeling of Solvated First Row Transition Metal Ions. 2006.

51. **Tagli Pitsi**. Nutrition Situation of Pre-School Children in Estonia from 1995 to 2004. 2006.

52. **Angela Ivask**. Luminescent Recombinant Sensor Bacteria for the Analysis of Bioavailable Heavy Metals. 2006.

53. **Tiina Lõugas**. Study on Physico-Chemical Properties and Some Bioactive Compounds of Sea Buckthorn (*Hippophae rhamnoides* L.). 2006.

54. **Kaja Kasemets**. Effect of Changing Environmental Conditions on the Fermentative Growth of *Saccharomyces cerevisae* S288C: Auxo-accelerostat Study. 2006.

55. **Ildar Nisamedtinov**. Application of ^{13}C and Fluorescence Labeling in Metabolic Studies of *Saccharomyces* spp. 2006.

56. **Alar Leibak**. On Additive Generalisation of Voronoï's Theory of Perfect Forms over Algebraic Number Fields. 2006.

57. **Andri Jagomägi**. Photoluminescence of Chalcopyrite Tellurides. 2006.

58. **Tõnu Martma**. Application of Carbon Isotopes to the Study of the Ordovician and Silurian of the Baltic. 2006.

59. **Marit Kauk**. Chemical Composition of $CuInSe_2$ Monograin Powders for Solar Cell Application. 2006.

60. **Julia Kois**. Electrochemical Deposition of $CuInSe_2$ Thin Films for Photovoltaic Applications. 2006.

61. **Ilona Oja Açik**. Sol-Gel Deposition of Titanium Dioxide Films. 2007.

62. **Tiia Anmann**. Integrated and Organized Cellular Bioenergetic Systems in Heart and Brain. 2007.

63. **Katrin Trummal**. Purification, Characterization and Specificity Studies of Metalloproteinases from *Vipera lebetina* Snake Venom. 2007.

64. **Gennadi Lessin**. Biochemical Definition of Coastal Zone Using Numerical Modeling and Measurement Data. 2007.

65. **Enno Pais**. Inverse problems to determine non-homogeneous degenerate memory kernels in heat flow. 2007.

66. **Maria Borissova**. Capillary Electrophoresis on Alkylimidazolium Salts. 2007.

67. **Karin Valmsen**. Prostaglandin Synthesis in the Coral *Plexaura homomalla*: Control of Prostaglandin Stereochemistry at Carbon 15 by Cyclooxygenases. 2007.

68. **Kristjan Piirimäe**. Long-Term Changes of Nutrient Fluxes in the Drainage Basin of the Gulf of Finland – Application of the PolFlow Model. 2007.

69. **Tatjana Dedova**. Chemical Spray Pyrolysis Deposition of Zinc Sulfide Thin Films and Zinc Oxide Nanostructured Layers. 2007.

70. **Katrin Tomson**. Production of Labelled Recombinant Proteins in Fed-Batch Systems in *Escherichia coli*. 2007.

71. **Cecilia Sarmiento**. Suppressors of RNA Silencing in Plants. 2008.

72. **Vilja Mardla**. Inhibition of Platelet Aggregation with Combination of Antiplatelet Agents. 2008.

73. **Maie Bachmann**. Effect of Modulated Microwave Radiation on Human Resting Electroencephalographic Signal. 2008.

74. **Dan Hüvonen**. Terahertz Spectroscopy of Low-Dimensional Spin Systems. 2008.

75. **Ly Villo**. Stereoselective Chemoenzymatic Synthesis of Deoxy Sugar Esters Involving *Candida antarctica* Lipase B. 2008.

76. **Johan Anton**. Technology of Integrated Photoelasticity for Residual Stress Measurement in Glass Articles of Axisymmetric Shape. 2008.

77. **Olga Volobujeva**. SEM Study of Selenization of Different Thin Metallic Films. 2008.

78. **Artur Jõgi**. Synthesis of 4'-Substituted 2,3'-dideoxynucleoside Analogues. 2008.

79. **Mario Kadastik**. Doubly Charged Higgs Boson Decays and Implications on Neutrino Physics. 2008.

80. **Fernando Pérez-Caballero**. Carbon Aerogels from 5-Methylresorcinol-Formaldehyde Gels. 2008.

81. **Sirje Vaask**. The Comparability, Reproducibility and Validity of Estonian Food Consumption Surveys. 2008.

82. **Anna Menaker**. Electrosynthesized Conducting Polymers, Polypyrrole and Poly(3,4-ethylenedioxythiophene), for Molecular Imprinting. 2009.

83. **Lauri Ilison**. Solitons and Solitary Waves in Hierarchical Korteweg-de Vries Type Systems. 2009.

84. **Kaia Ernits**. Study of In_2S_3 and ZnS Thin Films Deposited by Ultrasonic Spray Pyrolysis and Chemical Deposition. 2009.

85. **Veljo Sinivee**. Portable Spectrometer for Ionizing Radiation "Gammamapper". 2009.

86. **Jüri Virkepu**. On Lagrange Formalism for Lie Theory and Operadic Harmonic Oscillator in Low Dimensions. 2009.

87. **Marko Piirsoo**. Deciphering Molecular Basis of Schwann Cell Development. 2009.

88. **Kati Helmja**. Determination of Phenolic Compounds and Their Antioxidative Capability in Plant Extracts. 2010.

89. **Merike Sõmera**. Sobemoviruses: Genomic Organization, Potential for Recombination and Necessity of P1 in Systemic Infection. 2010.

90. **Kristjan Laes**. Preparation and Impedance Spectroscopy of Hybrid Structures Based on $CuIn_3Se_5$ Photoabsorber. 2010.

91. **Kristin Lippur**. Asymmetric Synthesis of 2,2'-Bimorpholine and its 5,5'-Substituted Derivatives. 2010.

92. **Merike Luman**. Dialysis Dose and Nutrition Assessment by an Optical Method. 2010.

93. **Mihhail Berezovski**. Numerical Simulation of Wave Propagation in Heterogeneous and Microstructured Materials. 2010.

94. **Tamara Aid-Pavlidis**. Structure and Regulation of BDNF Gene. 2010.

95. **Olga Bragina**. The Role of Sonic Hedgehog Pathway in Neuro- and Tumorigenesis. 2010.

96. **Merle Randrüüt**. Wave Propagation in Microstructured Solids: Solitary and Periodic Waves. 2010.

97. **Marju Laars**. Asymmetric Organocatalytic Michael and Aldol Reactions Mediated by Cyclic Amines. 2010.

98. **Maarja Grossberg**. Optical Properties of Multinary Semiconductor Compounds for Photovoltaic Applications. 2010.

99. **Alla Maloverjan**. Vertebrate Homologues of Drosophila Fused Kinase and Their Role in Sonic Hedgehog Signalling Pathway. 2010.

100. **Priit Pruunsild**. Neuronal Activity-Dependent Transcription Factors and Regulation of Human *BDNF* Gene. 2010.

101. **Tatjana Knjazeva**. New Approaches in Capillary Electrophoresis for Separation and Study of Proteins. 2011.

102. **Atanas Katerski**. Chemical Composition of Sprayed Copper Indium Disulfide Films for Nanostructured Solar Cells. 2011.

103. **Kristi Timmo.** Formation of Properties of $CuInSe_2$ and $Cu_2ZnSn(S,Se)_4$ Monograin Powders Synthesized in Molten KI. 2011.

104. **Kert Tamm**. Wave Propagation and Interaction in Mindlin-Type Microstructured Solids: Numerical Simulation. 2011.

105. **Adrian Popp**. Ordovician Proetid Trilobites in Baltoscandia and Germany. 2011.

106. **Ove Pärn**. Sea Ice Deformation Events in the Gulf of Finland and This Impact on Shipping. 2011.

107. **Germo Väli**. Numerical Experiments on Matter Transport in the Baltic Sea. 2011.

108. **Andrus Seiman**. Point-of-Care Analyser Based on Capillary Electrophoresis. 2011.

109. **Olga Katargina**. Tick-Borne Pathogens Circulating in Estonia (Tick-Borne Encephalitis Virus, *Anaplasma phagocytophilum*, *Babesia* Species): Their Prevalence and Genetic Characterization. 2011.

110. **Ingrid Sumeri**. The Study of Probiotic Bacteria in Human Gastrointestinal Tract Simulator. 2011.

111. **Kairit Zovo**. Functional Characterization of Cellular Copper Proteome. 2011.

112. **Natalja Makarytsheva**. Analysis of Organic Species in Sediments and Soil by High Performance Separation Methods. 2011.

113. **Monika Mortimer**. Evaluation of the Biological Effects of Engineered Nanoparticles on Unicellular Pro- and Eukaryotic Organisms. 2011.

114. **Kersti Tepp**. Molecular System Bioenergetics of Cardiac Cells: Quantitative Analysis of Structure-Function Relationship. 2011.

115. **Anna-Liisa Peikolainen**. Organic Aerogels Based on 5-Methylresorcinol. 2011.

116. **Leeli Amon**. Palaeoecological Reconstruction of Late-Glacial Vegetation Dynamics in Eastern Baltic Area: A View Based on Plant Macrofossil Analysis. 2011.

117. **Tanel Peets**. Dispersion Analysis of Wave Motion in Microstructured Solids. 2011.

118. **Liina Kaupmees**. Selenization of Molybdenum as Contact Material in Solar Cells. 2011.

119. **Allan Olspert**. Properties of VPg and Coat Protein of Sobemoviruses. 2011.

120. **Kadri Koppel**. Food Category Appraisal Using Sensory Methods. 2011.

121. **Jelena Gorbatšova**. Development of Methods for CE Analysis of Plant Phenolics and Vitamins. 2011.

122. **Karin Viipsi**. Impact of EDTA and Humic Substances on the Removal of Cd and Zn from Aqueous Solutions by Apatite. 2012.

123. **David Schryer**. Metabolic Flux Analysis of Compartmentalized Systems Using Dynamic Isotopologue Modeling. 2012.

124. **Ardo Illaste**. Analysis of Molecular Movements in Cardiac Myocytes. 2012.

125. **Indrek Reile**. 3-Alkylcyclopentane-1,2-Diones in Asymmetric Oxidation and Alkylation Reactions. 2012.

126. **Tatjana Tamberg**. Some Classes of Finite 2-Groups and Their Endomorphism Semigroups. 2012.

127. **Taavi Liblik**. Variability of Thermohaline Structure in the Gulf of Finland in Summer. 2012.

128. **Priidik Lagemaa**. Operational Forecasting in Estonian Marine Waters. 2012.

129. **Andrei Errapart**. Photoelastic Tomography in Linear and Non-linear Approximation. 2012.

130. **Külliki Krabbi**. Biochemical Diagnosis of Classical Galactosemia and Mucopolysaccharidoses in Estonia. 2012.

131. **Kristel Kaseleht**. Identification of Aroma Compounds in Food using SPME-GC/MS and GC-Olfactometry. 2012.

132. **Kristel Kodar**. Immunoglobulin G Glycosylation Profiling in Patients with Gastric Cancer. 2012.

133. **Kai Rosin**. Solar Radiation and Wind as Agents of the Formation of the Radiation Regime in Water Bodies. 2012.

134. **Ann Tiiman**. Interactions of Alzheimer's Amyloid-Beta Peptides with Zn(II) and Cu(II) Ions. 2012.

135. **Olga Gavrilova**. Application and Elaboration of Accounting Approaches for Sustainable Development. 2012.

136. **Olesja Bondarenko**. Development of Bacterial Biosensors and Human Stem Cell-Based *In Vitro* Assays for the Toxicological Profiling of Synthetic Nanoparticles. 2012.

137. **Katri Muska**. Study of Composition and Thermal Treatments of Quaternary Compounds for Monograin Layer Solar Cells. 2012.

138. **Ranno Nahku**. Validation of Critical Factors for the Quantitative Characterization of Bacterial Physiology in Accelerostat Cultures. 2012.

139. **Petri-Jaan Lahtvee**. Quantitative Omics-level Analysis of Growth Rate Dependent Energy Metabolism in *Lactococcus lactis*. 2012.

140. **Kerti Orumets**. Molecular Mechanisms Controlling Intracellular Glutathione Levels in Baker's Yeast *Saccharomyces cerevisiae* and its Random Mutagenized Glutathione Over-Accumulating Isolate. 2012.

141. **Loreida Timberg**. Spice-Cured Sprats Ripening, Sensory Parameters Development, and Quality Indicators. 2012.

142. **Anna Mihhalevski**. Rye Sourdough Fermentation and Bread Stability. 2012.

143. **Liisa Arike**. Quantitative Proteomics of *Escherichia coli*: From Relative to Absolute Scale. 2012.

144. **Kairi Otto**. Deposition of In_2S_3 Thin Films by Chemical Spray Pyrolysis. 2012.

145. **Mari Sepp**. Functions of the Basic Helix-Loop-Helix Transcription Factor TCF4 in Health and Disease. 2012.

146. **Anna Suhhova**. Detection of the Effect of Weak Stressors on Human Resting Electroencephalographic Signal. 2012.

147. **Aram Kazarjan**. Development and Production of Extruded Food and Feed Products Containing Probiotic Microorganisms. 2012.

148. **Rivo Uiboupin**. Application of Remote Sensing Methods for the Investigation of Spatio-Temporal Variability of Sea Surface Temperature and Chlorophyll Fields in the Gulf of Finland. 2013.

149. **Tiina Kriščiunaite**. A Study of Milk Coagulability. 2013.

150. **Tuuli Levandi**. Comparative Study of Cereal Varieties by Analytical Separation Methods and Chemometrics. 2013.

151. **Natalja Kabanova**. Development of a Microcalorimetric Method for the Study of Fermentation Processes. 2013.

152. **Himani Khanduri**. Magnetic Properties of Functional Oxides. 2013.

153. **Julia Smirnova**. Investigation of Properties and Reaction Mechanisms of Redox-Active Proteins by ESI MS. 2013.

154. **Mervi Sepp**. Estimation of Diffusion Restrictions in Cardiomyocytes Using Kinetic Measurements. 2013.

155. **Kersti Jääger**. Differentiation and Heterogeneity of Mesenchymal Stem Cells. 2013.

156. **Victor Alari**. Multi-Scale Wind Wave Modeling in the Baltic Sea. 2013.

157. **Taavi Päll**. Studies of CD44 Hyaluronan Binding Domain as Novel Angiogenesis Inhibitor. 2013.

158. **Allan Niidu**. Synthesis of Cyclopentane and Tetrahydrofuran Derivatives. 2013.

159. **Julia Geller**. Detection and Genetic Characterization of *Borrelia* Species Circulating in Tick Population in Estonia. 2013.

160. **Irina Stulova**. The Effects of Milk Composition and Treatment on the Growth of Lactic Acid Bacteria. 2013.

161. **Jana Holmar**. Optical Method for Uric Acid Removal Assessment During Dialysis. 2013.

162. **Kerti Ausmees**. Synthesis of Heterobicyclo[3.2.0]heptane Derivatives *via* Multicomponent Cascade Reaction. 2013.

163. **Minna Varikmaa**. Structural and Functional Studies of Mitochondrial Respiration Regulation in Muscle Cells. 2013.

164. **Indrek Koppel**. Transcriptional Mechanisms of BDNF Gene Regulation. 2014.

165. **Kristjan Pilt**. Optical Pulse Wave Signal Analysis for Determination of Early Arterial Ageing in Diabetic Patients. 2014.

166. **Andres Anier**. Estimation of the Complexity of the Electroencephalogram for Brain Monitoring in Intensive Care. 2014.

167. **Toivo Kallaste**. Pyroclastic Sanidine in the Lower Palaeozoic Bentonites – A Tool for Regional Geological Correlations. 2014.

168. **Erki Kärber**. Properties of ZnO-nanorod/In_2S_3/$CuInS_2$ Solar Cell and the Constituent Layers Deposited by Chemical Spray Method. 2014.

169. **Julia Lehner**. Formation of Cu_2ZnSnS_4 and $Cu_2ZnSnSe_4$ by Chalcogenisation of Electrochemically Deposited Precursor Layers. 2014.

170. **Peep Pitk**. Protein- and Lipid-rich Solid Slaughterhouse Waste Anaerobic Co-digestion: Resource Analysis and Process Optimization. 2014.

171. **Kaspar Valgepea**. Absolute Quantitative Multi-omics Characterization of Specific Growth Rate-dependent Metabolism of *Escherichia coli*. 2014.

172. **Artur Noole**. Asymmetric Organocatalytic Synthesis of 3,3'-Disubstituted Oxindoles. 2014.

173. **Robert Tsanev**. Identification and Structure-Functional Characterisation of the Gene Transcriptional Repressor Domain of Human Gli Proteins. 2014.

174. **Dmitri Kartofelev**. Nonlinear Sound Generation Mechanisms in Musical Acoustic. 2014.

175. **Sigrid Hade**. GIS Applications in the Studies of the Palaeozoic Graptolite Argillite and Landscape Change. 2014.

176. **Agne Velthut-Meikas**. Ovarian Follicle as the Environment of Oocyte Maturation: The Role of Granulosa Cells and Follicular Fluid at Pre-Ovulatory Development. 2014.

177. **Kristel Hälvin**. Determination of B-group Vitamins in Food Using an LC-MS Stable Isotope Dilution Assay. 2014.

178. **Mailis Päri**. Characterization of the Oligoadenylate Synthetase Subgroup from Phylum Porifera. 2014.

179. **Jekaterina Kazantseva**. Alternative Splicing of *TAF4*: A Dynamic Switch between Distinct Cell Functions. 2014.

180. **Jaanus Suurväli**. Regulator of G Protein Signalling 16 (RGS16): Functions in Immunity and Genomic Location in an Ancient MHC-Related Evolutionarily Conserved Synteny Group. 2014.

181. **Ene Viiard**. Diversity and Stability of Lactic Acid Bacteria During Rye Sourdough Propagation. 2014.

182. **Kristella Hansen**. Prostaglandin Synthesis in Marine Arthropods and Red Algae. 2014.

183. **Helike Lõhelaid**. Allene Oxide Synthase-lipoxygenase Pathway in Coral Stress Response. 2015.

184. **Normunds Stivrinš**. Postglacial Environmental Conditions, Vegetation Succession and Human Impact in Latvia. 2015.

185. **Mary-Liis Kütt**. Identification and Characterization of Bioactive Peptides with Antimicrobial and Immunoregulating Properties Derived from Bovine Colostrum and Milk. 2015.

186. **Kazbulat Šogenov**. Petrophysical Models of the CO_2 Plume at Prospective Storage Sites in the Baltic Basin. 2015.

187. **Taavi Raadik**. Application of Modulation Spectroscopy Methods in Photovoltaic Materials Research. 2015.